

An Experimental Investigation of Showerhead Film Cooling Performance in a Transonic Vane Cascade at Low Freestream Turbulence

Ruford J. Bolchoz, III

Thesis submitted to the faculty of Virginia Polytechnic Institute and State University in partial fulfillment of the requirements for the degree of

Master's of Science
in
Mechanical Engineering

Dr. Wing Ng, Chair
Dr. Thomas Diller
Dr. Brian Vick

May 14, 2008
Blacksburg, VA

Keywords: Heat Transfer, Turbine, Cascade, Film Cooling, Vane,
Transonic, Freestream Turbulence

Copyright © 2008 by Ruford Bolchoz, III

An Experimental Investigation of Showerhead Film Cooling Performance in a Transonic Vane Cascade at Low Freestream Turbulence

Ruford J. Bolchoz, III

THESIS ABSTRACT

In the drive to increase cycle efficiency, gas turbine designers have increased turbine inlet temperatures well beyond the metallurgical limits of engine components. In order to prevent failure and meet life requirements, turbine components must be cooled well below these hot gas temperatures. Film cooling is a widely employed cooling technique whereby air is extracted from the compressor and ejected through holes on the surfaces of hot gas path components. The cool air forms a protective film around the surface of the part. Accurate numerical prediction of film cooling performance is extremely difficult so experiments are required to validate designs and CFD tools.

In this study, a first stage turbine vane with five rows of showerhead cooling was instrumented with platinum thin-film gauges to experimentally characterize film cooling performance. The vane was tested in a transonic vane cascade in Virginia Tech's heated, blow-down wind tunnel. Two freestream exit Mach numbers of 0.76 and 1.0—corresponding to exit Reynolds numbers based on vane chord of 1.1×10^6 and 1.5×10^6 , respectively—were tested at an inlet freestream turbulence intensity of two percent and an integral length scale normalized by vane pitch of 0.05. The showerhead cooling scheme was tested at blowing ratios of 0 (no cooling), 1.5, and 2.0 and a density ratio of 1.35. Midspan Nusselt number and film cooling effectiveness distributions over the surface of the vane are presented.

Film cooling was found to augment heat transfer and reduce adiabatic wall temperature downstream of injection. In general, an increase in blowing ratio was shown to increase augmentation and film cooling effectiveness. Increasing Reynolds number was shown to increase heat transfer and reduce effectiveness. Finally, comparing low turbulence measurements ($Tu = 2\%$) to measurements performed at high freestream turbulence ($Tu = 16\%$) by Nasir *et al.* [13] showed that large-scale high freestream turbulence can reduce heat transfer coefficient downstream of injection.

ACKNOWLEDGEMENTS

This study was sponsored by Solar Turbines under the supervision of Drs. Hee-Koo Moon and Luzeng Zhang. I would like to thank them for their continued support throughout this project. I would also like to thank Drs. Mark Polanka and Richard Anthony of the Air Force Research Laboratory for providing the thin film gauges used in this study. Without the support of Solar Turbines and AFRL, this experiment would not have been possible.

I would also like to thank my committee members for providing the knowledge and guidance that our team needed to make this project a success. Dr. Ng provided me with the opportunity to work on an excellent team, and he continually pushed me to develop my own understanding of my research. He placed a lot of trust in our team and allowed us to be the decision makers which was a great confidence builder. Dr. Diller's advice regarding experimental techniques and interpretation of results was invaluable and cannot be overlooked. Lastly, Dr. Vick's instruction will be something that I will carry with me throughout my career.

The Mechanical Engineering staff and shop must also be thanked. Peggy Caldwell, Lynne Ellis, Johnny Cox, Bill Songer, and James Dowdy all provided assistance in this project. Bill Songer in the M.E. shop has been an extremely important contributor to this work. He has spent countless hours deciphering my drawings and machining part after part. His expertise and humor can't go without mention.

I would like to thank my team: Shakeel Nasir, Ashley Guy, and Colin Reagle. I learned more from them than I could possibly have discovered on my own—technically, socially, and culturally. I did not go a day on this team without learning something new. It was a privilege to work with them. I'd like to thank my friends Cape, Matt, and Felix, for struggling through this program with me, but most importantly for keeping me laughing. I'd also like to thank Bosco for greeting me at the door every day with a wagging tail and a bone in his mouth.

I'd like to thank Melia for sending me treats, making me smile, and always supporting my goals. Finally, I'd like to thank my entire family—parents, grandparents, sister, aunts and uncles—for continuing to support me in whatever I choose to do. My parents, Patty and Joey, have provided me with every opportunity that I could have asked for. They have pushed me to excel, and they've been there to guide me and listen to me along the way. They're the reason that I am where I am, and I can't thank them enough.

PREFACE

This thesis details an experimental investigation of showerhead film cooling performance in a transonic vane cascade at low freestream turbulence. The effects of blowing ratio, Reynolds/Mach number, and freestream turbulence on Nusselt number and adiabatic film cooling effectiveness are presented. The purpose of this work was to produce a data set that could be used in the validation of a computational model and that would compliment measurements performed previously at high freestream turbulence.

The work is divided into two parts. The first is a stand-alone paper that is intended for submission to the ASME International Gas Turbine Institute conference in 2009. The paper contains a brief description of the facility, the measurement technique, results, and discussion of those results. The second is a series of appendices which support the paper and provide additional detail.

TABLE OF CONTENTS

Thesis Abstract	ii
Acknowledgements	iii
Preface	iv
Table of Contents	v
List of Figures	vii
List of Tables	ix
Abstract	1
Introduction	2
Past Studies	2
Nomenclature	5
Greek	6
Subscripts	6
Experimental Setup and Instrumentation	7
Transonic Wind Tunnel	7
Cascade Test Section	8
Showerhead-Cooled Vane	8
Film Cooling Supply System	9
Instrumentation	10
Data Reduction	11
Heat Transfer Coefficient and Film Cooling Effectiveness	12
Recovery Temperature	14
Experimental Uncertainty	15
Vane Static Pressure Distribution	15
Vane Heat Transfer Coefficient and Effectiveness Results	16
Baseline Heat Transfer Coefficient	18
Effect of Blowing Ratio on Heat Transfer Coefficient	19
Effect of Blowing Ratio on Film Cooling Effectiveness	22
Effect of Reynolds Number/Mach Number on Heat Transfer Coefficient	24
Effect of Reynolds Number/Mach Number on Film Cooling Effectiveness	25
Effect of Turbulence on Heat Transfer Coefficient	27

Effect of Turbulence on Film Cooling Effectiveness.....	29
Conclusions	29
Acknowledgements.....	31
References	32
Appendix A: Film Cooling System.....	35
Film Cooling System Overview.....	35
Film Cooling System Plumbing.....	36
Compression and Storage.	36
Coolant Delivery.	36
Film Cooling System Operation	38
Appendix B: Gauge Installation	40
TFG Mounting	40
Thermocouple Mounting	41
Lead Wire Attachment	42
Test Section Installation	43
Additional References	44
Appendix C: Recovery Temperature Measurement.....	45
Appendix D: Uncertainty Analysis	48
Appendix E: Regression Technique at Low Freestream Turbulence	51
Appendix F: Tabulated Results.....	55
Appendix G: Sample Data.....	63
Appendix H: Net Heat Flux Reduction.....	66
Determining Net Heat Flux Reduction.....	66
Effect of Blowing Ratio on Net Heat Flux Reduction	66
Additional References	66
Appendix I: Data Reduction Code.....	68

LIST OF FIGURES

Figure 1. Virginia Tech Transonic Cascade	7
Figure 2. Vane Cascade.....	8
Figure 3. Profile of Showerhead-Cooled Vane.....	9
Figure 4. Sectioned View of Stagnation Row of Holes	9
Figure 5. Film-cooled Vane with Instrumentation.....	11
Figure 7. Determination of h and η	14
Figure 8. Local Mach Number Distribution	16
Figure 9. Acceleration Parameter Distribution.....	16
Figure 10. Uncooled Nu Distribution for Vane with and without Film Cooling Holes.....	19
Figure 11. Effect of BR on Nu at $M_{ex} = 0.76$	21
Figure 12. Effect of BR on Nu at $M_{ex} = 1.0$	22
Figure 13. Effect of BR on η at $M_{ex} = 0.76$	23
Figure 14. Effect of BR on η at $M_{ex} = 1.00$	24
Figure 15. Effect of Reynolds Number/Mach Number on Nu at BR = 1.5.....	25
Figure 16. Effect of Reynolds Number/Mach Number on Nu at BR = 2.0.....	25
Figure 17. Effect of Reynolds Number/Mach Number on η at BR = 1.5	26
Figure 18. Effect of Reynolds Number/Mach Number on η at BR = 2.0	27
Figure 19. Effect of Tu on Nu for $M_{ex} = 0.76$, BR = 0.....	28
Figure 20. Effect of Tu on Nu for $M_{ex} = 0.76$, BR = 2.0.....	28
Figure 21. Effect of Tu on η for $M_{ex} = 0.76$, BR = 2.0	29
Figure A1. Film Cooling System.....	35
Figure A2. Photograph of Film Cooling System.....	37
Figure A3. Coolant Supply Fitting.....	38
Figure A4. Time History of $M_{ex}=0.76$, BR=2.0 Tunnel Run.....	39
Figure B1. Platinum Thin-film Gauge Locations	41
Figure B2. Thermocouple Locations.....	42
Figure B3. Gauge Sheet and Thermocouples Installed on Film-Cooled Vane	43
Figure B4. Film-cooled Vane Assembled with Test Section Windows and Insert	44
Figure B5. Picture of Instrumented Vane Installed in Test Section.....	44

Figure C1. Determining h and T_r with BR= 0	46
Figure C2. Heat transfer coefficient for Mex=0.76, Tu=16%, BR=2.0, DR = 1.38.....	47
Figure C3. Film cooling effectiveness for Mex=0.76, Tu=16%, BR=2.0, DR = 1.38	47
Figure D1. Determination of h and η	48
Figure D2. Nusselt Number Distribution with Uncertainty Bands.....	49
Figure D3. Effectiveness Distribution with Uncertainty Bands	50
Figure E1. Freestream Conditions for $M_{ex} = 1.0$, BR = 1.5 Run.....	51
Figure E2. Regression Plot for Gauge 16 (s/C = 0.45)	52
Figure E3. Temperature History of Gauge 9 and 11 for Mex = 0.76, BR = 1.5.....	53
Figure E4. Regression for determining h and η at Gauge 9 for Mex = 0.76, BR = 1.5	54
Figure G1. Tunnel Freestream Conditions	63
Figure G2. Thin-film Gauge Temperature History of Gauge 5.....	64
Figure G3. Heat Flux History of Gauge 5	65
Figure G4. Heat Transfer Coefficient and Effectiveness During Transient Run	65
Figure H1. Effect of BR on $\Delta q''_{red}$ for Mex = 0.76.....	67
Figure H2. Effect of BR on $\Delta q''_{red}$ for Mex = 1.0.....	67

LIST OF TABLES

Table 1. Film-Cooled Vane Geometry.....	9
Table 2. Test Conditions	17
Table D1. Experimental Uncertainties	49
Table F1. Nusselt Number, Nu , for $M_{ex} = 0.76$	55
Table F2. Heat Transfer Augmentation, Nu/Nu_0 , for $M_{ex} = 0.76$	56
Table F3. Film Cooling Effectiveness, η , for $M_{ex} = 0.76$	57
Table F4. Net Heat Flux Reduction, $\Delta q''_{red}$, for $M_{ex} = 0.76$	58
Table F5. Nusselt Number, Nu , for $M_{ex} = 1.0$	59
Table F6. Heat Transfer Augmentation, Nu/Nu_0 , for $M_{ex} = 1.0$	60
Table F7. Film Cooling Effectiveness, η , for $M_{ex} = 1.0$	61
Table F8. Net Heat Flux Reduction, $\Delta q''_{red}$, for $M_{ex} = 1.0$	62

An Experimental Investigation of Showerhead Film Cooling Performance in a Transonic Vane Cascade at Low Freestream Turbulence

T. Bolchoz, S. Nasir, and W.F. Ng
Department of Mechanical Engineering
Virginia Polytechnic Institute and State University
Blacksburg, VA 24061

L.J. Zhang and H.K. Moon
Solar Turbines Incorporated
San Diego, CA 92101

ABSTRACT

This experiment investigates the effects of blowing ratio and exit Reynolds/Mach number on the film cooling performance of a showerhead-cooled first-stage turbine vane at low freestream turbulence ($Tu = 2\%$). The effect of freestream turbulence at design Mach number and blowing ratio ($M_{ex} = 0.76$, $BR = 2.0$) is also explored by comparing results with high freestream turbulence measurements ($Tu = 16\%$) performed on the same cascade by Nasir *et al.* [13]. To characterize film cooling performance, platinum thin-film gauges were used to measure Nusselt number and film cooling effectiveness distributions at the midspan of the vane. Two exit Mach numbers of 0.76 and 1.0—corresponding to exit Reynolds numbers based on vane chord of 1.1×10^6 and 1.5×10^6 , respectively—were tested at an inlet freestream turbulence intensity of two percent and an integral length scale normalized by vane pitch (A_x/P) of 0.05. A showerhead cooling scheme with five rows of cooling holes was tested at blowing ratios of 0 (no cooling), 1.5 and 2.0 and a density ratio of 1.35. Midspan Nusselt number and adiabatic film cooling effectiveness distributions over the vane surface are presented.

The primary effects of coolant injection were augmentation of Nusselt number and reduction of adiabatic wall temperature on the vane surface over the uncooled case. In general, increasing blowing ratio showed increases in augmentation over the vane surface and an increase in film cooling effectiveness as well. Both Nusselt number and film cooling effectiveness trends were influenced by a strong favorable pressure gradient and resulting flow acceleration on the suction surface. Increasing Reynolds number was shown to increase heat transfer levels and decrease effectiveness. On the pressure side, the increase in Reynolds number resulted in jet lift-off at both blowing ratios. Finally, comparing low freestream turbulence results with high freestream turbulence measurements by Nasir *et al.* [13] showed that large-scale high freestream turbulence can decrease heat transfer coefficient downstream of injection.

INTRODUCTION

In the drive to increase cycle efficiency, gas turbine designers have increased turbine inlet temperatures well beyond the metallurgical limits of engine components. In order to prevent failure and meet life requirements, turbine components must be cooled well below these hot gas temperatures. Film cooling is a widely employed cooling technique whereby air is extracted from the compressor and ejected through discrete holes drilled in the surface of turbine airfoils, tips, and endwalls. The air leaving these holes forms a film of cool air on the component surface which protects the part from hot gases exiting the combustor.

To date, numerical modeling has not been able to adequately predict film cooling performance at engine-realistic conditions. Factors such as hole shape, blowing ratio, momentum ratio, surface curvature, approach boundary layer state, Reynolds number, Mach number, freestream turbulence, turbulence length scale, and secondary flows make performance very difficult to numerically predict; however, steady progress is being made. Until computational methods are able to simulate these factors, engine designers must rely on experimental studies to validate designs and CFD tools.

The objective of this experiment was to investigate the effects of coolant injection rate on showerhead film cooling performance in a transonic vane cascade at low freestream turbulence. Although low freestream turbulence studies are not directly applicable to engine design, this experiment was performed with the intention of generating a data set that could assist in the validation of a computational model and that would compliment experiments performed previously at high freestream turbulence by Nasir *et al.* [13]. Three blowing ratios were tested at two exit Mach numbers corresponding to two exit Reynolds numbers. This paper will discuss the effects of blowing ratio, Reynolds/Mach number, and freestream turbulence on film cooling performance. Performance was characterized by measuring Nusselt number and adiabatic film cooling effectiveness at midspan along the surface of the vane.

PAST STUDIES

Film cooling performance has been a widely studied and heavily debated topic in literature for many years. Goldstein [1] demonstrated the basics of film cooling physics with flat plate studies. Bogard and Thole [2] as well as Han *et al.* [3] have compiled many of the

important film cooling studies that relate to gas turbines. This review covers some of the experimental work that has been performed on film-cooled vanes in high speed facilities.

One of the earliest studies performed on a film-cooled vane at high speed was by Turner *et al.* [4]. They studied the effects of Reynolds number, Mach number, coolant injection rate, and coolant-to-freestream temperature ratio on a C3X vane with showerhead cooling in a transonic cascade. Results showed that increasing coolant injection rate or Reynolds number caused an increase in heat transfer. They found that coolant injection increased heat transfer coefficient in the “preturbulent” region but has a minor effect after transition to a fully turbulent boundary layer. They also found that boundary layer transition moved slightly farther upstream with injection.

Years later, Arts and Bourguignon [5] investigated the effects of blowing ratio, Reynolds number, freestream turbulence, and row location on heat transfer coefficient and film cooling effectiveness on the pressure side of a high-pressure vane in a linear, transonic cascade. They found that heat transfer augmentation and film cooling effectiveness increased with blowing ratio. Increasing Reynolds number caused heat transfer augmentation and effectiveness to decrease for a pair of rows near stagnation. Increasing freestream turbulence intensity from 1 to 6 percent showed negligible effects on heat transfer augmentation, but it showed some influence on effectiveness.

Abuaf and Bunker [6] performed heat transfer coefficient and film cooling effectiveness measurements on a heavily film-cooled vane in a linear cascade with engine-representative flow conditions. The test vane had nine rows of showerhead cooling holes and five rows of suction side cooling holes. For the test condition presented, blowing ratio was as high as 2.7 in the showerhead region and as low as 1.4 in the set of suction side rows. The results showed that heat transfer augmentation increased significantly more on the suction side than the pressure side, and the accumulation of coolant from the showerhead and suction side rows produced higher film cooling effectiveness on the suction surface.

Drost and Bölcs [7] investigated the effects of blowing ratio, incoming boundary layer state, Reynolds/Mach number, and freestream turbulence on heat transfer coefficient and film cooling effectiveness for a vane using a transient liquid crystal technique. The test vane had cylindrical cooling hole rows on the pressure and suction surfaces. Increasing blowing ratio was found to increase augmentation and film cooling effectiveness although jets were seen to lift off

and reattach farther downstream for higher blowing ratios. On the suction side of the vane, a laminar incoming boundary layer showed up to thirty percent higher effectiveness just downstream of injection than a turbulent incoming boundary layer; however, both incoming boundary layers produced similar levels of effectiveness farther downstream. Results also indicated slightly higher augmentation for injection into a laminar boundary layer as compared to a turbulent boundary layer. Changing exit Reynolds/Mach number was shown to affect film cooling performance due to changes in boundary layer thickness and flow acceleration. Freestream turbulence had a complicated effect on film cooling performance, but high freestream turbulence ($Tu = 10\%$) was shown to increase film cooling effectiveness near injection for high blowing ratios ($BR > 1.5$) by increasing coolant dispersion into the boundary layer.

Guo *et al.* [8] used single-sided thin-film gauges on a semi-infinite substrate to measure heat transfer coefficient and film cooling effectiveness on a fully film-cooled vane in a transonic, annular cascade. Engine-representative conditions, including density ratio, were achieved, and results were only presented for a nominal pressure ratio of 1.02. Heat transfer augmentation was observed over the entire pressure surface, and some of the suction surface. Heat transfer coefficient levels falling below that of the uncooled case were reasoned to result from a thicker boundary layer for the cooled case. Film cooling effectiveness was highest on the pressure side where more rows of cooling holes were present.

Zhang *et al.* [9] used a pressure sensitive paint technique to study the effects of blowing ratio, Reynolds number, and Mach number at high freestream turbulence ($Tu = 12\%$) on film cooling effectiveness. The test vane had a single row of shaped film cooling holes on the suction surface. Results indicated that film cooling effectiveness increased with an increase in blowing ratio from 0.5 to 1.5, and jet lift-off was noted at a blowing ratio of 1.5. Significant spanwise variation of film cooling effectiveness was noted and attributed to uneven coolant ejection from the holes and insufficient mixing on the surface. Effectiveness was found to decrease with an increase in Reynolds number or a decrease in exit Mach number, but freestream effects were less significant with a high blowing ratio ($BR = 1.5$).

Reiss and Böls [10] investigated the effects of blowing ratio, incoming boundary layer state, and Reynolds/Mach number on the film cooling performance of a single row of cylindrical holes on the suction side of a vane using a transient liquid crystal technique. Results showed that spanwise averaged heat transfer coefficient increased with blowing ratio for a laminar incoming

boundary layer, but the effect of blowing ratio was weak with a turbulent incoming boundary layer. A turbulent incoming boundary layer was found to reduce film cooling effectiveness due to more intense mixing and to reduce lateral spread of the jets. Reynolds/Mach number effects were shown to vary depending on surface location and rate of injection.

Finally, Ames' work [11] on vane film cooling performance in a low speed facility should not go unmentioned. Ames studied the effects of coolant injection rate and freestream turbulence on heat transfer and adiabatic effectiveness distributions for a C3X vane. Several cooling configurations were tested, but the results for showerhead cooling are of interest to this study. Results showed that Stanton number augmentation on both suction and pressure surfaces increased with increasing showerhead coolant injection rate, but little effect of injection rate was seen after boundary layer transition. Film cooling effectiveness was found to increase with injection rate for high freestream turbulence, but the opposite was true for low freestream turbulence. Increasing freestream turbulence resulted in higher heat transfer levels but lower Stanton number augmentation for a given injection rate. Increased freestream turbulence also reduced film cooling effectiveness.

Very few studies available in literature have solely investigated the effects of showerhead film cooling on turbine vane heat transfer at engine-representative flow conditions, and to the authors' knowledge, no studies have characterized showerhead film cooling performance alone by Nusselt number and adiabatic film cooling effectiveness at such conditions. This experimental study is part of larger study whose ultimate goal is to characterize showerhead film cooling performance of a first-stage vane at realistic exit Reynolds numbers and Mach numbers with high freestream turbulence. The results presented in this paper detail the investigation of film cooling performance at low freestream turbulence ($Tu = 2\%$), and the study is meant to compliment measurements performed by Nasir *et al.* [13] at high freestream turbulence ($Tu = 16\%$).

NOMENCLATURE

A	area
BR	blowing ratio
C	vane chord
d	cooling hole diameter

DR	density ratio
h	heat transfer coefficient
k	acceleration parameter or thermal conductivity
M	Mach number
\dot{m}	mass flow rate
Nu	Nusselt number
P	vane pitch
p	cooling hole pitch
Pr	Prandtl number
PS	pressure side
q''	heat flux
$\Delta q''_{red}$	net heat flux reduction
Re	Reynolds number
s	vane surface distance from stagnation point
SS	suction side
T	temperature
Tu	streamwise freestream turbulence intensity
U	local velocity

Greek

α	injection angle (spanwise)
γ	compound angle (streamwise)
ϕ	overall film cooling effectiveness
Λ_x	integral turbulence length scale
η	adiabatic film cooling effectiveness
ρ	local density of air

Subscripts

0	no film cooling
∞	freestream
a	air
aw, w	adiabatic wall, wall

c	coolant
ex, i	exit, inlet
g	gas
o	stagnation
r	recovery
s	surface

EXPERIMENTAL SETUP AND INSTRUMENTATION

Transonic Wind Tunnel

This experiment was performed in Virginia Tech's blow-down wind tunnel, depicted in Figure 1. The facility is capable of supplying the transonic, two-dimensional cascade with a constant pressure for 25 seconds. This same facility was used by Nasir *et al.* [11, 13], Carullo *et al.* [14], Nix *et al.* [15], Holmberg and Diller [16], Smith *et al.* [17], and Popp *et al.* [18]. Air is supplied by storage tanks which are pressurized up to 1380 kPa (200 psig) using a four-stage Ingersoll-Rand compressor. A control valve regulates flow from these tanks to achieve a desired test section pressure which can range from 20.7 kPa (3 psig) to 69.0 kPa (10 psig) depending on the test conditions. Before entering the test section, air travels through a passive heat exchanger which provides a cascade inlet temperature up to 120°C at the start of the run. After the heat exchanger, air flows through a rectangular contraction and into the test section. Air leaves the test section through a duct which exhausts to the atmosphere.

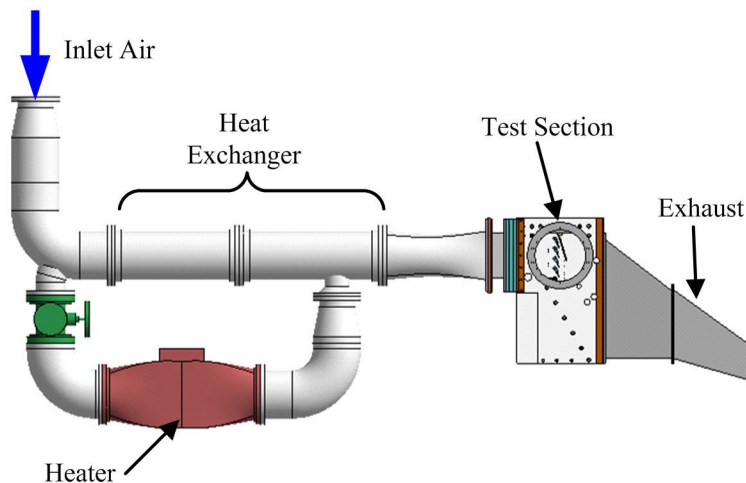


Figure 1. Virginia Tech Transonic Cascade

Cascade Test Section

The cascade used in this experiment is depicted in Figure 2. It contained four full vanes and two partial vanes, resulting in four full passages and one partial passage. A tailboard was placed along the exit angle of the topmost partial vane to ensure periodicity. Cascade inlet and exit conditions were measured using a Pitot-static probe and T-type stagnation temperature thermocouple near the inlet of the test section along with static pressure taps on the endwall upstream and downstream of the vanes. A vertical slot located $0.45C$ upstream of the vane row was used for turbulence and velocity distribution measurements. Film cooling experiments previously performed by Nasir *et al.* [13] used a passive mesh grid generating turbulence intensity levels of 16 percent with an integral length scale normalized by vane pitch (Λ_x/P) of 0.23; however, the passive grid was removed for this experiment. The resulting turbulence intensity was two percent with Λ_x/P of 0.05. Turbulence measurements are described in Nasir *et al.* [11]. All measurements were performed on Vane 2 shown in Figure 2.

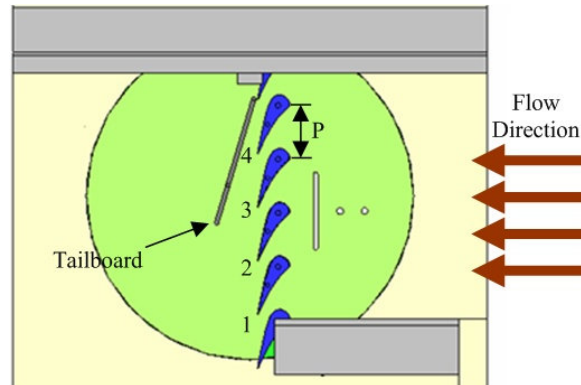


Figure 2. Vane Cascade

Showerhead-Cooled Vane

The showerhead-cooled vane used in this experiment had five rows of staggered cylindrical holes. The center row was placed at the geometric stagnation point while the remaining rows were spaced at four and eight hole diameters on either side. A cylindrical plenum supplied air to all five rows, and each row was spaced three hole diameters apart within the plenum as seen in Figure 3. Cooling holes were spaced by a hole-pitch-to-diameter (p/d) of 4.35. All holes were oriented with a 45° injection angle (spanwise), shown in Figure 4, and a 90° compound angle (streamwise). The vane profile is representative of the first-stage turbine

vane of a small industrial gas turbine, and it was scaled 1.5 times to obtain an appropriate nominal exit Reynolds number. Exit Reynolds number is based on vane chord, C , which was defined as the distance between the geometric stagnation point and trailing edge of the vane (See Figure 3). Additionally, the vane was made of Macor, a machinable ceramic material with low thermal conductivity. Table 1 summarizes the geometry, which was also used by Nasir *et al.* [13].

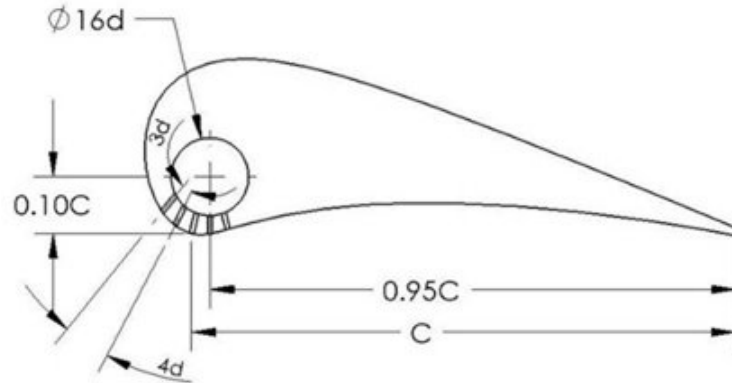


Figure 3. Profile of Showerhead-Cooled Vane

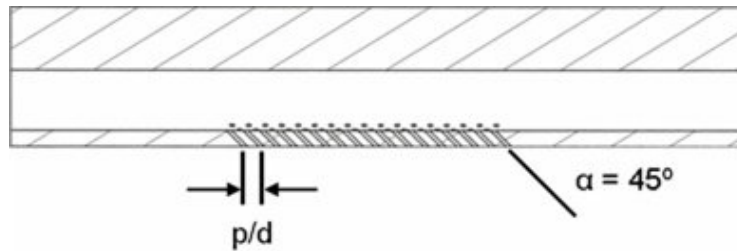


Figure 4. Sectioned View of Stagnation Row of Holes

Table 1. Film-Cooled Vane Geometry

Vane Chord	C	91.2 mm (3.59 in.)
Pitch	P	83.0 mm (3.27 in.)
Cooling Hole Diameter	d	0.787 mm (0.031 in.)
Cooling Hole Spacing	p/d	4.35
Injection Angle (spanwise)	α	45°
Compound Angle (streamwise)	γ	90°
Vane Span		152.4 mm (6.00 in.)
Cooled Span		59.2 mm (2.33 in.)
Vane Inlet and Exit Angle		0° and 73.5°

Film Cooling Supply System

Cooling air was supplied by a storage tank pressurized to 830 kPa (120 psig). A dryer kept relative humidity of the coolant air to less than four percent. Coolant flow was set via a control valve at the tank exit. Air flow was directed from the tank through a heat exchanger

which was used to heat the coolant air to match the temperature of the film-cooled vane prior to a run ($\sim 26^\circ\text{C}$).

In this experiment, coolant flow was set by coolant-to-freestream mass flux ratio or blowing ratio, BR , for the entire showerhead region. Blowing ratio for showerhead cooling was defined by Colban *et al.* [19] as:

$$BR = \frac{\rho_c U_c}{\rho_\infty U_\infty} = \frac{\dot{m}_c}{A_{\text{holes}} \rho_i U_i} \quad (1)$$

Coolant mass flux was determined by measuring the mass flow rate of the coolant with an orifice meter and dividing by the total area of the showerhead cooling holes. Freestream mass flux was determined from cascade inlet conditions measured by the Pitot-static probe and T-type thermocouple. Local surface pressure variations will undoubtedly cause blowing ratio variation from row to row, but this variation is small in the showerhead region.

Coolant-to-freestream density ratio, DR , was measured in this experiment. Using a Pitot-static probe at the inlet to the film cooling plenum, and a T-type thermocouple in the plenum near midspan, coolant density was found and compared to cascade inlet density using the following relation:

$$DR = \frac{\rho_c}{\rho_\infty} \quad (2)$$

The density ratio for this set of experiments was between 1.3 and 1.4. Although these density ratios are lower than typical engine density ratios, Bogard and Thole [2] have suggested that coolant density has a secondary effect on film cooling performance when considering the effects of injection rate and freestream conditions.

Instrumentation

Platinum thin-film gauges were used to characterize heat transfer in this experiment. The gauges were similar to those developed by Doorly and Oldfield [20], and they were manufactured by Air Force Research Laboratories according to Joe's procedure [21]. Once calibrated and installed on the film-cooled vane, the gauges measured surface temperature history with high spatial resolution and minimal flow disruption. Each thin film gauge had a 3.18 mm (0.125 in) long and $0.6 \mu\text{m}$ (2.3×10^{-5} in) thick platinum sensor centered at midspan.

The gauge cover a range from s/C of -0.58 on the pressure surface to 0.72 on the suction surface. More discussion on the use of platinum thin-film gauges regarding calibration, physical properties, and data reduction can be found in Nasir *et al.* [11] and Cress [22]. Guo *et al.* [8] have also documented the use of single-sided thin-film gauges for film cooling experiments.

Since the gauges were installed on a substrate with low thermal conductivity and the coolant temperature was set to match the vane temperature prior to a run, one-dimensional conduction into a semi-infinite medium was assumed. With this assumption, a simple transient heat conduction finite difference code was used to determine heat flux, q'' , at each gauge location based on the surface temperature history measured by that gauge.

The film-cooled vane used in this experiment had a total of twenty platinum thin-film gauges instrumented on the surface. Eleven gauges were located on the suction side of the vane, and nine gauges were located on the pressure side. Additionally, eight T-type foil thermocouples with a $12.7\ \mu\text{m}$ (0.0005 in) thickness were installed on the vane surface to measure the initial temperature of the airfoil prior to an experimental run. Figure 5 shows the gauges and thermocouples mounted on the vane before its installation in the cascade.

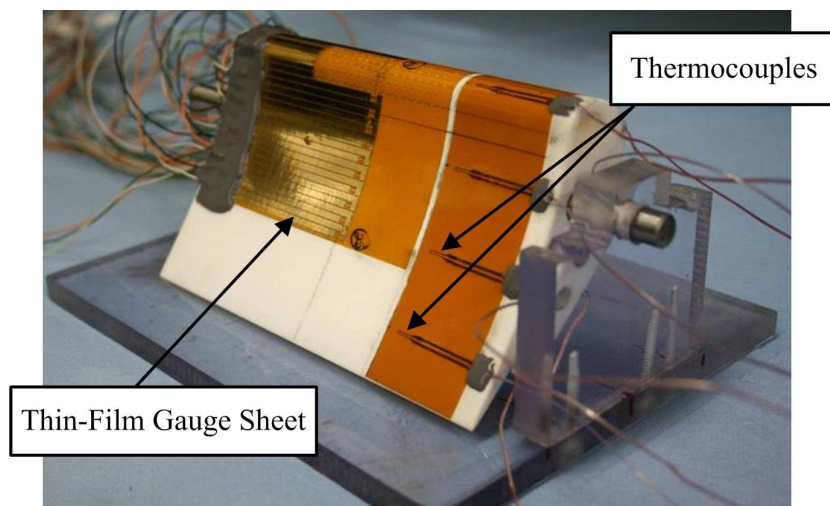


Figure 5. Film-cooled Vane with Instrumentation

DATA REDUCTION

In this study, film cooling performance was characterized by midspan Nusselt number and film cooling effectiveness. The following sections describe the technique used to measure both parameters from a single run.

Heat Transfer Coefficient and Film Cooling Effectiveness

Heat transfer into a surface in a high speed, film-cooled environment can be described by the following relation:

$$q'' = h(T_{aw} - T_w) \quad (3)$$

where T_w is the temperature of the surface or wall, and T_{aw} is the driving temperature for heat transfer. Adiabatic wall temperature, T_{aw} , is the wall temperature if the surface is assumed to be adiabatic ($q'' = 0$). The value of T_{aw} depends on the freestream temperature, coolant temperature, and the mixing between the freestream and coolant [1, 10]. Expressing heat transfer in terms of adiabatic wall temperature defines heat transfer coefficient as a function of the flowfield aerodynamics, independent of temperature boundary conditions. Adiabatic wall temperature for high speed flows can be nondimensionalized by expressing it in terms of adiabatic film cooling effectiveness:

$$\eta = \frac{T_{aw} - T_r}{T_c - T_r} \quad (4)$$

Film cooling performance is characterized by h and η , and it is often necessary to perform multiple experiments to determine these two quantities for a given set of conditions. However, this is not the case in the Virginia Tech facility. Quasi-steady flow conditions along with transient freestream and vane temperatures allow measurement of heat transfer coefficient and film cooling effectiveness from a single run. This data reduction technique is outlined in Smith *et al.* [17]. Equations 3 and 4 can be arranged to yield:

$$\frac{q''}{T_r - T_c} = h \left(\frac{T_r - T_w}{T_r - T_c} \right) - h\eta \quad (5)$$

where q'' and T_w are measured with thin-film gauges; T_c is measured by a thermocouple near midspan in the supply plenum; and T_r is experimentally measured without film cooling. Measurement of recovery temperature is discussed in the following section.

In the form above, Equation 5 is equivalent to the slope-intercept expression for a straight line: $y = mx + b$. This linear relationship is further illustrated by plotting experimental values for the nondimensional temperature term on the right hand side of Equation 5 along the x-axis and the

experimental values for the left hand side of Equation 5 along the y-axis. The slope of the resulting line represents the heat transfer coefficient, and adiabatic film cooling effectiveness is given by the x-intercept—where q'' goes to zero. Slope and intercept are determined by calculating a linear least squares regression of the plotted data. This technique was performed at each measurement location for each tunnel run. Figure 6 shows a sample of the measured experimental values used in the regression technique for one gauge, and the corresponding regression is shown in Figure 7.

In subsequent sections, results for heat transfer coefficient will be presented in terms of Nusselt number:

$$Nu = \frac{hC}{k_a} \quad (6)$$

Nusselt number for each gauge was determined using the method described above and averaged for several runs at identical conditions.

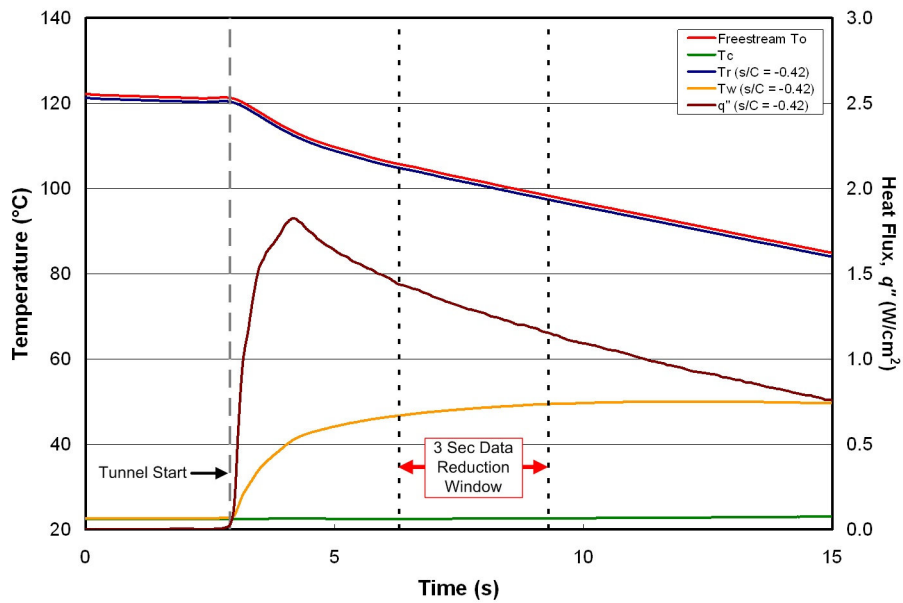


Figure 6. Experimental Data Used to Determine h and η

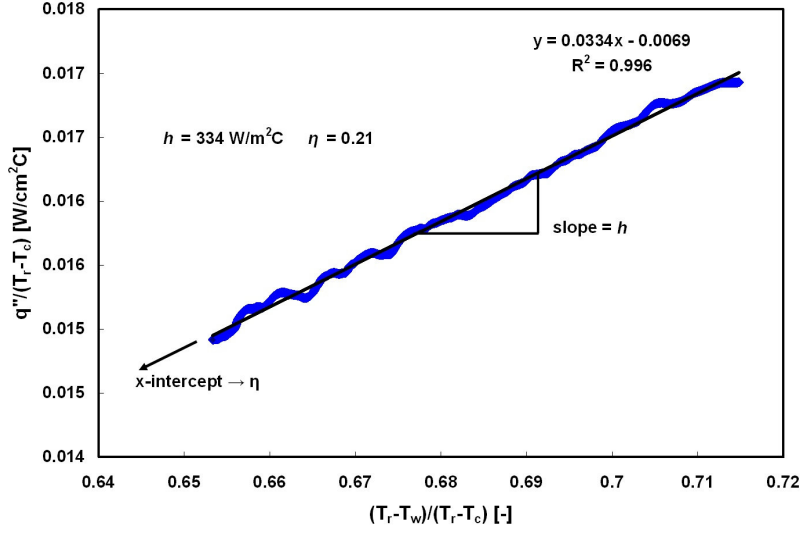


Figure 7. Determination of h and η

Recovery Temperature

Recovery Temperature, T_r , in Equation 5 was experimentally determined in a high speed flow with no film injection ($BR = 0$). With no film cooling, heat transfer on the airfoil surface can be described by:

$$q_0'' = h_0(T_r - T_w) \quad (7)$$

where h_0 is the heat transfer coefficient for the uncooled case; T_w is the wall temperature measured by the thin-film gauge; and q_0'' is heat flux calculated based on the wall temperature and a 1-D, semi-infinite heat conduction assumption. The difference between the freestream total temperature and the recovery temperature is constant as long as flow conditions are steady, so Equation 7 can be rewritten as:

$$q_0'' = h_0(T_{o,\infty} - T_w) - h_0(T_{o,\infty} - T_r) \quad (8)$$

Using Equation 8, h_0 and T_r were found by plotting q_0'' versus $(T_{o,\infty} - T_w)$ for each gauge during a steady part of the run. The resulting line is again a linear relationship where slope represents heat transfer coefficient, h_0 , and the x-intercept represents $(T_{o,\infty} - T_r)$. $(T_{o,\infty} - T_r)$ was then used to determine the recovery temperature at each gauge for film-cooled experiments using $T_{o,\infty}$ for that particular experiment. More explanation of this technique is detailed in Smith *et al.* [17] and Popp *et al.* [18].

EXPERIMENTAL UNCERTAINTY

The overall uncertainty of heat transfer coefficient and film cooling effectiveness were determined by combining two methods. First, Moffat's [23] small perturbation uncertainty method was used to estimate bias and precision uncertainties of the $q''/(T_r-T_c)$ and $(T_r-T_w)/(T_w-T_c)$ values plotted in Figure 7. Then, Brown and Coleman's [24] linear regression analysis was used to obtain the uncertainty of the least squares linear regression for each gauge based upon the uncertainties determined by Moffat's method. The uncertainty in slope and intercept represented the uncertainties in h and η . All uncertainties are reported within a 95% confidence interval, and each test condition was performed at least three times to account for run-to-run repeatability. The overall average uncertainty in heat transfer coefficient and effectiveness was $\pm 8.0\%$ and ± 0.055 , respectively. Uncertainty is higher in film cooling effectiveness because the reduction technique requires extrapolation to determine η . It should also be noted that uncertainty in both heat transfer coefficient and effectiveness is higher than the uncertainty reported by Nasir *et al.* [13] ($\pm 6.5\%$ in h and ± 0.032 in η) for similar measurements with large-scale high freestream turbulence. This will be discussed further when the results are presented.

VANE STATIC PRESSURE DISTRIBUTION

Prior to film cooling experiments, a vane model instrumented with static pressure taps was used to determine the local Mach number distributions, shown in Figure 8, for the two exit Mach number conditions. The Mach number gradually increases from the stagnation to the trailing edge on the pressure side, showing no velocity peaks. The flow on the suction side continuously accelerates up to the geometric throat at s/C of 0.51. For the exit Mach 0.8 case, the flow decelerates immediately after the throat; whereas, the flow for the exit Mach 1.0 case continues to accelerate beyond the throat, becoming supersonic. A trailing edge shock from the adjacent vane impinging on the suction surface at s/C of 0.58 causes multiple flow decelerations after the throat for the higher Mach number case.

The distribution of acceleration parameter, k , on the smooth vane surface for each exit Mach number is provided in Figure 9. A positive acceleration parameter indicates flow acceleration and a negative value indicates deceleration. Values of k above the critical value of 3×10^{-6} have been observed by Jones and Launder [25] and Mayle [26] to be the criterion for

boundary layer relaminarization. It should be noted that the suction side maintains an acceleration parameter above the critical value until $s/C = 0.28$.

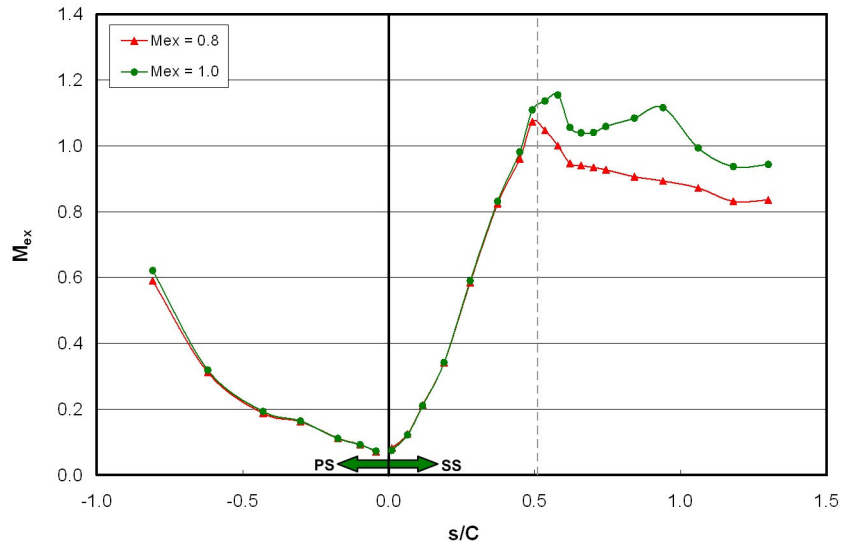


Figure 8. Local Mach Number Distribution

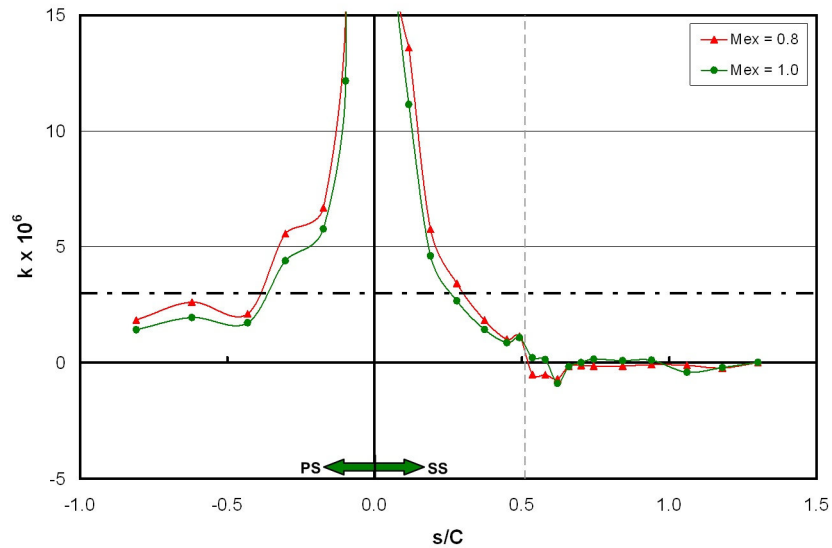


Figure 9. Acceleration Parameter Distribution

VANE HEAT TRANSFER COEFFICIENT AND EFFECTIVENESS RESULTS

Heat transfer coefficient and film cooling effectiveness measurements were performed at exit Mach numbers of 0.76 and 1.00 with an inlet freestream turbulence intensity of two percent and an integral length scale normalized by vane pitch (A_{ν}/P) of 0.05. In this study, exit Mach

number and Reynolds number were coupled due to limitations of the facility. Reynolds numbers based on exit conditions and vane chord (defined in Figure 3) for the respective exit Mach number conditions are shown in Table 2. Blowing ratios of 0, 1.5, and 2.0 were studied at both exit Mach number conditions. Results for a blowing ratio of zero represent tests with no coolant injection. Additionally, the coolant-plenum-to-freestream pressure ratios corresponding to each blowing ratio tested are provided in Table 2.

Table 2. Test Conditions

Case	Tu	M_{ex}	Exit Re_C	BR	$p_{o,c}/p_{o,\infty}$
1	2% ($A_x/P = 0.05$)	0.76	1.1×10^6	0	0
2				1.5	1.07
3				2.0	1.12
4		1.00	1.5×10^6	0	0
5				1.5	1.07
6				2.0	1.12

As mentioned earlier, the uncertainty for heat transfer coefficient and effectiveness for showerhead film cooling measurements at low freestream turbulence ($Tu = 2\%$, $A_x/P = 0.05$) was found to be significantly higher than tests performed by Nasir *et al.* [13] with large-scale high freestream turbulence ($Tu = 16\%$, $A_x/P = 0.23$). The reasons for this increase in uncertainty stem from a relatively high sensitivity of heat transfer coefficient and effectiveness to small changes in freestream and film cooling conditions. This sensitivity resulted in increased run-to-run variation of h and η for a given set of conditions, driving uncertainty in both parameters upward. Realizing this, a considerable effort was made to obtain several runs for each test case with as little variation in freestream and blowing conditions as possible; despite the effort, run-to-run variation was the major contributor to uncertainty in this experiment.

Although all gauges exhibited increased sensitivity to freestream and cooling conditions at low freestream turbulence, two factors were particularly influential on the increase in average uncertainty. The first contributing factor occurred on the suction surface at measurement locations upstream of the throat between s/C of 0.34 and 0.51; these gauges showed the highest sensitivity to variations in local pressure. For instance, two identical runs for an exit Mach number of 0.76 and blowing ratio of 2.0 resulted in a 10% variation in h and 0.07 absolute variation in η for these gauges; whereas other gauges for this case varied less than 4% in h and 0.02 in η . Since these gauges lie just upstream of the throat, their exaggerated sensitivity to

freestream conditions could be due to compressibility effects as well as a changing boundary layer state in this region.

The second, and perhaps most influential, factor in increasing uncertainty occurred on the pressure side with a blowing ratio of 1.5 and an exit Mach number of 0.76. At this condition, unsteadiness in heat transfer coefficient and effectiveness was seen on the pressure side. For gauges between s/C of -0.15 and -0.20, the regression technique to find h and η produced prohibitively high uncertainty due to this unsteadiness so results for these gauges have not been included. Other pressure side gauges showed time-varying effects as well but with less severity. Although variations in local static pressure were assumed to be negligible when determining blowing ratio for the showerhead cooling rows, a very low coolant-plenum-to-freestream pressure ratio ($p_{o,c}/p_{o,\infty} \sim 1.07$) at a blowing ratio of 1.5 may explain this phenomenon. Slightly higher local static surface pressure for the cooling rows on the pressure side would result in a lower local pressure ratio ($p_{o,c}/p_s$), increasing the possibility of unsteady coolant ejection with local pressure variations. Any unsteady ejection from the cooling holes on the pressure side would result in time-varying jet interaction with the boundary layer as well as spanwise variations in film cooling performance. Overall, the unsteadiness present at a blowing ratio of 1.5 and an exit Mach number of 0.76 adversely impacted run-to-run variation, causing increased uncertainty for this case.

Neither of these behaviors was seen in experiments with high freestream turbulence by Nasir *et al.* [13], possibly because strong interaction between the coolant jets and the large-scale turbulence dominated these effects at high freestream turbulence. Despite the increase in uncertainty relative to high turbulence experiments, important conclusions regarding the effects of blowing ratio and Reynolds number can still be drawn.

Baseline Heat Transfer Coefficient

Before studying the effects of blowing ratio and Reynolds/Mach number on film cooling performance, baseline heat transfer distributions on the vane with showerhead cooling holes were established with no coolant injection (BR = 0). In Figure 10, the results are compared to uncooled measurements on a smooth vane (no cooling holes) performed by Nasir *et al.* [12] at similar freestream conditions.

For an exit Mach number of 0.76, heat transfer coefficient on the pressure surface compares very well with the smooth vane, indicating that the holes do not produce much boundary layer disturbance for the pressure surface. However, the suction surface shows a noticeable difference in heat transfer with the addition of film cooling holes. The disturbance caused by the cooling holes appears to slightly increase heat transfer augmentation prior to transition, and the boundary layer transition location moves upstream from s/C of 0.57 to 0.45.

For an exit Mach number of 1.00, the addition of cooling holes causes an increase in heat transfer coefficient over the entire pressure surface. At this exit Mach number condition, the holes disturb the boundary layer enough on the pressure side to show a significant heat transfer augmentation over the smooth vane. On the suction side, the presence of film cooling holes appears to cause immediate boundary layer transition, but the transition length is affected by a favorable pressure gradient and resulting flow acceleration between s/C of 0.29 and 0.34. The effect of acceleration on suction surface heat transfer will be discussed more in the following section.

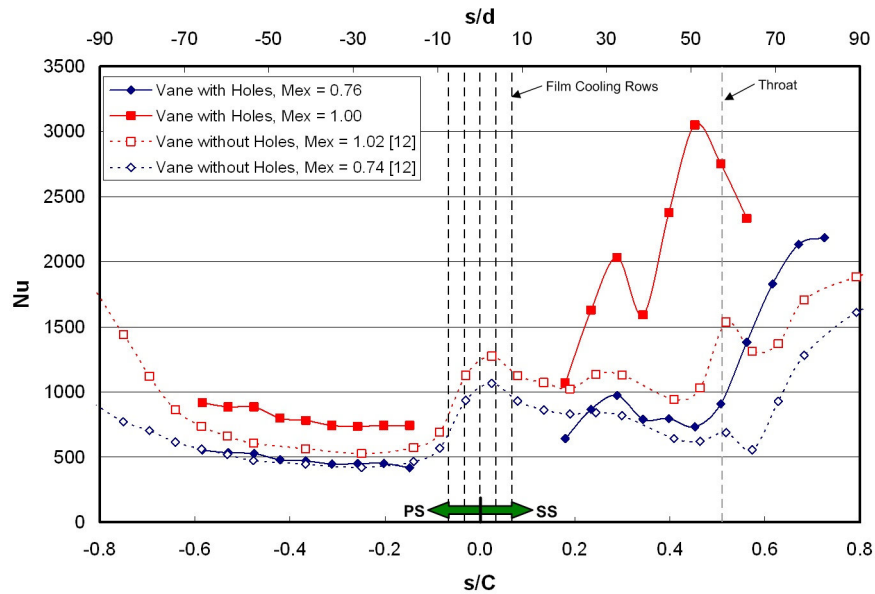


Figure 10. Uncooled Nu Distribution for Vane with and without Film Cooling Holes

Effect of Blowing Ratio on Heat Transfer Coefficient

The effect of blowing ratio on Nusselt number distribution along the vane surface at exit Mach numbers of 0.76 and 1.00 is shown in Figure 11 and Figure 12, respectively. Results are plotted against nondimensional surface distance (s/C and s/d). The Nusselt number distribution with no film injection ($BR = 0$) is included for comparison. As mentioned previously, results for

two gauges near injection on the pressure side of the vane have been removed for a blowing ratio of 1.5 at both Mach numbers due to flow unsteadiness experienced at these locations. Figures 11 and 12 clearly illustrate that the primary effect of coolant injection is augmentation of heat transfer on the vane surface downstream of injection for both exit Mach number conditions. This effect is due to increased mixing and local turbulence within the boundary layer as a result of coolant injection.

At an exit Mach number of 0.76, cooling augments heat transfer downstream of injection on both surfaces of the vane. Increasing blowing ratio from 1.5 to 2.0 causes an increase in heat transfer augmentation over the pressure surface with the effect of the higher blowing ratio being carried farther downstream. Similar results have been reported widely in literature such as references [4, 5, 7, 11, 27, and 28]. The effect of blowing ratio on the suction surface is within the measurement uncertainty of the experiment, but the surface heat transfer distributions with film cooling follow a trend similar to the uncooled case. In all three cases, heat transfer peaks downstream of injection and then decreases rapidly until $s/C = 0.34$ on the suction surface; following this decrease, heat transfer remains low until transition occurs at s/C of 0.45. Previous experiments at high freestream turbulence by Nasir *et al.* [13] have shown that this decrease in heat transfer could be due to a disturbed boundary layer tending towards relaminarization due to high flow acceleration ($k > 3 \times 10^{-6}$) in the presence of a favorable pressure gradient. This effect of acceleration on heat transfer distribution was also noted by Turner *et al.* [4] for showerhead cooling. Transition location at s/C of 0.45 is unaffected by increasing blowing ratio. Downstream of the throat, the uncooled case shows higher heat transfer than the film-cooled cases. This is likely due to the diminished effect of injection after transition and a thinner boundary layer for the uncooled case.

At an exit Mach number of 1.00, cooling continues to augment heat transfer downstream of injection on both surfaces. On the pressure side, increasing blowing ratio causes an increase in augmentation. Additionally, jet lift-off on the pressure side can be seen for both blowing ratios. Lift-off is indicated by low heat transfer augmentation downstream of injection that increases once the jet reattaches or moves close enough to the surface to interact with the boundary layer. A blowing ratio of 2.0 shows jet interaction with the boundary layer by $s/C = -0.20$, but the lower blowing ratio shows a gradual increase in boundary layer disturbance. In addition to the influence of increased mass flow at the higher blowing ratio, curvature could have

some effect on this phenomenon. Bogard and Thole [2] have stated that high momentum jets tend to stick better to concave surfaces than low momentum jets due to the pressure gradient normal to the curved surface. This would cause increased boundary layer disturbance and consequently increased heat transfer for the higher blowing ratio. On the suction side, the effect of blowing ratio is apparent in Figure 12; increasing blowing ratio from 1.5 to 2.0 shows a drastic increase in augmentation over the entire surface. The boundary layer is again heavily influenced by high acceleration between s/C of 0.23 and 0.34. It should be noted that three gauges between s/C of 0.62 and 0.73 have been removed from the exit Mach 1.00 results because they showed the possibility of a shockwave interaction with the turbulent boundary layer. The linear regression technique showed a high level of unsteadiness in the flow due to this interaction, resulting in high uncertainty in heat transfer coefficient and effectiveness for these gauges.

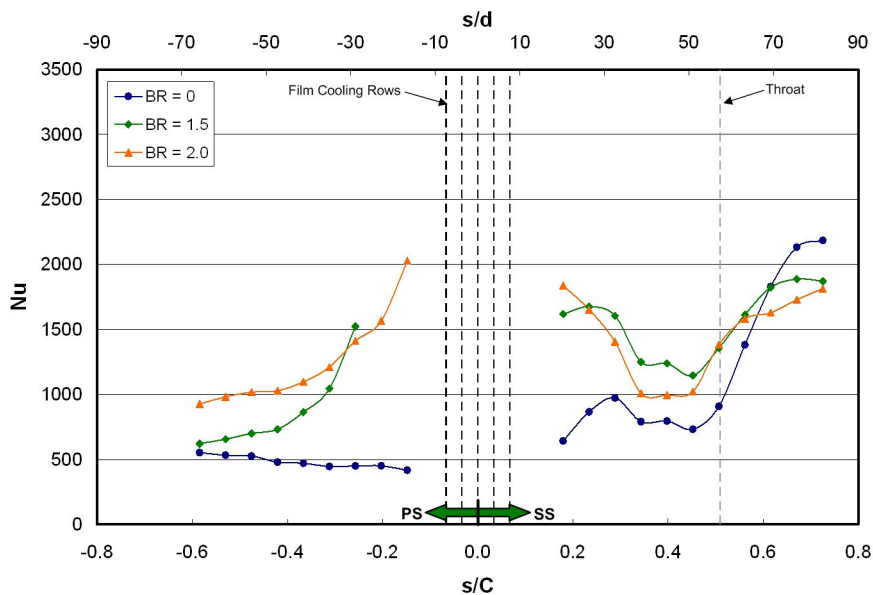


Figure 11. Effect of BR on Nu at $M_{ex} = 0.76$

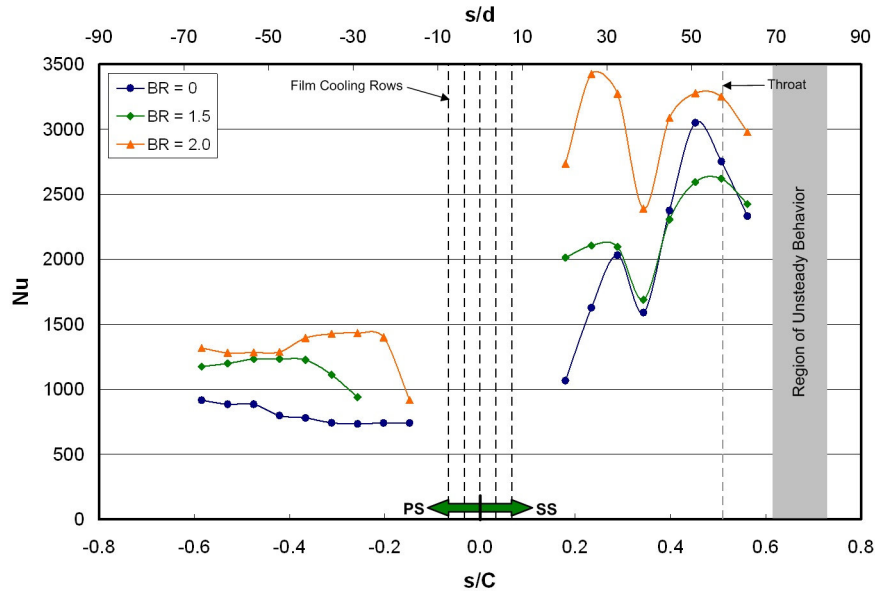


Figure 12. Effect of BR on Nu at $M_{ex} = 1.0$

Effect of Blowing Ratio on Film Cooling Effectiveness

Another important effect of coolant injection was reduction of adiabatic wall temperature downstream of injection on both vane surfaces. As described earlier, the adiabatic wall temperature was measured in terms of adiabatic film cooling effectiveness, η . The effect of blowing ratio on film cooling effectiveness at exit Mach 0.76 and 1.00 is shown in Figure 13 and Figure 14, respectively. Results are plotted against nondimensional surface distance (s/C and s/d). For reasons mentioned previously, results for two gauges near injection on the pressure side of the vane have been removed again for a blowing ratio of 1.5 at both Mach numbers.

At exit Mach 0.76, effectiveness is highest near injection and decays downstream on both surfaces. On the pressure surface, a blowing ratio of 1.5 shows relatively quick decay with effectiveness going to zero by s/C of -0.53. Increasing blowing ratio causes an increase in effectiveness, and the effect of the higher blowing ratio again carries farther downstream. On the suction surface, the effect of blowing ratio is within the measurement uncertainty of the experiment; however, the decay of effectiveness is affected by the acceleration between s/C of 0.23 and 0.34 mentioned earlier. Effectiveness becomes zero after the throat. Although some gauges indicate negative effectiveness far downstream on both surfaces, the levels are within our uncertainty.

Effectiveness decays downstream of injection at exit Mach 1.00 as well. On the pressure surface, increasing blowing ratio causes an increase in effectiveness. Evidence of lift-off is seen again for both blowing ratios. The higher blowing ratio shows a peak in effectiveness at s/C of -0.20 where the film returns to the surface, and the lower blowing ratio shows almost no effectiveness—possibly indicating that the film never fully returns to the surface. On the suction surface, increasing blowing ratio from 1.5 to 2.0 causes a significant increase in effectiveness. The lower blowing ratio is seen to have zero effectiveness by s/C of 0.29, but a blowing ratio of 2.0 shows film coverage over the entire surface. The influence of acceleration is also seen again between s/C of 0.29 to 0.40. It appears that effectiveness becomes negative at s/C of 0.40 for the lower blowing ratio, but this is within the experimental uncertainty. Effectiveness also appears to increase downstream of s/C of 0.45 for both blowing ratios, but no coolant is expected to be present on the surface this far downstream.

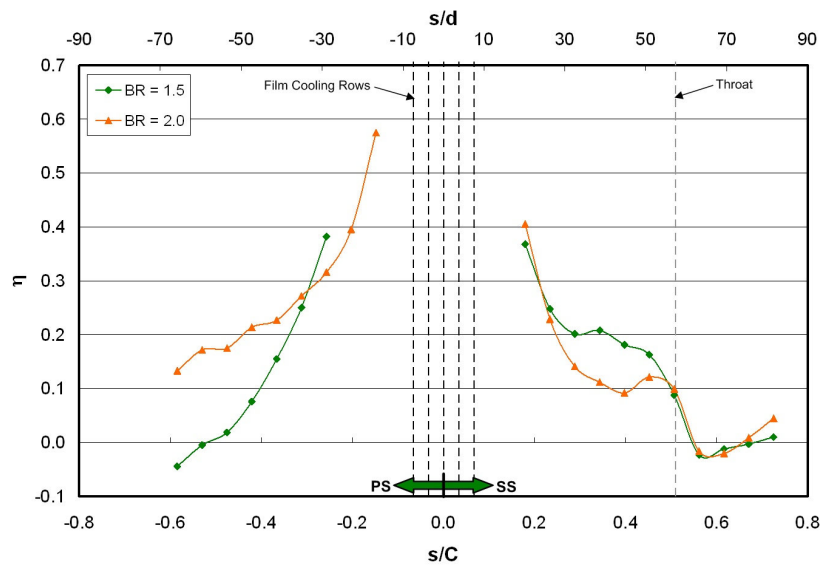


Figure 13. Effect of BR on η at $M_{ex} = 0.76$

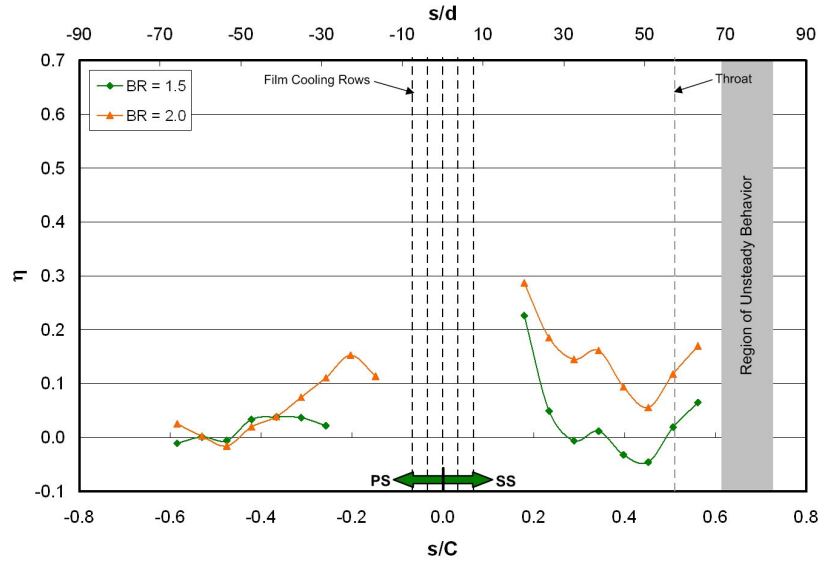


Figure 14. Effect of BR on η at $M_{ex} = 1.00$

Effect of Reynolds Number/Mach Number on Heat Transfer Coefficient

As mentioned previously, exit Mach number and exit Reynolds number are coupled in the Virginia Tech transonic cascade, so an increase in exit Mach number corresponds to an increase in exit Reynolds number. Exit Mach numbers of 0.76 and 1.00 correspond to Reynolds numbers of 1.1×10^6 and 1.5×10^6 , respectively. For consistency with previous discussion, data in the following sections are plotted by referencing the Mach number for the appropriate exit Mach number and exit Reynolds number condition.

Film cooling performance was affected by changing exit Reynolds number and Mach number conditions. Nusselt number distributions showing the effect of increasing Reynolds/Mach number at blowing ratios of 1.5 and 2.0 are shown in Figure 15 and Figure 16, respectively. In general, an increase in heat transfer was seen over both vane surfaces; this effect can be attributed to a decrease in boundary layer thickness over the surface and change in boundary layer state at some locations due to the increase in Reynolds number.

The pressure surface exhibits an increase in heat transfer with increasing Reynolds number and Mach number for both blowing ratios—excluding the area affected by lift-off at the higher Reynolds/Mach number case. The suction surface shows an increase in heat transfer with increasing Reynolds number and Mach number for both blowing ratios as well. This increase in heat transfer is again due to a thinner boundary layer caused by the increase in Reynolds number. This effect of increasing Reynolds number has been observed by many including Turner [4] and

Arts [5]. The higher Reynolds/Mach number case appears to produce a fully turbulent boundary layer on the suction surface for both blowing ratios. This boundary layer is heavily influenced by the favorable pressure gradient between s/C of 0.23 and 0.34.

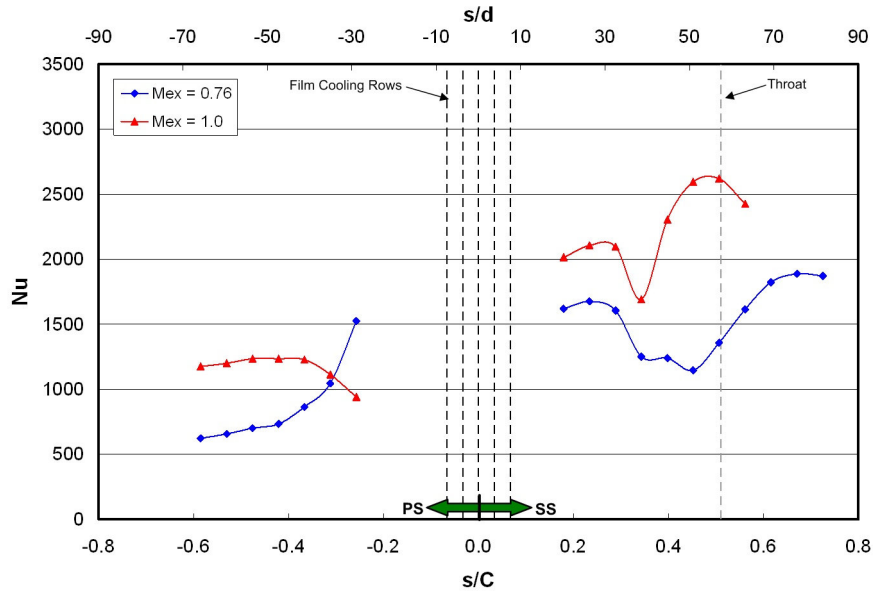


Figure 15. Effect of Reynolds Number/Mach Number on Nu at BR = 1.5

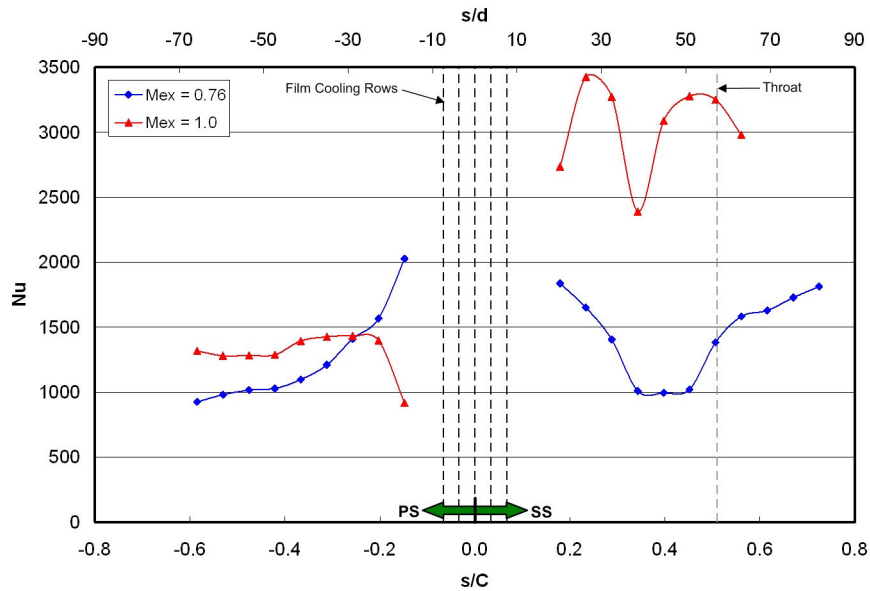


Figure 16. Effect of Reynolds Number/Mach Number on Nu at BR = 2.0

Effect of Reynolds Number/Mach Number on Film Cooling Effectiveness

Increasing Reynolds number and Mach number also influenced film cooling effectiveness. Drost and Bölc's [7] have shown that simultaneously increasing Reynolds number

and Mach number can affect film cooling effectiveness; they reasoned that the change in effectiveness was a result of changing flow acceleration and boundary layer thickness as functions of increasing Reynolds number. Effectiveness distributions showing the effect of increasing Reynolds/Mach number at blowing ratios of 1.5 and 2.0 are shown in Figure 17 and Figure 18, respectively.

On the pressure surface, effectiveness levels are drastically higher for both blowing ratios at an exit Mach number of 1.00 and Reynolds number of 1.5×10^6 than at the lower Reynolds/Mach number case. A thinner boundary layer present at the higher Reynolds number makes it difficult for the coolant to interact with the boundary layer, increasing jet dissipation into the freestream. This effect was seen by Reiss and Bölcş [27] as well. Jet lift-off at this condition only compounds the problem.

On the suction surface, a blowing ratio of 1.5 shows a decrease in effectiveness for increasing Reynolds number and Mach number. At a Mach number of 0.76 and a Reynolds number of 1.1×10^6 , effectiveness extends to the throat, but at the higher Reynolds number, effectiveness is gone by s/C of 0.29. This can also be attributed to less jet interaction with and penetration into the thinned boundary layer at a higher Reynolds number. A blowing ratio of 2.0 shows similar values of effectiveness at both Reynolds/Mach number conditions.

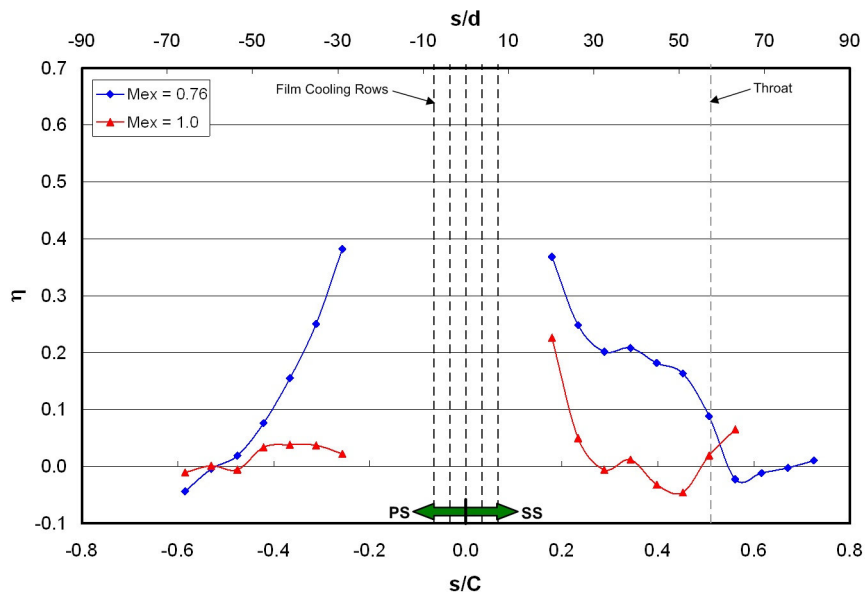


Figure 17. Effect of Reynolds Number/Mach Number on η at BR = 1.5

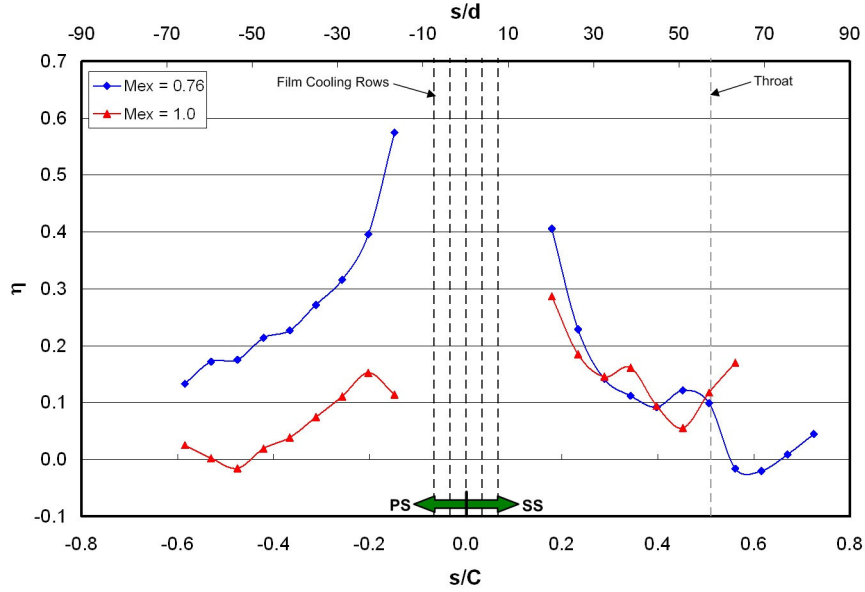


Figure 18. Effect of Reynolds Number/Mach Number on η at BR = 2.0

Effect of Turbulence on Heat Transfer Coefficient

As mentioned previously, the purpose of this experiment was to generate a low freestream turbulence data set that could assist in the development of a CFD model and that would compliment measurements already performed by Nasir *et al.* [13] with large-scale, high freestream turbulence ($Tu = 16\%$, $A_x/P = 0.23$). This section discusses the effects of freestream turbulence on heat transfer at the design exit Mach number of 0.76 without cooling and with a design blowing ratio of 2.0.

The effect of large-scale, high freestream turbulence on Nusselt number distribution for a smooth, uncooled vane has already been studied by Nasir *et al.* [12]; however, the baseline results presented earlier showed that cooling holes can significantly alter the Nusselt number distribution downstream. The effect of turbulence on a vane with film cooling holes but without coolant injection (BR = 0) is shown in Figure 19. The results confirm the findings of Nasir *et al.* [12]. Turbulence augments heat transfer over the entire pressure surface and over the suction surface until the boundary layer becomes fully turbulent. Additionally, the transition location moves slightly upstream for the high turbulence case.

The effect of freestream turbulence on heat transfer coefficient with film cooling can be seen in Figure 20 for an exit Mach number of 0.76 and a blowing ratio of 2.0. On the pressure surface of the vane, the low turbulence case shows higher Nusselt number downstream of injection than the sixteen percent freestream turbulence case, but the difference between the two

cases becomes minimal by s/C of -0.42 . The large scale high freestream turbulence is believed to reduce jet strength and actually reduce local turbulence by breaking up the jet's vortex pair; however, the jet retains its strength at low freestream turbulence. This results in an increase in Nusselt number for the low freestream turbulence case. On the suction surface, the low freestream turbulence case again shows higher Nusselt number downstream of injection again. However, both cases show similar levels from s/C of 0.23 to 0.34 where acceleration has a large influence on reducing heat transfer by forcing the boundary layer towards relaminarization. After s/C of 0.34 , the high turbulence case shows higher heat transfer coefficient than the low turbulence case due to earlier transition.

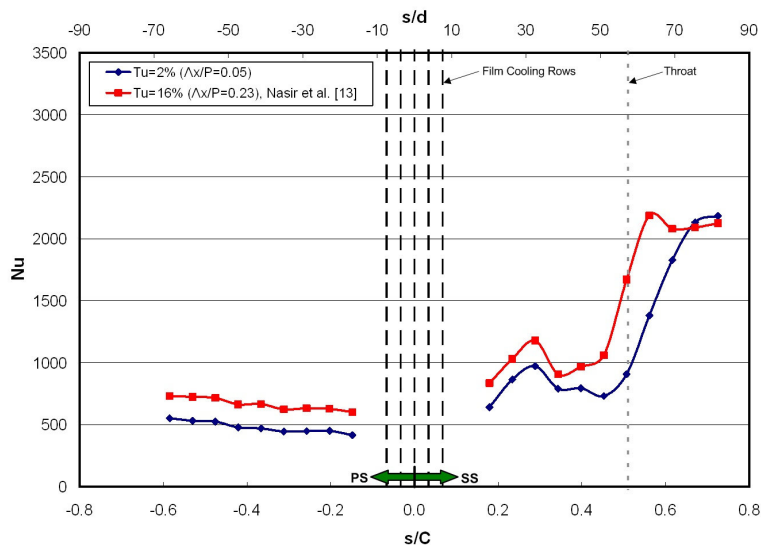


Figure 19. Effect of Tu on Nu for $M_{ex} = 0.76$, $BR = 0$

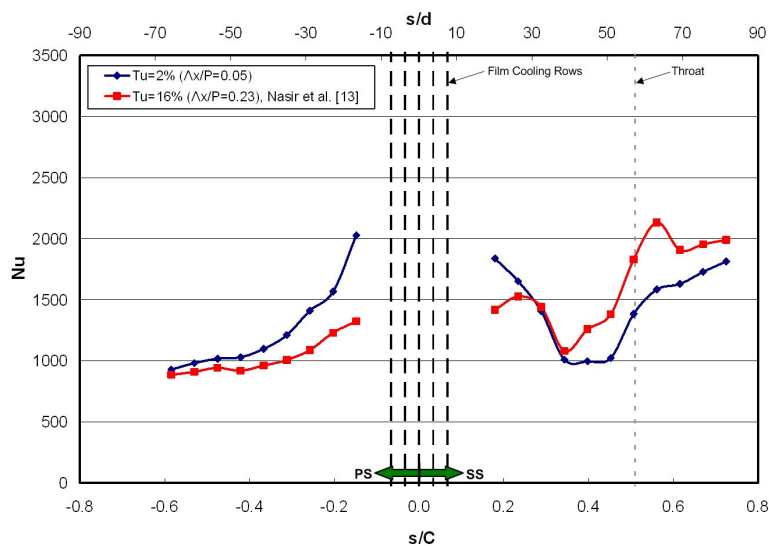


Figure 20. Effect of Tu on Nu for $M_{ex} = 0.76$, $BR = 2.0$

Effect of Turbulence on Film Cooling Effectiveness

High freestream turbulence has been shown to significantly reduce film cooling effectiveness downstream of injection by many studies such as those of Ames [11], Polanka *et al.* [29], and Ekkad *et al.* [30]. Increasing freestream turbulence serves to enhance mixing, resulting in increased coolant dissipation into the freestream. Figure 21 presents the effect of freestream turbulence on film cooling effectiveness for a design exit Mach number of 0.76 and a design blowing ratio of 2.0 by comparing results from this experiment with those of Nasir *et al.* [13]. On the pressure surface, it appears that high freestream turbulence reduces film cooling effectiveness, but the difference is within the measurement uncertainty. On the suction side, the effect of turbulence is indistinguishable and within our uncertainty as well.

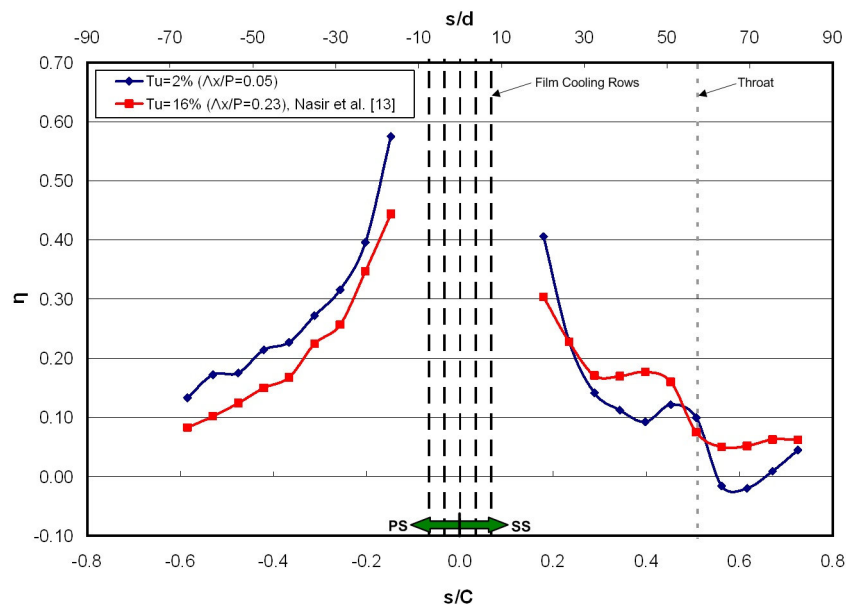


Figure 21. Effect of Tu on η for $M_{ex} = 0.76$, $BR = 2.0$

CONCLUSIONS

Showerhead film cooling performance in a transonic vane cascade was experimentally measured at low freestream turbulence. Two exit Mach numbers of 0.76 and 1.00—corresponding to exit Reynolds numbers based on vane chord of 1.1×10^6 and 1.5×10^6 , respectively—were tested with an inlet freestream turbulence intensity of two percent and an integral length scale normalized by vane pitch (Λ/P) of 0.05. A showerhead cooling scheme with five rows of cooling holes was tested with blowing ratios of 0 (no cooling), 1.5 and 2.0 with

a density ratio around 1.35. Midspan Nusselt number and adiabatic film cooling effectiveness distributions over the vane surface were presented demonstrating the effects of blowing ratio, Reynolds/Mach number, and freestream turbulence on film cooling performance.

The purpose of this investigation was to produce an experimental data set for film cooling performance at low freestream turbulence to be used in the validation of a computational model and to compliment measurements performed with more engine-realistic, high freestream turbulence by Nasir *et al.* [13]. Measurements exhibited an increase in run-to-run variation when compared to the tests performed by Nasir *et al.* [13] at sixteen percent freestream turbulence. This increase in variation has been attributed to characteristics of the flowfield at low freestream turbulence. Run-to-run variation adversely impacted uncertainty; however, important conclusions regarding the effects of blowing ratio, Reynolds/Mach number, and freestream turbulence can still be drawn.

One of the primary effects of coolant injection was increasing Nusselt number on the vane surface over the uncooled case ($BR = 0$). In general, increasing blowing ratio from 1.5 to 2.0 caused an increase in heat transfer augmentation over the vane surface. Coolant injection also served to reduce the adiabatic wall temperature on the vane surface downstream of injection when compared to the uncooled case ($BR = 0$). Increasing blowing ratio from 1.5 to 2.0 generally showed an increase in film cooling effectiveness over the vane surface.

Increasing Reynolds number and Mach number caused an increase in heat transfer on the vane surface for all blowing ratios tested due to a decrease in boundary layer thickness with an increase in Reynolds number. Film cooling effectiveness generally decreased with increasing Reynolds number and Mach number because the decrease in boundary layer thickness inhibited coolant interaction with boundary layer.

Measurements were compared to large-scale high freestream turbulence measurements by Nasir *et al.* [13]. For an exit Mach number of 0.76 and a blowing ratio of 2.0, the low freestream turbulence case showed higher heat transfer coefficient just downstream of injection on the pressure and suction surfaces of the vane. However, the high turbulence case showed greater heat transfer coefficient farther downstream due to earlier boundary layer transition.

Although the results of this study are not directly applicable to gas turbine engine design, this experiment has demonstrated that the flow physics on a showerhead-film-cooled airfoil at high speed and low freestream turbulence are no less complicated than at high freestream

turbulence. Using the current measurement technique, it can be more difficult to accurately measure film cooling performance at low freestream turbulence than at an engine-representative turbulence level. The results of this experiment emphasize the need to continue to develop measurement techniques which can provide three-dimensional as well as time-resolved information in order to further the understanding of film cooling physics.

Acknowledgements

This work was sponsored by Solar Turbines Incorporated. We would like to express our gratitude towards Drs. Richard Anthony and Marcus Polanka from the Air Force Research Laboratory at Wright-Patterson AFB for their help with the manufacturing and use of the thin-film gauges. We would also like to thank Ashley Guy, Colin Reagle, and Bill Songer for their valuable assistance in setting up this experiment.

REFERENCES

- [1] Goldstein, R.J., 1971, "Film Cooling," *Advances in Heat Transfer*, 7, pp. 321-380.
- [2] Bogard, D.G., and Thole, K.A., 2006, "Gas Turbine Film Cooling," *ASME J. Propulsion and Power*, 22, pp. 249-270.
- [3] Han, J.-C., Dutta, S., and Ekkad, S.V., 2000, *Gas Turbine Heat Transfer and Cooling Technology*, Taylor & Francis, New York.
- [4] Turner, E.R., Wilson, M.D., Hylton, L.D., and Kaufman, R.M., 1985, "Turbine Vane External Heat Transfer: Vol. 1: Analytical and Experimental Evaluation of Surface Heat Transfer Distributions with Leading Edge Showerhead Film Cooling," NASA CR-174827.
- [5] Arts, T., and Bourguignon, A.E., 1990, "Behavior of a Coolant Film with Two rows of Holes along the Pressure Side of a High Pressure Nozzle Guide Vane," *ASME J. Turbomach.*, 112, pp. 512-520.
- [6] Abuaf, N., Bunker, R., and Lee, C.P., 1997, "Heat Transfer and Film Cooling Effectiveness in a Linear Airfoil Cascade," *ASME J. Turbomach.*, 119, pp. 302-309.
- [7] Drost, U., and Bölcs, A., 1999, "Investigation of Detailed Film Cooling Effectiveness and Heat Transfer Distribution on a Gas Turbine Airfoil," *ASME J. Turbomach.*, 121, 1999, pp. 233-242.
- [8] Guo, S.M., Lai, C.C., Jones, T.V., Oldfield, M.L.G., Lock, G.D., and Rawlinson, A.J., 1998, "The Application of Thin-film Technology to Measure Turbine-Vane Heat Transfer and Effectiveness in a Film-Cooled, Engine-Simulated Environment," *Intl. J. Heat and Fluid Flow*, 19, pp. 594-600.
- [9] Zhang, L. J., Baltz, M., Pudupatty, R., and Fox, M., 1999, "Turbine Nozzle Film Cooling Study Using the Pressure Sensitive Paint (PSP) Technique," ASME GT-1999-196.
- [10] Reiss, H., and Bölcs, A., 2000, "The Influence of the Boundary Layer State and Reynolds Number on Film Cooling and Heat Transfer on a Cooled Nozzle Guide Vane," ASME GT-2000-205.
- [11] Ames, F.E., 1996, "Experimental Study of Vane Heat Transfer and Film Cooling at Elevated Levels of Turbulence," NASA CR-198525.
- [12] Nasir, S., Carullo, J.S., Ng, W.F., Thole, K.A., Wu, H., Zhang, L.J., and Moon, H.K., 2007, "Effects of Large Scale High Freestream Turbulence, and Exit Reynolds Number on Turbine Vane Heat Transfer in a Transonic Cascade," ASME IMECE-2007-44098.

- [13] Nasir, S., Bolchoz, T., Ng, W.F., Zhang, L.J., Moon, H.K., and Anthony, R.J., 2008, "Showerhead Film Cooling Performance of a Turbine Vane in a Transonic Cascade," ASME IMECE-2008-66528.
- [14] Carullo, J.S., Nasir, S., Cress, R.D., Ng, W.F., Thole, K.A., Zhang, L.J., and Moon, H.K., 2007, "The Effects of Freestream Turbulence, Turbulence Length Scale, and Exit Reynolds Number on Turbine Blade Heat Transfer in a Transonic Cascade," ASME GT-2007-27859.
- [15] Nix, A.C., Diller, T.E., and Ng, W.F., 2007, "Experimental Measurements and Modeling of the Effects of Large-Scale Freestream Turbulence on Heat Transfer," *ASME J. Turbomach.*, **129**, pp. 542-550.
- [16] Holmberg, D.G., and Diller, T.E., 2005, "Simultaneous Heat Flux and Velocity Measurements in a Transonic Turbine Cascade," *ASME J. Turbomach.*, **127**, pp. 502-506.
- [17] Smith, D.E., Bubb, J.V., Popp, O., Grabowski, H.C., Diller, T.E. Schetz, J.A. and Ng, W.F., 2000, "An Investigation of Heat Transfer in a Film Cooled Transonic Turbine Cascade, Part I: Steady Heat Transfer," ASME GT-2000-202.
- [18] Popp, O., Smith, D.E., Bubb, J.V., Grabowski, H.C., Diller, T.E. Schetz, J.A. and Ng, W.F., 2000, "An Investigation of Heat Transfer in a Film Cooled Transonic Turbine Cascade, Part II: Unsteady Heat Transfer," ASME GT-2000-203.
- [19] Colban, W., Gratton, A., and Thole, K.A., 2006, "Heat Transfer and Film-Cooling Measurements on a Stator Vane with Fan-Shaped Cooling Holes," *ASME J. Turbomach.*, **128**, pp. 53-61.
- [20] Doorly, J.E., and Oldfield, M.L.G., 1987, "The Theory of Advanced Multi-Layer Thin Film Heat Transfer Gages," *Intl. J. Heat and Mass Transfer*, 30, pp. 1159-1168.
- [21] Joe, C.R., 1997, "Unsteady Heat Transfer on the Turbine Research Facility at Wright Laboratory," Ph.D. Dissertation, Syracuse University.
- [22] Cress, R.D., 2006, "Turbine Blade Heat Transfer Measurements in a Transonic Flow Using Thin film Gages," Master's Thesis, Virginia Polytechnic Institute and State University.
- [23] Moffat, R. J., 1988, "Describing Uncertainties in Experimental Results," *Exp. Thermal and Fluid Science*, 1, pp. 3-17.
- [24] Brown, K.H., Coleman, H.W., and Steele, W.G., 1995, "Estimating Uncertainty Intervals for Linear Regression," AIAA-1995-0796.

- [25] Jones, W.P., and Launder, B. E., 1972, "The Prediction of Laminarization with a Two-Equation Model of Turbulence," *Intl. J. Heat and Mass Transfer*, 15, pp. 301-314.
- [26] Mayle, R.E., 1991, "The Role of Laminar-Turbulent Transition in Gas Turbine Engines," *ASME J. Turbomach.*, 113, pp. 509-537.
- [27] Reiss, H., and Bölcs, A., 2000, "Experimental Study of Showerhead Cooling on a Cylinder Comparing Several Configurations Using Cylindrical and Shaped Holes," *ASME J. Turbomach.*, 122, 2000, pp. 161-169.
- [28] Ou, S., Han, J.-C., Mehendale, A.B., and Lee, C.P., 1994, "Unsteady Wake Over a Linear Turbine Blade Cascade with Air and CO₂ Film Injection: Part I—Effect on Heat Transfer Coefficients," *ASME J. Turbomach.*, **116**, pp. 721-729.
- [29] Polanka, M.D., Witteveld, V.C., and Bogard, D.G., 1999, "Film Cooling Effectiveness in the Showerhead Region of a Gas Turbine Vane Part I: Stagnation Region and Near-Pressure Side," ASME GT-1999-048
- [30] Ekkad, S.V., Mehendale, A.B., Han, J.C., and Lee, C.P., 1997, "Combined Effect of Grid Turbulence and Unsteady Wake on Film Effectiveness and Heat Transfer Coefficient of a Gas Turbine Blade with Air and CO₂ Film Injection," *ASME J. Turbomach.*, 119, pp.594-600.

APPENDIX A: FILM COOLING SYSTEM

This appendix describes the film cooling system used in the film-cooled vane experiments. An overview of the system will be given, followed by details regarding plumbing and instrumentation, and ending with a description of the operation of the system.

Film Cooling System Overview

The film cooling system used in this experiment was an adaptation of the system used by Smith et al. [17]. A diagram of the setup can be seen in Figure A1. The coolant system is a blow-down configuration similar to the tunnel air supply. A large storage tank located in the lab is pressurized by a five horsepower Ingersoll-Rand compressor. The air is filtered and dried below four percent relative humidity before entering the storage tank. For film cooling experiments, the tank is charged to 120 psi to provide adequate mass flow for the test. The volume of the tank is large enough that there is minimal blow-down effect during a run.

Coolant flow rate is controlled by a ball valve and measured by an orifice plate located just downstream of the tank. After passing through the orifice plate, the coolant flows through a copper coil immersed in a water bath. The water bath serves to heat the air to the initial temperature of the vane, reducing internal conduction within the airfoil during the run. Once heated, the air flows into the vane plenum via a fitting designed to pass air through the test section window. Coolant proceeds through the plenum and is ejected through the showerhead film cooling holes.

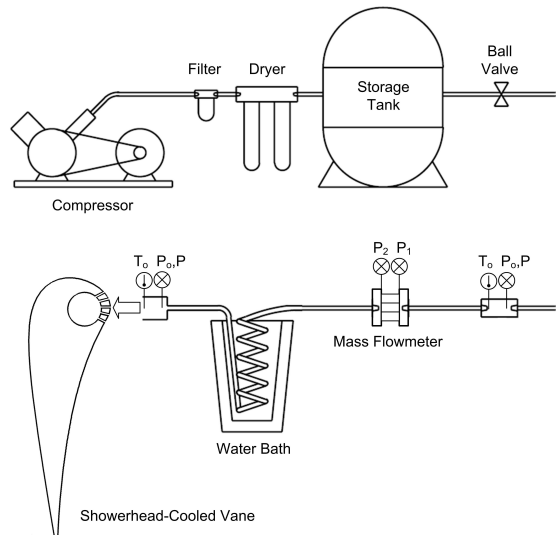


Figure A1. Film Cooling System

Film Cooling System Plumbing

The film cooling system is plumbed to provide adequate mass flow for a five-row showerhead-cooled vane. The system can be divided into two parts: compression/storage and coolant delivery.

Compression and Storage. The compression and storage components include the compressor, the storage tank, filter, dryer, and any components used to connect or seal these. The compressor itself is an Ingersoll-Rand 2475N5 two-stage, reciprocating compressor housed in a storage shed outside of the lab. It supplies 16.8 ACFM at a maximum pressure of 175 psi. Immediately downstream of the compressor is a filter and Ingersoll-Rand HRM regenerative dryer that keeps relative humidity below four percent. Following the dryer, air travels into the lab and is stored in a large tank. All connections between the compressor and storage tank are made with brass compression fittings on 0.5” copper tubing.

The storage tank has several available inlet/outlet ports which vary in size. The two largest ports are four-inch diameter pipes. For this experiment, one of these ports is sealed with a blank flange, and the other is sealed with a flange tapped for a one-inch NPT connection from which coolant is extracted. Both flanges are sealed to the tank using appropriately rated fiberglass gaskets. Two smaller ports exist on the tank. One is plugged with a pressure gauge so that tank pressure can be monitored, and the other is connected to the compressor via tubing from the dryer.

The entire compression and storage system is rated for use at or below 125 psi. All of the components have individual maximum pressure ratings of 150 psi or more, but a lower limit has been set for added safety.

Coolant Delivery. Coolant is extracted from the storage tank via a 1” NPT connection tapped in the tank’s lower flange. Flow rate from the tank is controlled by a 0.5” ball valve connected to the tank by this NPT port. Air passes through the ball valve and travels through 0.5” high-pressure polyethylene tubing to a work bench supporting instrumentation and a water bath—pictured in Figure A2. Coolant first travels through a set of tees which house a Pitot-static probe and a T-type thermocouple; these are used to determine the density of the coolant just before passing through the orifice meter. The Lambda Square orifice meter houses upstream and downstream static pressure taps to determine pressure drop across the calibrated orifice. Pitot-

static probe pressures and orifice meter differential pressure are measured using MKS Baratron 223B pressure transducers.

After the flowmeter, air travels through a copper coil immersed in a water bath. The temperature of this water bath is monitored with a T-type thermocouple and adjusted according to the temperature of the vane before a run so that the coolant temperature and initial vane temperature match to within $\sim 1^\circ\text{C}$. This helps reduce internal conduction around the plenum and showerhead holes.

Once heated to the appropriate temperature, coolant travels through tubing and is passed through the test section window via a fitting that threads through the Lexan window and forms a face seal around the circular plenum. This fitting, pictured in Figure A3, contains another Pitot-static probe to monitor plenum pressure. The pressures from this probe are measured by the PSI 8400 system. Additionally, an identical fitting is threaded through the aluminum window and used to insert a T-type thermocouple near the midspan of the blade to measure coolant temperature. Because of Macor's low thermal conductivity, it was assumed that the temperature of the coolant exiting the holes was the same temperature as the air inside the plenum.

All connections for coolant delivery to the vane are made using 0.5" brass Swagelok compression fittings on either 0.5" polyethylene or copper tubing. Swagelok-to-NPT adapters are used where necessary. All tubing and fittings are rated to 150 psi or higher; however, the tubing connecting the MKS pressure transducers is not. For this reason, the maximum pressure in the line should not exceed 30 psi.

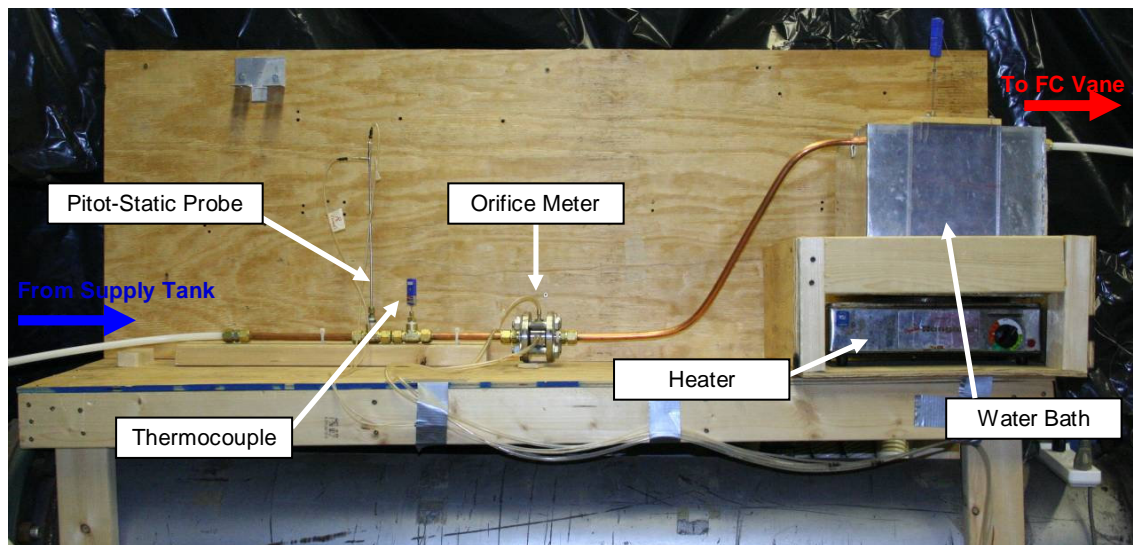


Figure A2. Photograph of Film Cooling System

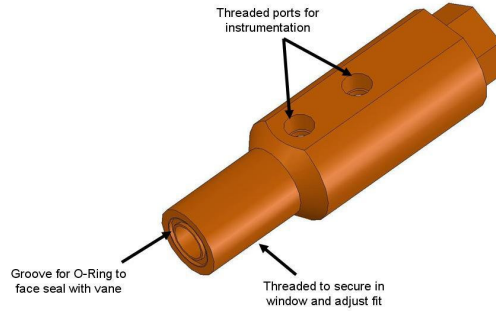


Figure A3. Coolant Supply Fitting

Film Cooling System Operation

Operation of the film cooling system is fairly simple. Prior to a run, the storage tank is charged to 120 psi. Once pressurized, the compressor and dryer are turned off. When the tunnel is ready to run, an operator will slowly open the ball valve on the film cooling tank, allowing air to flow through the system. Using the digital multimeter to display the total pressure at the plenum inlet measured by the MKS, the operator sets the pressure to a value previously found to provide the correct blowing ratio for those conditions. Once this pressure is set, operators may leave the room and run the tunnel. It has been found that a control scheme for the coolant is not required because the external pressure imposed by the freestream flow is enough to cause the coolant pressure to follow a similar trend. After performing a few runs to find the correct pressure setting, blowing ratios can be repeated reasonably well from run to run.

During the run, pressure and temperature data are recorded by the NI DAQ and the PSI 8400 systems. Using a MATLAB code, data is reduced on the spot to check exit Mach number, blowing ratio, and density ratio. Blowing ratio for film cooling is determined by Equation 1. Mass flow of the coolant is measured by orifice plate using the following relation:

$$\dot{m}_c = C_d A_{op} \sqrt{2\rho\Delta P} \quad (A1)$$

where C_d is the discharge coefficient of 0.62, A_{op} is the area of the orifice plate ($3.95 \times 10^{-5} \text{ m}^2$), ρ is the density of air, and ΔP is the pressure drop across the plate. The Pitot-static probe and T-type thermocouple upstream of the orifice plate provide the temperature and pressure needed to calculate the density of the air traveling through the orifice plate.

Below, Figure A4 shows an example of blowing ratio and density ratio history for a tunnel run with an exit mach number of 0.76, a blowing ratio of 2.0, and a density ratio of 1.4

during the data reduction period illustrated by dashed red lines. Although blowing ratio is not steady during the run, variation is small during the data reduction period.

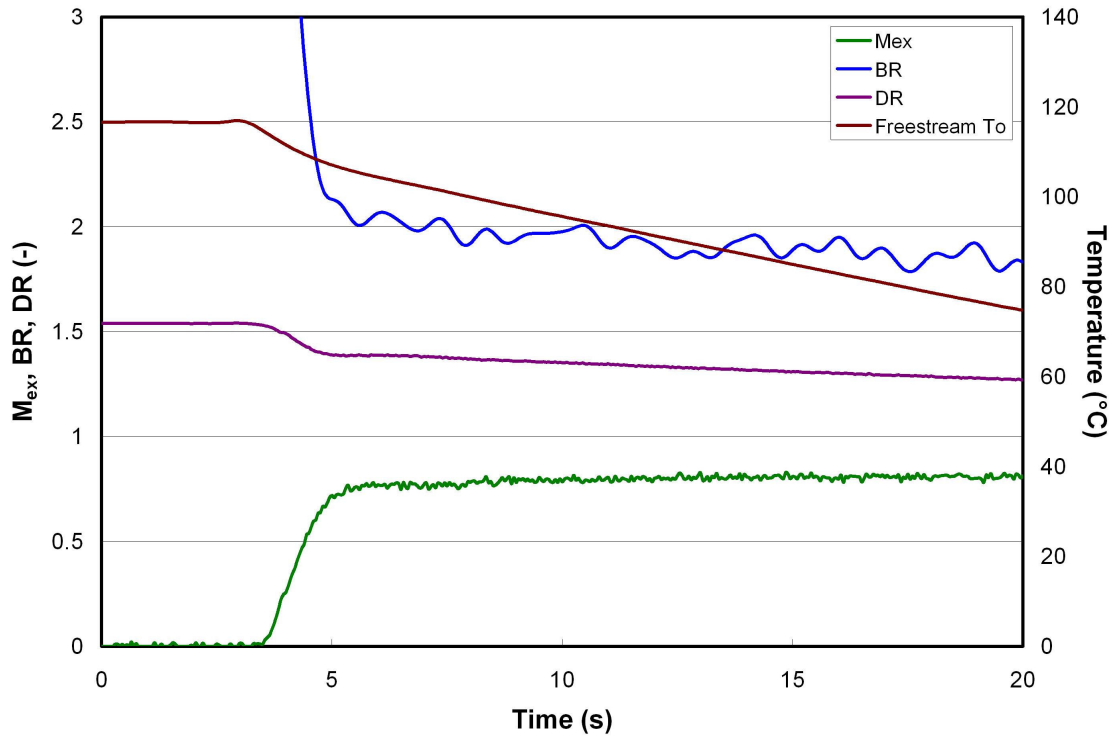


Figure A4. Time History of Mex=0.76, BR=2.0 Tunnel Run

APPENDIX B: GAUGE INSTALLATION

This appendix discusses the mounting, soldering, and installation of the platinum thin-film gauges used in this experiment as well as the installation of several thermocouples onto the vane.

TFG Mounting

The platinum thin film gauges (TFGs) used in film cooling experiments were manufactured by Air Force Research Laboratories. The gauges are the same type used by Carullo et al. [14] and Nasir et al. [11]. Each thin film gauge uses a platinum sensor approximately 3.18 mm (0.125 in.) long attached to copper leads. The platinum sensor changes resistance with temperature and gives a fast response measurement with high spatial resolution between gauges. Twenty-five gauges are sputtered onto a Kapton sheet ($k = 0.12 \text{ W/m}^2\text{K}$) with a 50 μm thickness. Each sheet of gauges is given an adhesive backing approximately 20 μm in thickness.

Before mounting the gauges, the gauge sheet was cut to the appropriate size, and the Macor airfoil was thoroughly cleaned. The gauges were aligned with the midspan of the airfoil and the cooling hole rows, and then the sheet was carefully adhered to the pressure and suction surfaces. Air bubbles were eliminated beneath the sheet by using a soft paper towel to apply the sheet from the stagnation region toward the trailing edge.

After the sheet was applied, an X-acto knife was used to scrape away the copper leads and platinum sensors of four gauges that were covering the cooling hole rows. Once the gauges covering holes were removed, a hot soldering iron with a fine tip was used to pierce a hole in the Kapton at each hole location. Using a soldering iron to create holes prevented the Kapton sheet from tearing. Once the holes were made, excess Kapton was removed from the holes by hand using a pin-vise-mounted drill bit with a diameter equivalent to the cooling hole diameter. Each cooling hole was visually inspected to ensure uniformity between holes and eliminate the possibility of hole blockage. Figure B1 shows the location of each gauge on the vane, and nondimensional surface distance locations can be found in Appendix F. Figure B3 shows the gauge sheet mounted on the film-cooled vane.

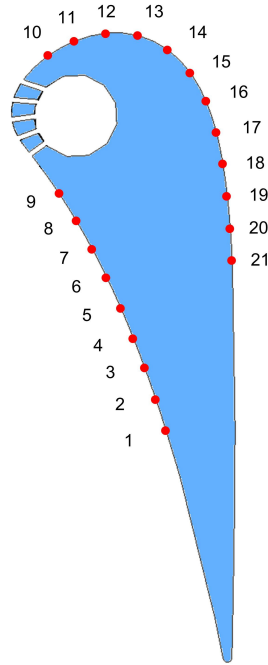


Figure B1. Platinum Thin-film Gauge Locations

Thermocouple Mounting

In addition to the thin film gauges, ten T-type thermocouples were installed on the film-cooled vane. The purpose of these thermocouples was to measure temperature uniformity between runs and to monitor the initial core temperature of the Macor airfoil before and during a run. Figure B2 shows the streamwise thermocouple locations.

Eight T-type foil thermocouples manufactured by RDF were placed on the surface of the vane opposite the TFGs. To attach the thermocouples (TCs), an adhesive-backed strip of Kapton was placed on a table with the adhesive side facing upwards. The foil TCs were placed on the strip of Kapton aligning the sensors in the spanwise direction with one inch of space between each TC and the leads oriented in the spanwise direction. The strip of Kapton was then adhered to the Macor surface with the first TC located one inch from the trailing edge on the suction surface. Figure B3 shows the thermocouples mounted on the film-cooled vane.

Two miniature T-type thermocouples manufactured by Omega were placed in small holes drilled 1.5 inches deep from the endwall opposite the TFGs. The thermocouples were placed in the holes with the lead wires running out, and then a high-thermal-conductivity epoxy manufactured by Omega was used to fill the holes and secure the thermocouples in place.

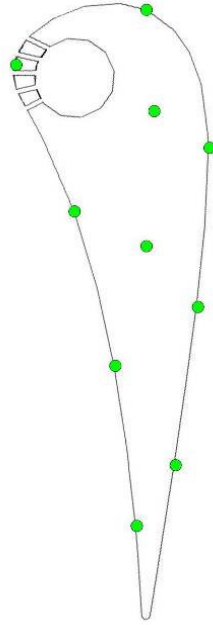


Figure B2. Thermocouple Locations

Lead Wire Attachment

After mounting the TFGs and TCs to the vane surface and drilling holes in the Kapton for the film cooling holes, the TFG lead wires were soldered onto the TFG leads. They were soldered following the same procedure as Carullo [31], except the soldering iron was set at a lower temperature (420°C rather than 575°C). The gauges used in this experiment appeared to have a different surface treatment than gauges used previously, and the temperature setting used before caused the gauge to burn through when soldering. Once soldered, the gauges were calibrated in an oven using the procedure discussed by Cress [32]. After calibration, the lead/TFG junctions were covered with JB Weld to increase the robustness of the junction. At this point, the thermocouple lead wires were also soldered to the foil thermocouples and their junctions were covered with JB Weld. Figure B3 shows the lead wires and junctions.

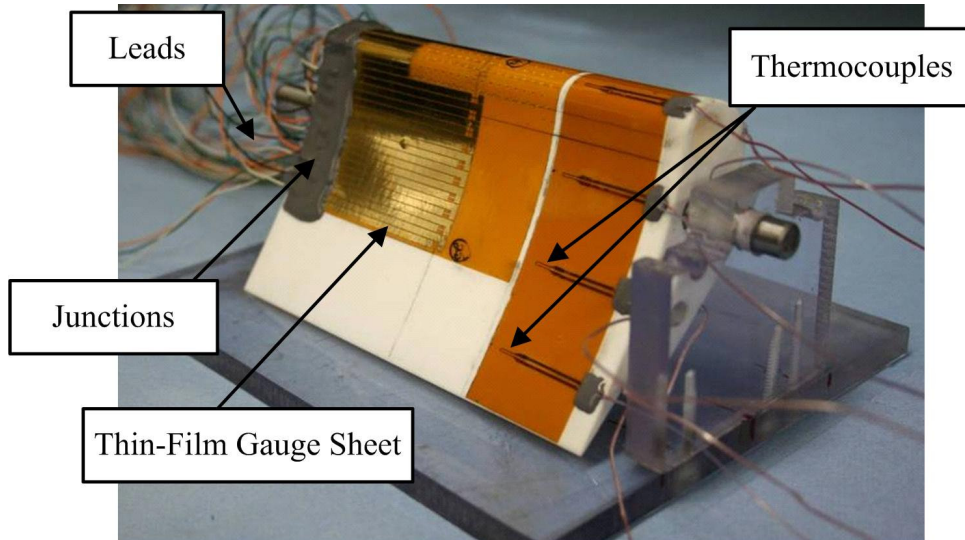


Figure B3. Gauge Sheet and Thermocouples Installed on Film-Cooled Vane

Test Section Installation

After JB welding all lead wire junctions, the film-cooled vane was mounted on the test section window where it remained for the remainder of the experiment. To do this, the film-cooled vane was attached to a Lexan test section window using dowel pins inserted through the window and into the vane. The TFG lead wires were pulled through holes drilled in the Lexan near the surface of the vane. Silicone caulk was used to cover the lead wires and seal the vane to the Lexan window.

An aluminum insert was attached to the other side of the vane using dowel pins, and the thermocouple lead wires were pulled through holes drilled in the aluminum near the vane surface. Again, silicone caulk was used to cover the lead wires and seal the vane to the insert. Figure B4 and Figure B5 show the vane attached to the window and insert.

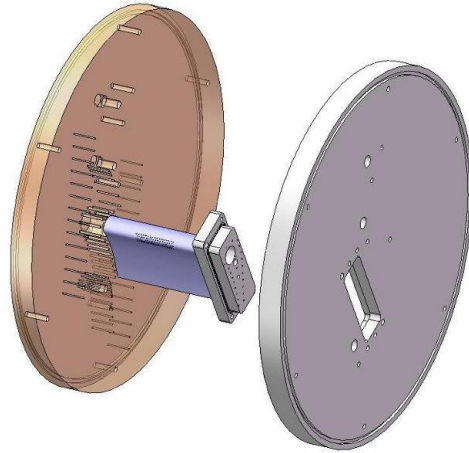


Figure B4. Film-cooled Vane Assembled with Test Section Windows and Insert

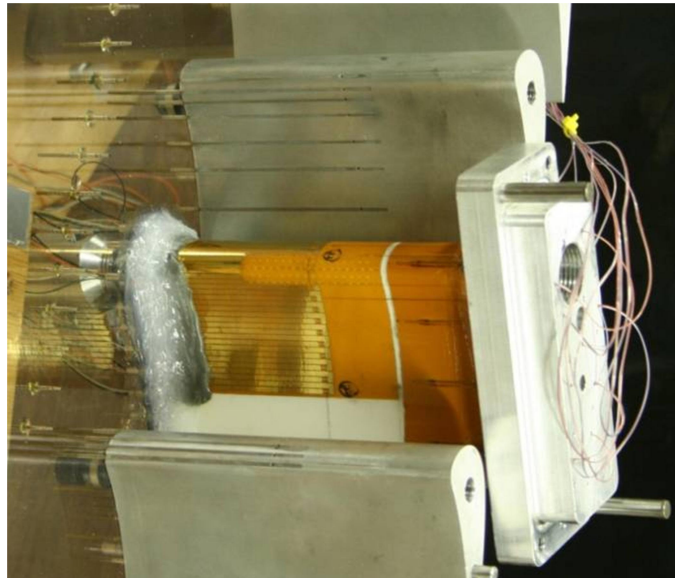


Figure B5. Picture of Instrumented Vane Installed in Test Section

Additional References

[31] Carullo, J.S., 2006, "Effects of Freestream Turbulence, Turbulence Length Scale, and Reynolds Number on Turbine Blade Heat Transfer in a Transonic Cascade," Master's Thesis, Virginia Polytechnic Institute and State University.

[32] Cress, R.D., 2006, "Turbine Blade Heat Transfer Measurements in a Transonic Flow Using Thin film Gages," Master's Thesis, Virginia Polytechnic Institute and State University.

APPENDIX C: RECOVERY TEMPERATURE MEASUREMENT

As discussed in the “Measurement of Recovery Temperature” section of the report, h and η are determined using a linear regression technique with the data obtained from a single run. The data is plotted with the quantity $q''/(T_r-T_c)$ on the Y-axis and $(T_r-T_w)/(T_r-T_c)$ on the X-axis, and a line is fit to the result. This line corresponds to Equation 5 with the slope of the line representing h and the y-intercept representing η .

Originally, recovery temperature, T_r , for this technique was calculated using the following equation:

$$T_r = T_{o,\infty} \left[\frac{1 + r \frac{\gamma - 1}{2} M_{loc}^2}{1 + \frac{\gamma - 1}{2} M_{loc}^2} \right] \quad (C1)$$

where r is the recovery factor approximated assuming a fully turbulent boundary layer, $T_{o,\infty}$ is the freestream total temperature, and M_{loc} is the local Mach number at the vane surface. For this experiment, r was assumed to be $Pr^{1/3}$ (0.892) for a fully turbulent boundary layer. This technique has been used by several groups including Guo *et al.* [8] and Abuaf *et al.* [6].

Recovery temperature was also measured for the film cooled vane. With the BR=0 data, the equation below was used to determine T_r for film cooled experiments.

$$q'' = h(T_{o,\infty} - T_w) - h(T_{o,\infty} - T_r) \quad (C2)$$

Using Equation C2, h and T_r were determined by plotting q'' versus $(T_{o,\infty}-T_w)$. The result gives us a line of the form $y = mx + b$ where the slope of the line is heat transfer coefficient and the X-intercept of the line is $(T_{o,\infty}-T_r)$. $(T_{o,\infty}-T_r)$ was determined at each measurement location and then used to find the recovery temperature using $T_{o,\infty}$ from the film cooled runs. Figure C1 shows an example of this technique. More explanation of this technique can be seen in Popp *et al.* [18].

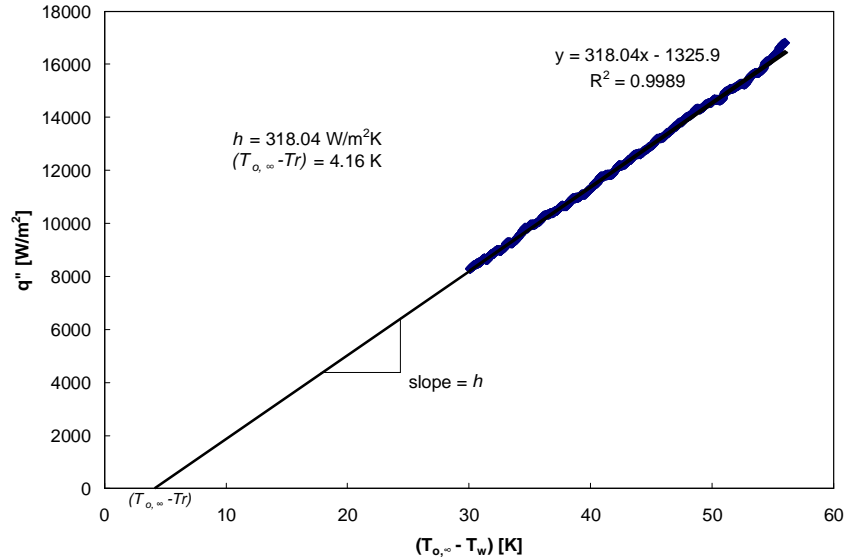


Figure C1. Determining h and T_r with $BR=0$

At some locations, the measured recovery temperature proved to vary noticeably from the recovery temperature found using an assumed recovery factor. This is due to factors such as flow acceleration and pressure gradient and their effect on the boundary layer and boundary layer transition that the previously assumed recovery factor does not take into account. Discrepancies between the two methods of determining T_r occur where the previously mentioned factors are significant.

With the measured recovery temperature, heat transfer coefficient and effectiveness were found using Equation 5 on page 21 of this report. Figure C3 shows the effectiveness distribution found with a measured recovery temperature versus the distribution found using an assumed recovery factor. The suction side trend using the measured recovery temperature is significantly different than the trend using the assumed recovery factor. The “valley” in effectiveness seen by assuming a recovery factor is not present, and effectiveness clearly decays downstream of injection. The two techniques showed minor differences on the pressure side. The heat transfer coefficient distribution did not change significantly except in the region near the throat where a noticeable decrease occurred; this can be seen in Figure C2 on the next page.

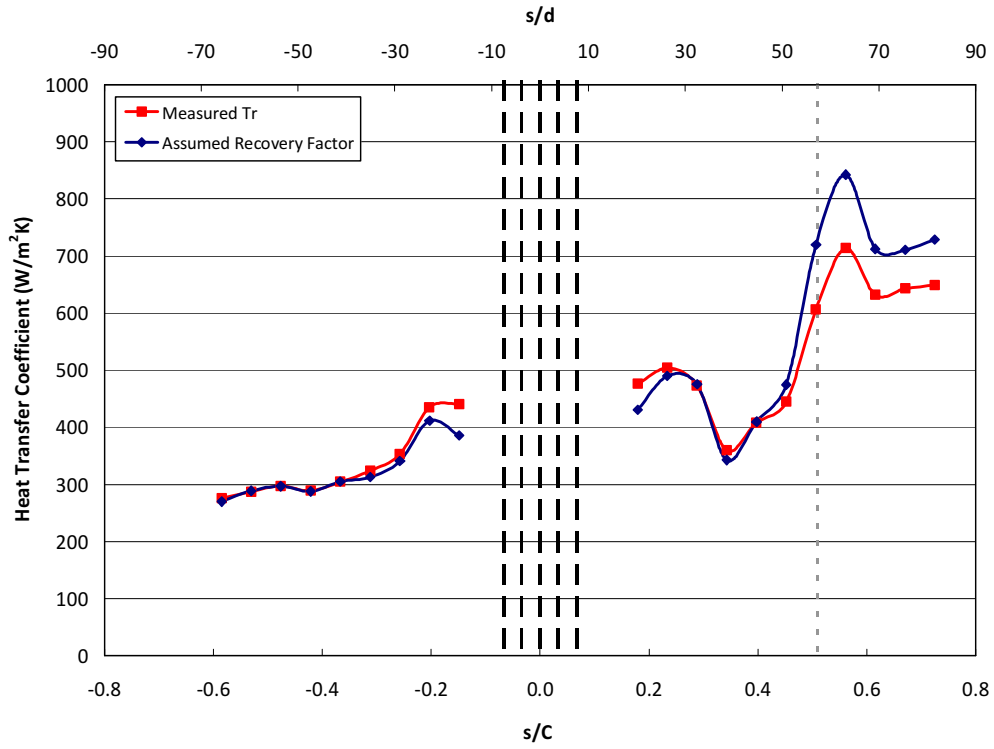


Figure C2. Heat transfer coefficient for $M_{ex}=0.76$, $T_u=16\%$, $BR=2.0$, $DR = 1.38$

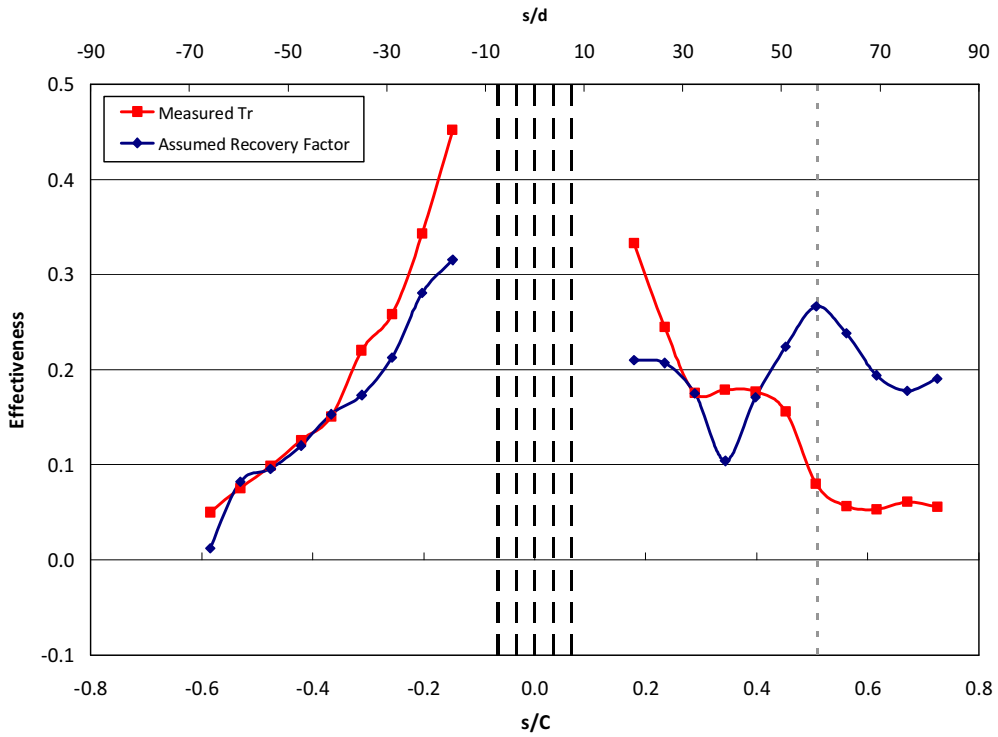


Figure C3. Film cooling effectiveness for $M_{ex}=0.76$, $T_u=16\%$, $BR=2.0$, $DR = 1.38$

APPENDIX D: UNCERTAINTY ANALYSIS

This appendix describes the method used to determine the experimental uncertainty in heat transfer coefficient and film cooling effectiveness. As discussed in the “Data Reduction” section of this report, heat transfer coefficient was determined by the slope of the least-squares line fit shown in Figure D1. By the nature of the experiment, each data point shown in Figure D1 has bias and precision uncertainty in both X and Y coordinates. Uncertainty in each of these coordinates was determined within a 95% confidence interval using Moffat’s small perturbation method [23].

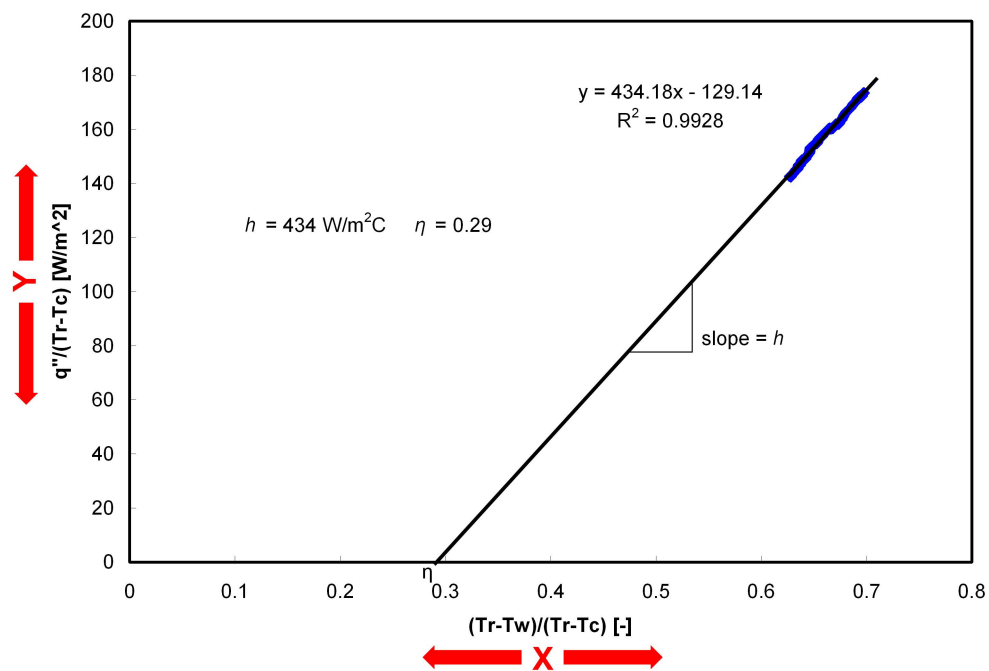


Figure D1. Determination of h and η

Knowing the uncertainty in X and Y coordinates for each data point, Brown and Coleman’s [24] method was used to determine the uncertainty in the linear regression. Covariance was assumed to be negligible in this experiment. The result of Brown’s analysis produces an uncertainty in the linear regression’s slope and x-intercept which represent the uncertainty in heat transfer coefficient and film cooling effectiveness, respectively. For each test condition, measurements were performed at least three times to establish repeatability. The total average uncertainty of the heat transfer coefficient was determined to be $\pm 9.6\%$. Because η is determined from extrapolating the data shown in Figure 8, its uncertainty is larger. The total average uncertainty in η is ± 0.062 .

Uncertainties in M_{ex} , DR, and BR were determined with Moffat's [23] small perturbation method within the 95% confidence interval. Uncertainty values for intermediate and final results are shown in Table D1. Samples of data plotted with the uncertainty bands for each gauge are provided for Nusselt number and effectiveness in Figure D2 and Figure D3, respectively; these plots correspond to Figure 11 and Figure 13 from the report.

Table D1. Experimental Uncertainties

Value	Average Uncertainty
q''	$\pm 7.6\%$
h	$\pm 8.0\%$
η	± 0.055
M_{ex}	$\pm 1.3\%$
DR	$\pm 0.4\%$
BR	$\pm 1.4\%$

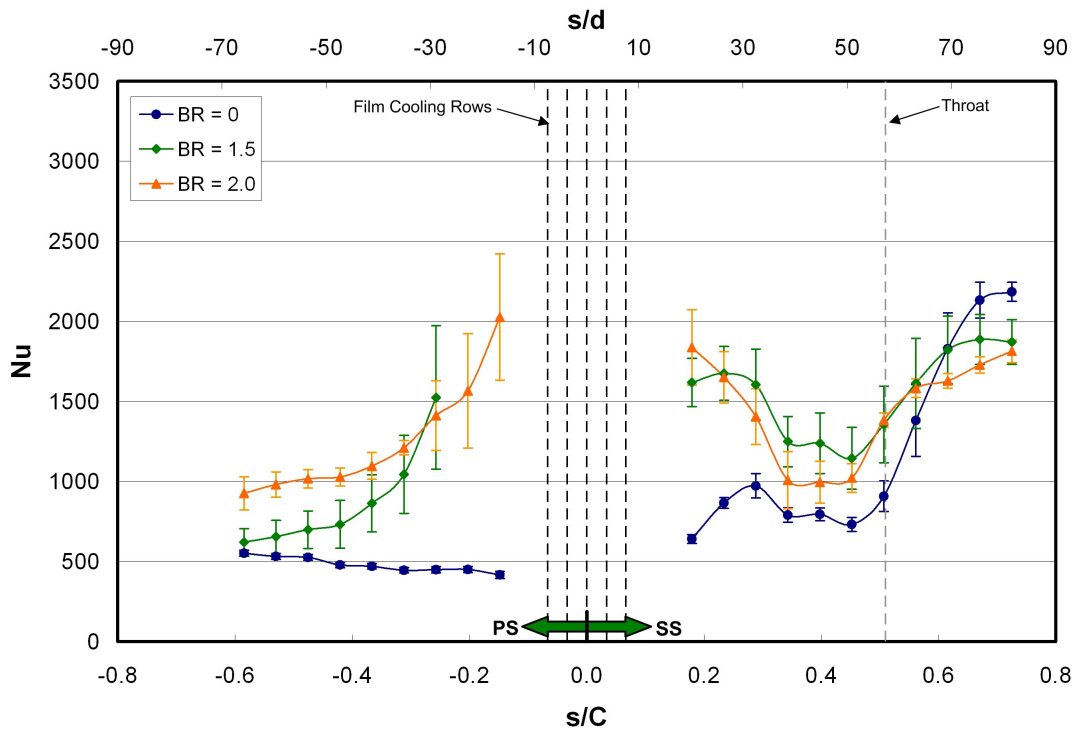


Figure D2. Nusselt Number Distribution with Uncertainty Bands

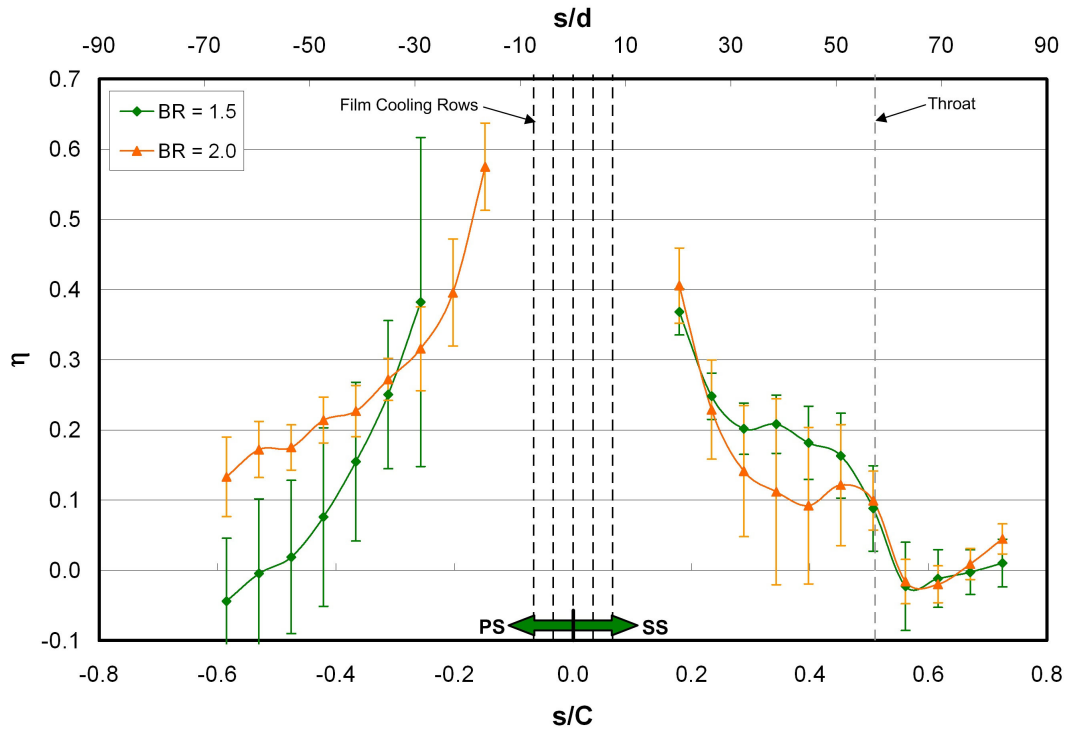


Figure D3. Effectiveness Distribution with Uncertainty Bands

APPENDIX E: REGRESSION TECHNIQUE AT LOW FREESTREAM TURBULENCE

Uncertainty in h and η were significantly higher for low freestream turbulence tests than for large-scale high freestream turbulence experiments. The increase in uncertainty at high freestream turbulence was largely due to an increase in run-to-run variation of heat transfer coefficient and effectiveness. It was observed that the low turbulence results were highly sensitive to changes in freestream and cooling conditions when compared to the sixteen percent turbulence case.

Although this sensitivity affected all of the gauges, run-to-run variation was particularly high in two locations. The first was just upstream of the throat on the suction side of the vane. In this location, slight changes in freestream pressure were seen to cause drastic slope and intercept changes in the linear regression applied to find h and η . This effect was particularly clear as the tunnel ramped up to pressure or at exit Mach 1.0 where small “bump” in freestream pressure was present due to the tunnel control system. Figure E1 shows the freestream conditions for a run at exit Mach 1.0 with a blowing ratio of 1.5.

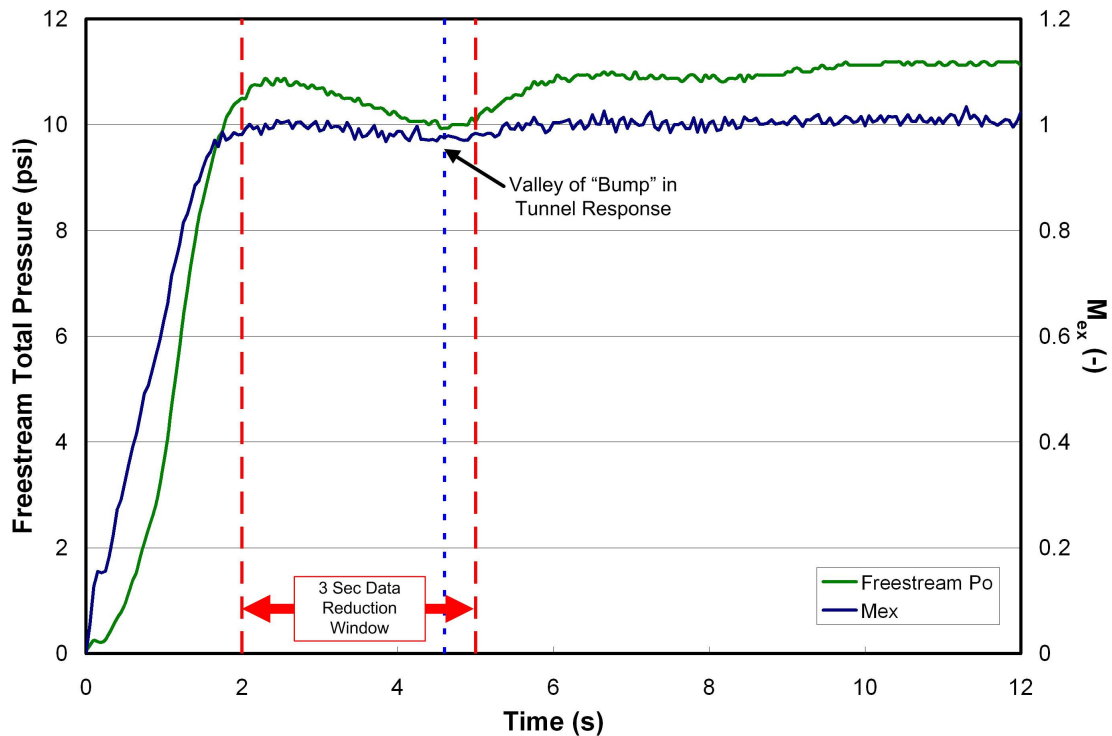


Figure E1. Freestream Conditions for $M_{ex} = 1.0$, $BR = 1.5$ Run

The “bump” in the freestream total pressure caused an obvious change in heat transfer coefficient and film cooling effectiveness measured by the gauge. This is most clearly illustrated by viewing the regression plot shown in Figure E2 for a gauge upstream of the throat for this run. The red lines in the plot indicate the start and end of the time over which data is typically reduced, and the blue dashed line indicates the point in time at which the valley of the “bump” in freestream total pressure occurs. From the start of reduction ($t = 2$ seconds), the trend was fairly linear until the valley in total pressure, beyond which the slope shifted drastically. This shift significantly skewed the regression used to find h and η . In some cases, the data reduction window was moved in time or shortened slightly to avoid this effect. Despite this effort, smaller changes in pressure—though never as severe—were also seen to have an effect on the regression. The high sensitivity of these gauges to fluctuations in pressure led to an increase in run-to-run variation. This sensitivity was not seen with high freestream turbulence.

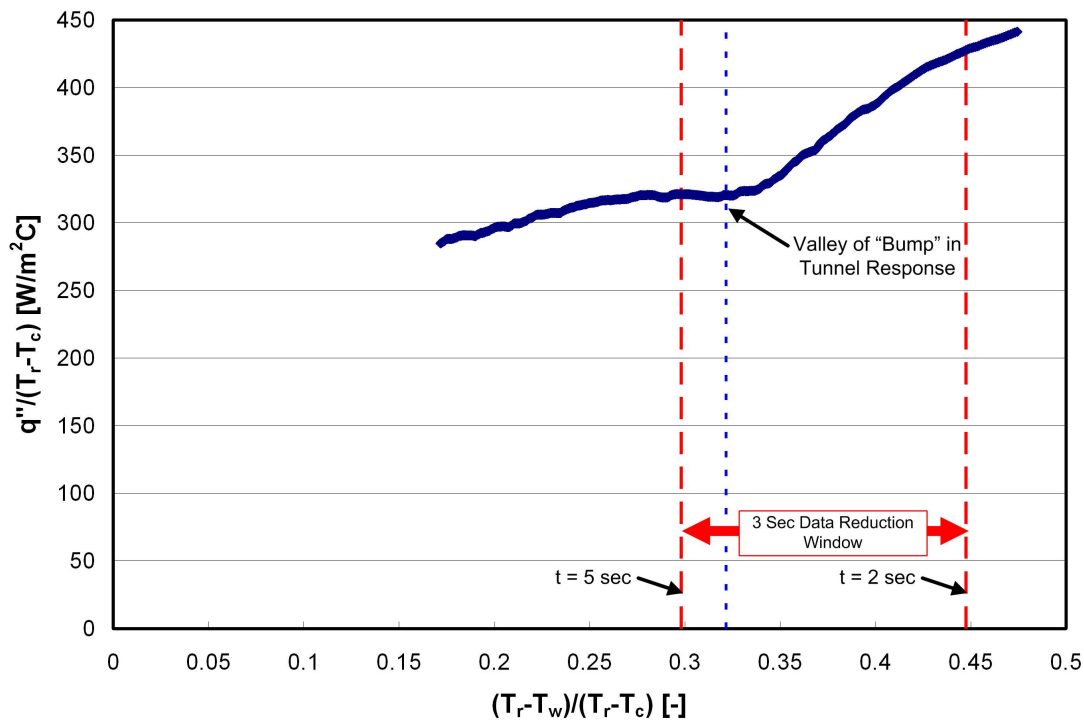


Figure E2. Regression Plot for Gauge 16 ($s/C = 0.45$)

Run-to-run variation also increased significantly on the pressure side just downstream of injection for a blowing ratio of 1.5. It is possible that flow unsteadiness at this blowing ratio is the cause. Figure E3 shows a temperature history for one pressure side gauge (Gauge 9) just downstream of injection compared to a suction side gauge (Gauge 11) that is a similar distance

away from the injection site. Although temperatures are not expected to be equal, temperature histories typically follow a trend similar to Gauge 11. The pressure side, however, shows an unusual trend with temperature climbing as the tunnel ramps up and then reaching a plateau. Once this plateau is reached, the rate of change of temperature seems to fluctuate erratically. This fluctuation seems to indicate some unsteady behavior which can be seen in the regression plot shown in Figure E4. This unsteadiness resulted in increased run-to-run variation which led to increased uncertainty and loss of measurement in the case of Gauges 8 and 9 on the pressure side.

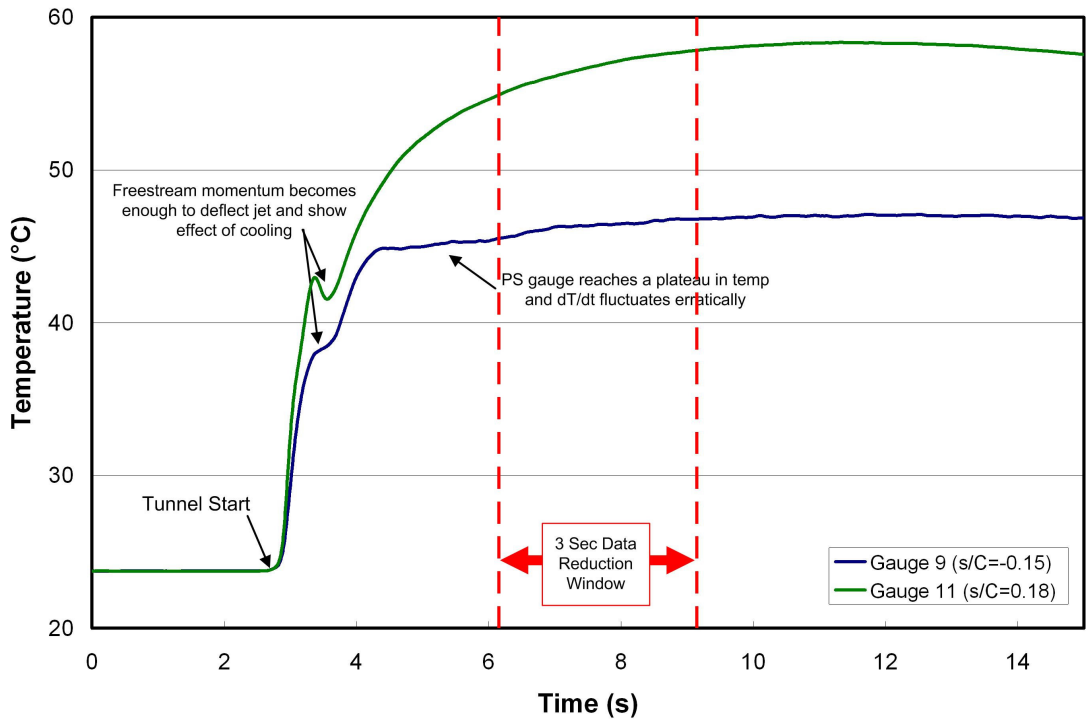


Figure E3. Temperature History of Gauge 9 and 11 for $Mex = 0.76$, $BR = 1.5$

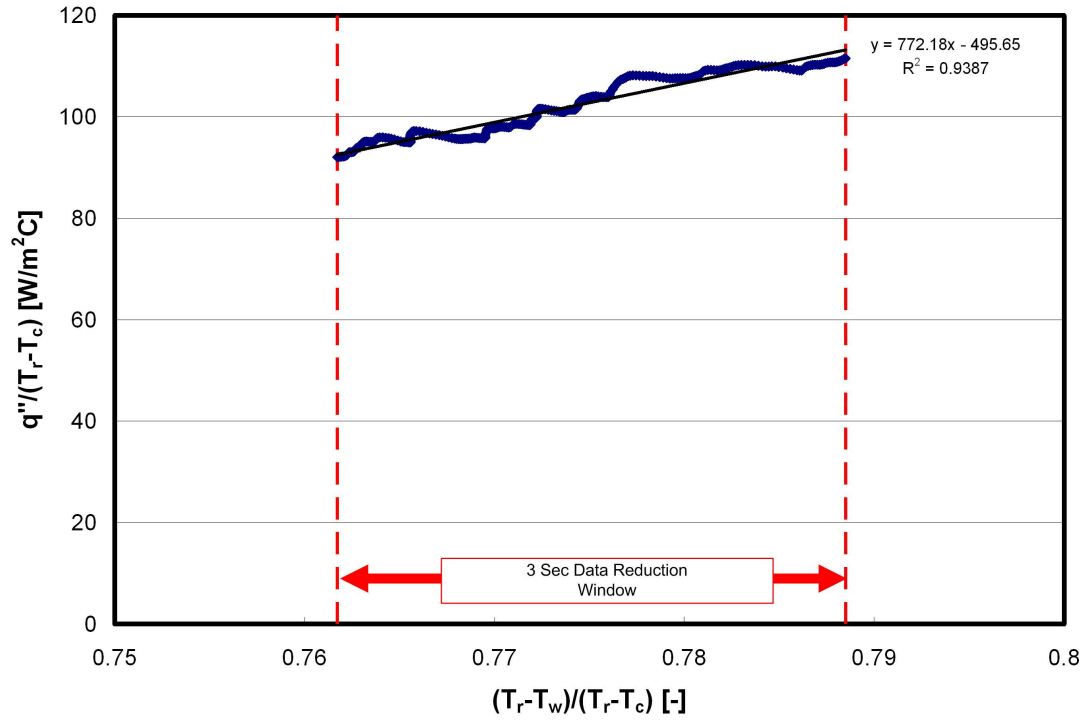


Figure E4. Regression for determining h and η at Gauge 9 for Mex = 0.76, BR = 1.5

APPENDIX F: TABULATED RESULTS

Table F1. Nusselt Number, Nu , for $M_{ex} = 0.76$

Gauge	Location		Nu @ Blowing Ratio:		
	s/C	s/d	0.0	1.5	2.0
1	-0.585	-67.7	553	622	927
2	-0.530	-61.4	533	655	982
3	-0.476	-55.1	526	700	1017
4	-0.421	-48.8	479	733	1029
5	-0.366	-42.5	470	864	1097
6	-0.312	-36.1	446	1045	1211
7	-0.257	-29.8	449	1525	1411
8	-0.203	-23.5	451		1567
9	-0.148	-17.2	417		2027
10	0.125	14.5			
11	0.179	20.8	642	1619	1838
12	0.234	27.1	866	1675	1652
13	0.288	33.4	974	1605	1406
14	0.343	39.7	791	1250	1009
15	0.398	46.1	796	1239	996
16	0.452	52.4	732	1145	1022
17	0.507	58.7	908	1357	1383
18	0.561	65.0	1382	1613	1583
19	0.616	71.4	1829	1823	1629
20	0.671	77.7	2133	1888	1729
21	0.725	84.0	2185	1872	1814

Table F2. Heat Transfer Augmentation, Nu/Nu_0 , for $Mex = 0.76$

Gauge	Location		Nu/Nu ₀ @ Blowing Ratio:	
	s/C	s/d	1.5	2.0
1	-0.585	-67.7	1.13	1.68
2	-0.530	-61.4	1.23	1.84
3	-0.476	-55.1	1.33	1.93
4	-0.421	-48.8	1.53	2.15
5	-0.366	-42.5	1.84	2.33
6	-0.312	-36.1	2.34	2.71
7	-0.257	-29.8	3.39	3.14
8	-0.203	-23.5		3.48
9	-0.148	-17.2		4.86
10	0.125	14.5		
11	0.179	20.8	2.52	2.87
12	0.234	27.1	1.93	1.91
13	0.288	33.4	1.65	1.44
14	0.343	39.7	1.58	1.28
15	0.398	46.1	1.56	1.25
16	0.452	52.4	1.56	1.40
17	0.507	58.7	1.49	1.52
18	0.561	65.0	1.17	1.15
19	0.616	71.4	1.00	0.89
20	0.671	77.7	0.88	0.81
21	0.725	84.0	0.86	0.83

Table F3. Film Cooling Effectiveness, η , for $M_{ex} = 0.76$

Gauge	Location		η @ Blowing Ratio:	
	s/C	s/d	1.5	2.0
1	-0.585	-67.7	-0.04	0.13
2	-0.530	-61.4	0.00	0.17
3	-0.476	-55.1	0.02	0.18
4	-0.421	-48.8	0.08	0.21
5	-0.366	-42.5	0.15	0.23
6	-0.312	-36.1	0.25	0.27
7	-0.257	-29.8	0.38	0.32
8	-0.203	-23.5		0.40
9	-0.148	-17.2		0.57
10	0.125	14.5		
11	0.179	20.8	0.37	0.41
12	0.234	27.1	0.25	0.23
13	0.288	33.4	0.20	0.14
14	0.343	39.7	0.21	0.11
15	0.398	46.1	0.18	0.09
16	0.452	52.4	0.16	0.12
17	0.507	58.7	0.09	0.10
18	0.561	65.0	-0.02	-0.02
19	0.616	71.4	-0.01	-0.02
20	0.671	77.7	0.00	0.01
21	0.725	84.0	0.01	0.04

Table F4. Net Heat Flux Reduction, $\Delta q''_{red}$, for $M_{ex} = 0.76$

Gauge	Location		$\Delta q''_{red}$ @ Blowing Ratio:	
	s/C	s/d	1.5	2.0
1	-0.585	-67.7	-0.21	-0.30
2	-0.530	-61.4	-0.24	-0.31
3	-0.476	-55.1	-0.29	-0.37
4	-0.421	-48.8	-0.34	-0.38
5	-0.366	-42.5	-0.36	-0.45
6	-0.312	-36.1	-0.36	-0.48
7	-0.257	-29.8	-0.23	-0.49
8	-0.203	-23.5		-0.18
9	-0.148	-17.2		0.80
10	0.125	14.5		
11	0.179	20.8	0.03	0.07
12	0.234	27.1	-0.13	-0.18
13	0.288	33.4	-0.09	-0.10
14	0.343	39.7	-0.03	-0.04
15	0.398	46.1	-0.09	-0.06
16	0.452	52.4	-0.14	-0.11
17	0.507	58.7	-0.27	-0.27
18	0.561	65.0	-0.21	-0.18
19	0.616	71.4	-0.02	0.08
20	0.671	77.7	0.11	0.20
21	0.725	84.0	0.16	0.23

Table F5. Nusselt Number, Nu , for $M_{ex} = 1.0$

Gauge	Location		Nu @ Blowing Ratio:		
	s/C	s/d	0.0	1.5	2.0
1	-0.585	-67.7	553	622	927
2	-0.530	-61.4	533	655	982
3	-0.476	-55.1	526	700	1017
4	-0.421	-48.8	479	733	1029
5	-0.366	-42.5	470	864	1097
6	-0.312	-36.1	446	1045	1211
7	-0.257	-29.8	449	1525	1411
8	-0.203	-23.5	451		1567
9	-0.148	-17.2	417		2027
10	0.125	14.5			
11	0.179	20.8	642	1619	1838
12	0.234	27.1	866	1675	1652
13	0.288	33.4	974	1605	1406
14	0.343	39.7	791	1250	1009
15	0.398	46.1	796	1239	996
16	0.452	52.4	732	1145	1022
17	0.507	58.7	908	1357	1383
18	0.561	65.0	1382	1613	1583
19	0.616	71.4	1829	1823	1629
20	0.671	77.7	2133	1888	1729
21	0.725	84.0	2185	1872	1814

Table F6. Heat Transfer Augmentation, Nu/Nu_0 , for $M_{ex} = 1.0$

Gauge	Location		Nu/Nu ₀ @ Blowing Ratio:	
	s/C	s/d	1.5	2.0
1	-0.585	-67.7	1.13	1.68
2	-0.530	-61.4	1.23	1.84
3	-0.476	-55.1	1.33	1.93
4	-0.421	-48.8	1.53	2.15
5	-0.366	-42.5	1.84	2.33
6	-0.312	-36.1	2.34	2.71
7	-0.257	-29.8	3.39	3.14
8	-0.203	-23.5		3.48
9	-0.148	-17.2		4.86
10	0.125	14.5		
11	0.179	20.8	2.52	2.87
12	0.234	27.1	1.93	1.91
13	0.288	33.4	1.65	1.44
14	0.343	39.7	1.58	1.28
15	0.398	46.1	1.56	1.25
16	0.452	52.4	1.56	1.40
17	0.507	58.7	1.49	1.52
18	0.561	65.0	1.17	1.15
19	0.616	71.4	1.00	0.89
20	0.671	77.7	0.88	0.81
21	0.725	84.0	0.86	0.83

Table F7. Film Cooling Effectiveness, η , for $M_{ex} = 1.0$

Gauge	Location		η @ Blowing Ratio:	
	s/C	s/d	1.5	2.0
1	-0.585	-67.7	-0.04	0.13
2	-0.530	-61.4	0.00	0.17
3	-0.476	-55.1	0.02	0.18
4	-0.421	-48.8	0.08	0.21
5	-0.366	-42.5	0.15	0.23
6	-0.312	-36.1	0.25	0.27
7	-0.257	-29.8	0.38	0.32
8	-0.203	-23.5		0.40
9	-0.148	-17.2		0.57
10	0.125	14.5		
11	0.179	20.8	0.37	0.41
12	0.234	27.1	0.25	0.23
13	0.288	33.4	0.20	0.14
14	0.343	39.7	0.21	0.11
15	0.398	46.1	0.18	0.09
16	0.452	52.4	0.16	0.12
17	0.507	58.7	0.09	0.10
18	0.561	65.0	-0.02	-0.02
19	0.616	71.4	-0.01	-0.02
20	0.671	77.7	0.00	0.01
21	0.725	84.0	0.01	0.04

Table F8. Net Heat Flux Reduction, $\Delta q''_{red}$, for $M_{ex} = 1.0$

Gauge	Location		$\Delta q''_{red}$ @ Blowing Ratio:	
	s/C	s/d	1.5	2.0
1	-0.585	-67.7	-0.21	-0.30
2	-0.530	-61.4	-0.24	-0.31
3	-0.476	-55.1	-0.29	-0.37
4	-0.421	-48.8	-0.34	-0.38
5	-0.366	-42.5	-0.36	-0.45
6	-0.312	-36.1	-0.36	-0.48
7	-0.257	-29.8	-0.23	-0.49
8	-0.203	-23.5		-0.18
9	-0.148	-17.2		0.80
10	0.125	14.5		
11	0.179	20.8	0.03	0.07
12	0.234	27.1	-0.13	-0.18
13	0.288	33.4	-0.09	-0.10
14	0.343	39.7	-0.03	-0.04
15	0.398	46.1	-0.09	-0.06
16	0.452	52.4	-0.14	-0.11
17	0.507	58.7	-0.27	-0.27
18	0.561	65.0	-0.21	-0.18
19	0.616	71.4	-0.02	0.08
20	0.671	77.7	0.11	0.20
21	0.725	84.0	0.16	0.23

APPENDIX G: SAMPLE DATA

This appendix presents a sampling of data used for the calculation of heat transfer coefficient and film cooling effectiveness for one gauge on the film cooled vane with freestream conditions of $M_{ex} = 0.76$, $BR = 2.0$, $Tu = 2\%$ and $\Lambda_x/P = 0.05$. Data is presented for Gauge 5, which is located at $s/C = -0.37$ on the pressure surface.

A time trace of tunnel freestream conditions is shown below in Figure G1. The window of time in which data can be used to calculate h and η is shown within the red dotted lines. Exit Mach number, density ratio, and blowing ratio are constant during this window, and total temperature is falling. The transient temperature and otherwise steady freestream conditions permit the calculation of h and η during a single run. Outside of the three second window of time shown, the semi-infinite assumption can begin to fail for some gauges. For this reason, a three second window has been chosen to ensure that h and η are calculated for all gauges during the same period of time.

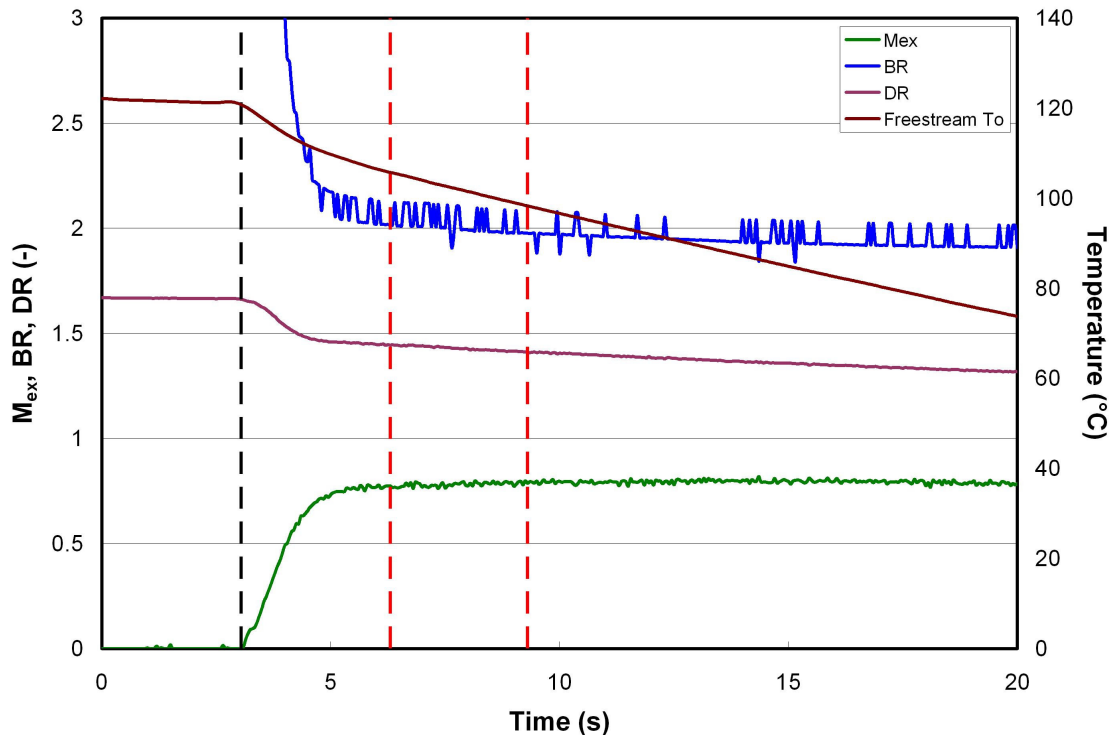


Figure G1. Tunnel Freestream Conditions

Thin film gauge (TFG) voltages are sampled at 1 kHz during the experiment by a National Instruments AT-MIO-16XE-50 System. The TFGs are resistance temperature devices, and prior to testing, all of the gauges are calibrated to determine each one's resistance-

temperature relationship following the procedure outlined by Cress [22]. A Wheatstone bridge is used to convert each gauge's resistance change to a change in voltage that can be read by the data acquisition system. This voltage change is later converted to temperature change following Cress' procedure [22], and the initial temperature of the gauge is obtained from the 10 thermocouples on the vane prior to the run. Figure G1 shows the temperature trace for Gauge 7 during the run.

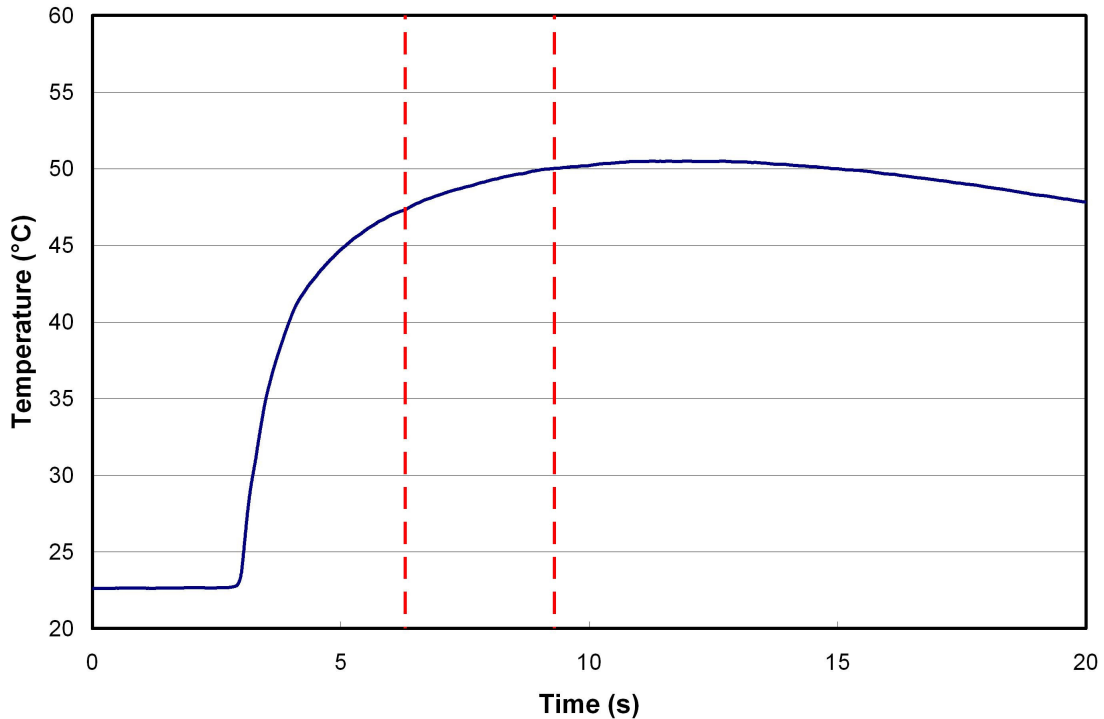


Figure G2. Thin-film Gauge Temperature History of Gauge 5

Using the gauge temperature, a finite difference code is used to determine heat flux assuming 1-D heat conduction on a semi-infinite substrate. The initial temperature of the low thermal conductive semi-infinite substrate (Macor) is determined by the 10 thermocouples prior to the run. 1-D heat conduction can be assumed since the vane is at uniform temperature prior to the start of the run. Figure G3 shows the heat flux into the vane at Gauge 5 during the run.

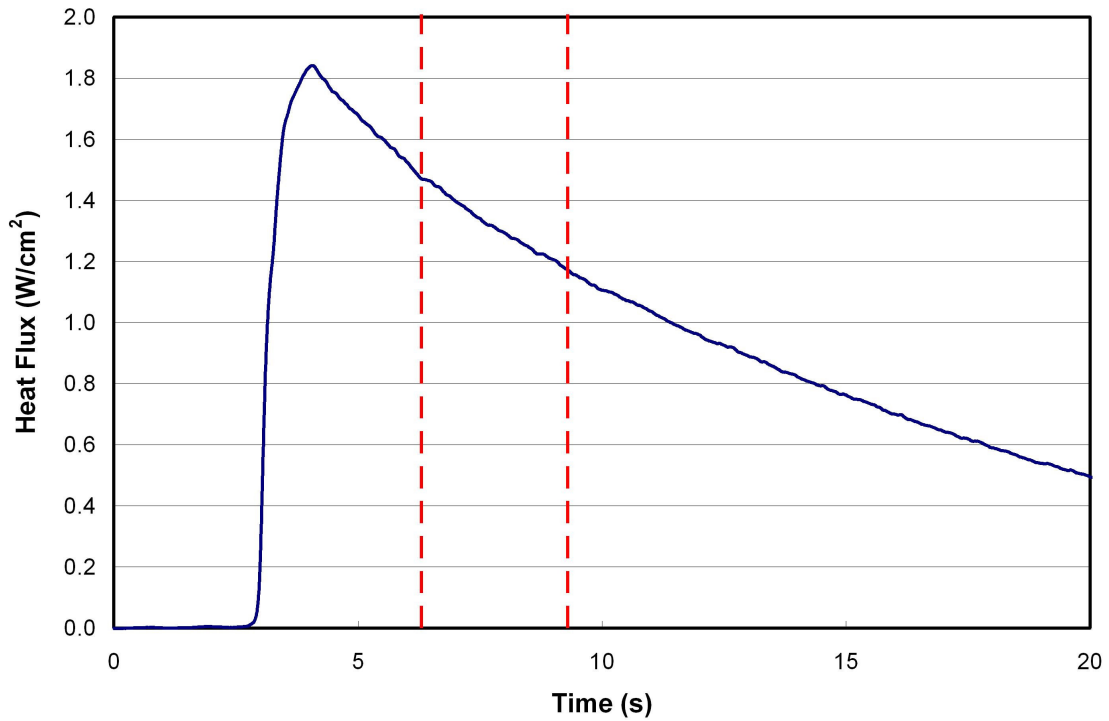


Figure G3. Heat Flux History of Gauge 5

With heat flux, heat transfer coefficient and film cooling effectiveness can be found using the linear regression technique discussed in the “Data Reduction” section of this report. A sample plot demonstrating this technique can be seen in Figure G4. The slope of the line fit shown represents heat transfer coefficient during the run, and the x-intercept of the line represents the film cooling effectiveness.

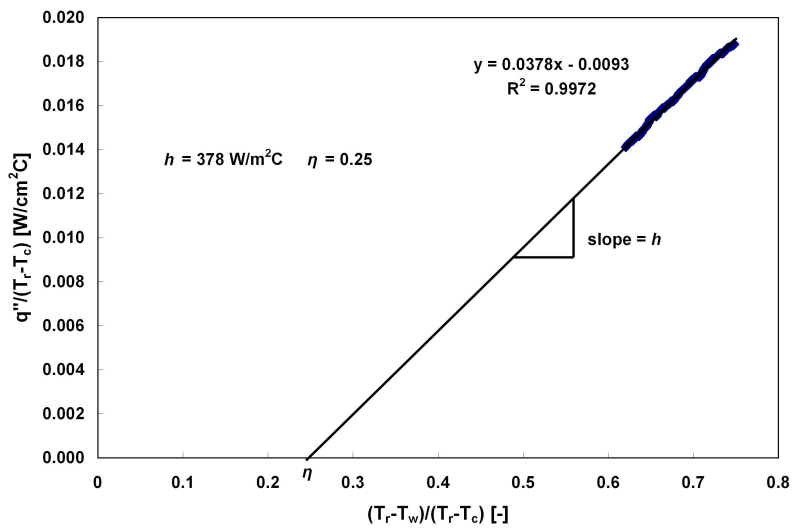


Figure G4. Heat Transfer Coefficient and Effectiveness During Transient Run

APPENDIX H: NET HEAT FLUX REDUCTION

Determining Net Heat Flux Reduction

While film cooling reduces adiabatic wall temperature, it also augments heat transfer by enhancing local turbulence. Therefore, a balance must be struck between heat transfer augmentation and reduction of adiabatic wall temperature to create a beneficial cooling scheme. To evaluate the merit of a particular scheme, it is helpful to consider reduction of heat flux into the vane which clearly illustrates this balance. Net heat flux reduction, $\Delta q_{red}''$, is determined by:

$$\Delta q_{red}'' = \frac{q_o'' - q_f''}{q_o''} = 1 - \frac{q_f''}{q_o''} = 1 - \frac{h}{h_0} \left(1 - \frac{\eta}{\phi} \right) \quad (8)$$

with the overall cooling effectiveness, ϕ , defined as:

$$\phi = \frac{T_w - T_g}{T_c - T_g} \quad (9)$$

Overall cooling effectiveness is typically around 0.5 to 0.7, depending on external and internal cooling design. A value of $\phi = 0.6$ has been assumed for this analysis. Drost *et al.* [7] and Lu *et al.* [33] used the same value of ϕ for high-speed and low-speed facilities, respectively. A positive value of net heat flux reduction indicates that heat flux into the vane is reduced by film cooling, and a negative value indicates that heat flux is increased.

Effect of Blowing Ratio on Net Heat Flux Reduction

Interestingly, experimental results indicate that net heat flux reduction for both blowing ratios at both Mach numbers is negative along the entire measurement surface. These results can be seen in Figure H1 and Figure H2. In all cases tested, the high heat transfer augmentation due to injection far outweighs any thermal dilution provided by the coolant. Positive net heat flux reduction is seen downstream of the throat at both mach numbers because of heat transfer augmentation less than one occurring in those locations.

Additional References

[33] Lu, Y., Dhungel, A., Ekkad, S.V., and Bunker, R.S., 2007, "Effect of Trench Width and Depth on Film Cooling from Cylindrical Holes Embedded in Trenches," ASME GT-2007-27388.

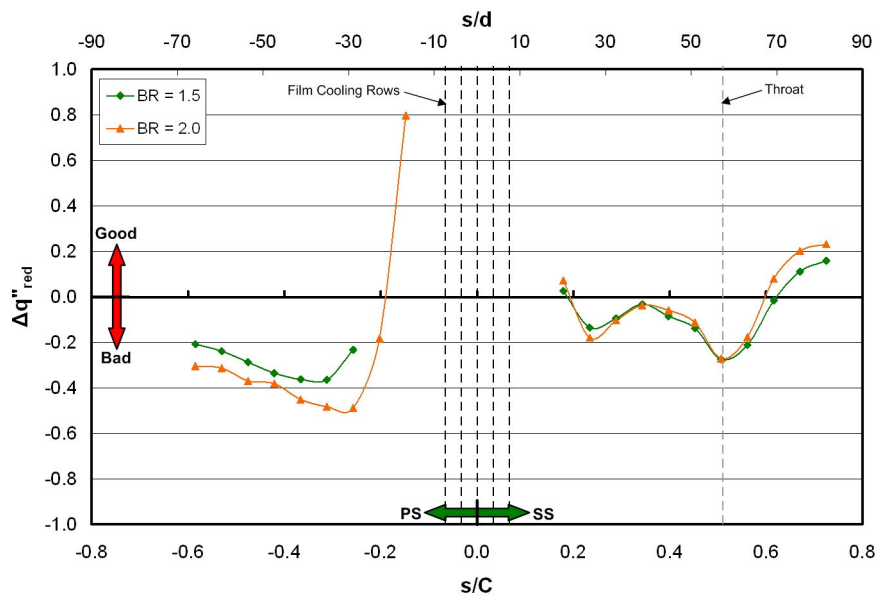


Figure H1. Effect of BR on $\Delta q''_{red}$ for $M_{ex} = 0.76$

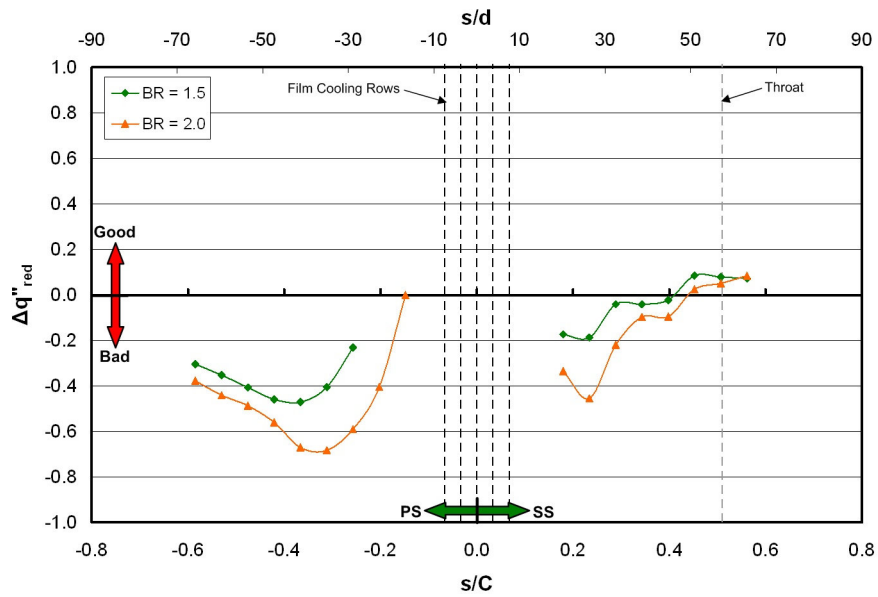


Figure H2. Effect of BR on $\Delta q''_{red}$ for $M_{ex} = 1.0$

APPENDIX I: DATA REDUCTION CODE

This appendix contains two MATLAB .m-files used to reduce experimental data. Data was saved in three files: an input file, an NI file, and a PSI file. The input file contained all of the data relevant to a particular day of testing such as gauge calibrations, gauge pre-run resistances, Wheatstone bridge voltage, atmospheric pressure, and local Mach numbers measured in previous experiments. The NI file contained all thin-film gauge voltages, MKS pressure transducer voltages, and thermocouple temperatures for a particular run. Finally, the PSI file contained all pressures measured by the PSI 8400 for the same run. The MATLAB code reads all three files, computes all quantities of interest, plots relevant information, and saves the processed data in an excel spreadsheet to be further analyzed. A modified version of this code was used to determine heat transfer coefficient and ($T_{o,\infty}-T_f$).

MATLAB Data Reduction Code:

```
%Data reduction code for film-cooled vane experiments
%Trey Bolchoz 8/1/07

clc,clear,close all

global N fs

%%%%%%%%%%%%%%%%%%%%%%%%%%%%%%%%%%%%%%%%%%%%%%%%%%%%%%%%%%%%%%%%%%%%%%%%
%Inputs
%%%%%%%%%%%%%%%%%%%%%%%%%%%%%%%%%%%%%%%%%%%%%%%%%%%%%%%%%%%%%%%%%%%%%%%%
%Reduction times
reductime = 3;
tunnel_delay = 2.00;
lagPSI = 0.00;
Td_select = '';

%Input for loading files
fn_drive = 'z';
fn_turbulence = '2';
fn_exit_mach = '1_01';
fn_BR = '1_5';
date = '3_13_08';
run_number = '4';
save_tag = '_reduced_FD_meas_Td_10sec_0_39lag_1_75delay';
input_tag = '_a';
event = 0; %1 = before, 2 = after, 3 = both averaged

%Calculate/Display/Save Option
filter = 1; %Filter NI data? (1=yes,0=no)
recovery = 2; %Assumed r = 1, Measured Td = 2
conv_TFG=1; %Convert TFG voltages to temp?(1=yes,0=no)
determine_q = 1; %Determine flux?(1=yes,0=no)
choose_code = 2; %Reduce using?(1=laplace,2=finite difference)
separate_plen = 0; %Reduce 9,10,11 w/other BC for FD code?(1=yes,0=no)
savedata = 2; %Save Data?(0=no,1=blowing only,2=all)

%Geometry
num_holes = 83;
hole_diam = 0.031; %hole diameter in inches
C = 3.591; %Chord (inches)

%Input Sampling frequencies
```

```

fs = 1000; %NI Sampling Rate
psi_fs = 20; %PSI Sampling Rate

%Input Ttot lag
lagTC =0.35; %lag freestream by seconds

%Input recovery factor
r = 0.892; %Recovery factor for turbulent flow

%Display Run Parameters in Command Window
disp(['Date: ' date])
disp(['Turbulence: ' fn_turbulence '%'])
disp(['Exit Ma: ' fn_exit_mach])
disp(['BR: ' fn_BR])
disp(['Run: ' run_number])
disp(['Code: ' num2str(choose_code)])
disp(['Reduce Time: ' num2str(reduces_time) ' seconds'])
disp(['Ttot Lag: ' num2str(lagTC) ' seconds'])
if recovery == 1;
    disp(['Treccovery: Assumed Recovery Factor = ' num2str(r)])
elseif recovery == 2;
    disp(['Treccovery: Measured Td (' num2str(event) ')'])
end

%Gage Names
numberofgage = 21;
numberofTC = 10;
gagename = ['Gage 01';'Gage 02';'Gage 03';'Gage 04';...
    'Gage 05';'Gage 06';'Gage 07';'Gage 08';'Gage 09';'Gage 10';...
    'Gage 11';'Gage 12';'Gage 13';'Gage 14';'Gage 15';'Gage 16';...
    'Gage 17';'Gage 18';'Gage 19';'Gage 20';'Gage 21'];
gagename2 = [1:1:numberofgage];

%Arrays for Td from BR = 0 Runs
if fn_turbulence == '16'
    if fn_exit_mach == '0_60'
        Td = [];
    elseif fn_exit_mach == '0_80'
        Td = [];
    elseif fn_exit_mach == '1_01'
        Td = [];
    end
elseif fn_turbulence == '2'
    if fn_exit_mach == '0_80'
        Td = [];
    elseif fn_exit_mach == '1_01'
        Td = [];
    end
end

end

%%%%%%%%%%%%%%%%%%%%%%%%%%%%%%%%%%%%%%%%%%%%%%%%%%%%%%%%%%%%%%%%%%%%%%%%
%Load/Sort/Filter/Lag Data Files
%%%%%%%%%%%%%%%%%%%%%%%%%%%%%%%%%%%%%%%%%%%%%%%%%%%%%%%%%%%%%%%%%%%%%%%%
%File Name Strings
%-----
fn1 = '\Solar_Research\Film_Cooled\Film Cooled Vane\Tunnel Test\Final Vane\';
fn2 = '_Turbulence\Mach ';
fn3 = '\BR_';
fn4 = '\';
fn5 = '\NI_';
fn6 = '\PSI_';
fn7 = 'Run_';
fn8 = '.lvm';
fn9 = '.xls';

%Input File
fn_input = [fn_drive fn1 fn_turbulence fn2 fn_exit_mach fn3 fn_BR fn4 ...
    date '\Input ' date input_tag fn9];
%NI File
fn_NI = [fn_drive fn1 fn_turbulence fn2 fn_exit_mach fn3 fn_BR fn4 date...
    fn5 fn7 run_number fn8];

```

```

%PSI File
fn_PSI = [fn_drive fn1 fn_turbulence fn2 fn_exit_mach fn3 fn_BR fn4 date...
         fn6 fn7 run_number];
%Save file name
savename = [fn_drive fn1 fn_turbulence fn2 fn_exit_mach fn3 fn_BR fn4...
           date fn4 ' ' fn7 run_number '_reduced' save_tag '.xls'];

%Title for plots
plot_name = ['Date:' date ' Turb: ' fn_turbulence '% M_e_x: ' ...
           fn_exit_mach ' BR: ' fn_BR 'Run ' run_number];

%Load Files
%-----
NI_data_prefilt = dlmread(fn_NI);
PSI_data_prelag = dlmread(fn_PSI,'\t',1,0);
input = xlsread(fn_input,'input','B2:H22');

Vbridgesupply = input(1,6); %Voltage supplied to Wheatstone bridge
Patm_Pa = input(1,7);      %Atmospheric pressure in bars
Patm = Patm_Pa/6894.75;    %Atmospheric converted to Pa
Kelvin_con = 273.15;      %Conversion from deg C to Kelvin

%Assign individual gage properties/values from input file
%-----
for i = 1:numberofgage
    Kcalib(i) = input(i,1); %TFG calibration slope (ohm/degC)
    R20(i) = input(i,2);   %TFG resistance at 20degC
    x_c(i) = input(i,3);   %x/c location of gage
    M_loc(i) = input(i,4); %local mach number at gage location
    Rprun(i) = input(i,5); %Pre-run resistance of TFG
end
clear i

%Filter NI Data
%-----
if filter == 1
    aba = size(NI_data_prefilt); %Number of data columns
    [d,e] = butter(5,20/500);    %Define filter
    for i = 2:aba(2)             %every column except time
        NI_data(:,i) = filtfilt(d,e,NI_data_prefilt(:,i));
    end
    clear i

    %digital Filter for 60hz noise
    % n = 1024;
    % Nyq = fs/2;
    % for i = 2:aba(2)
    % % W = [29./Nyq 31./Nyq 59./Nyq 61./Nyq 179./Nyq 181./Nyq 299./...
    % % Nyq 301./Nyq];
    % W = [59./Nyq 61./Nyq 179./Nyq 181./Nyq 299./Nyq 301./Nyq];
    % b = fir1(n, W, 'stop');
    % NI_data(:,i) = filtfilt(b,1,NI_data_prefilt(:,i));
    % end
    % clear i n
elseif filter == 0
    NI_data = NI_data_prefilt;
end

%Time Data
%-----
time = NI_data_prefilt(:,1);
time = time-time(1); %convert b/c DAQ may not start at t = 0
N = length(NI_data);
Npsi = length(PSI_data_prelag);

%Name/Sort NI data
%-----
%NI Column Structure:

```

```

%time,Ttot_free,Ttot_plen_slide,Ttot_plen_fit,Ttot_line,TFG voltages,
%TC's, MKS

%TC's and MKS's
for i = 1:N
    %TC's
    Ttot_free_prelag(i) = NI_data(i,2);
    Ttot_plen_slide(i) = NI_data(i,3);
    Ttot_plen_fit(i) = NI_data(i,4);
    Ttot_line(i) = NI_data(i,5);

    %MKS(Psi)
    Orifice_dP(i) = NI_data(i,5+numberofgage+numberofTC+3);
    Orifice_up_Ptot(i) = NI_data(i,5+numberofgage+numberofTC+1);
    Orifice_up_Pstat(i) = NI_data(i,5+numberofgage+numberofTC+2);

end
clear i

%TFG's
for i = 1:numberofgage
    for j = 1:N
        TFG_volt(j,i) = NI_data(j,5+i);
    end
end
clear i j

%TC's
for i = 1:numberofTC
    for j = 1:N
        TC(j,i) = NI_data(j,5+numberofgage+i);
    end
end
clear i j

%Lag Ttot freestream
Ttot_free = zeros(1,N);
if lagTC>0;
    T_lag = Ttot_free_prelag(lagTC*fs:N);
else
    T_lag = Ttot_free_prelag(1:N);
end
for i = 1:length(T_lag)
    Ttot_free(i) = Ttot_free(i)+T_lag(i);
end
clear i

%Lag PSI System
PSI_data = zeros(Npsi,32);
if lagPSI>0
    PSI_lag = PSI_data_prelag(lagPSI*psi_fs:Npsi,:);
else
    PSI_lag = PSI_data_prelag(1:Npsi,:);
end
for i = 1:length(PSI_lag)
    PSI_data(i,:) = PSI_data(i,:)+PSI_lag(i,:);
end
clear PSI_data_prelag

%Name PSI data (units of PSI)
%-----
tpsi = 0;
psi_count = 1;
for i = 1:Npsi
    Ptot_free_up(i) = PSI_data(psi_count,1);
    Pstat_free_up(i) = PSI_data(psi_count,2);
    Pstat_up_1(i) = PSI_data(psi_count,9);
    Pstat_up_2(i) = PSI_data(psi_count,10);
    Pstat_down_1(i) = PSI_data(psi_count,5);
    Pstat_down_2(i) = PSI_data(psi_count,6);
    Pstat_down_3(i) = PSI_data(psi_count,7);
end

```

```

Pstat_down_4(i) = PSI_data(psi_count,8);
Ptot_plen(i)= PSI_data(psi_count,3);
Pstat_plen(i)= PSI_data(psi_count,4);
Pstat_down_avg(i)=(Pstat_down_1(i)+Pstat_down_2(i)+Pstat_down_3(i)+...
    Pstat_down_4(i))/4;
Pr_up(i)=(Ptot_free_up(i)+Patm)/(Pstat_free_up(i)+Patm);
Pr_down(i)=(Ptot_free_up(i)+Patm)/(Pstat_down_avg(i)+Patm);
M_up(i)=sqrt(2/0.4*(Pr_up(i)^(.4/1.4)-1));
M_down(i)=sqrt(2/0.4*(Pr_down(i)^(.4/1.4)-1));

%Vane static taps (psi)
j=1;
for tap = 11:32
    Pstat_vane(i,j) = PSI_data(psi_count,tap);
    Pr_vane(i,j) = (Ptot_free_up(i)+Patm)/(Pstat_vane(i,j)+Patm);
    M_vane(i,j) = sqrt(2/0.4*(Pr_vane(i,j)^(.4/1.4)-1));
    j=j+1;
end
clear tap j
time_psi(i)=ttpsi;
ttpsi = ttpsi+1/psi_fs; %makes a time vector same length as psi data
if psi_count < Npsi
    psi_count = psi_count+1;
else
    psi_count = 600;
end
end
clear i
clear NI_data NI_data_prefilt PSI_data

%Oversample NI data for calculating BR
%-----
z = 1;
for a = 1:50:N
    %Tunnel Ttot
    Ttot_free_OS(z) = Ttot_free(a);
    %Plenum total temp @ fitting
    Ttot_plen_fit_OS(z) = Ttot_plen_fit(a);
    %Plenum total temp w/sliding TC
    Ttot_plen_slide_OS(z) = Ttot_plen_slide(a);
    %Line total temp upstream of orifice
    Ttot_line_OS(z) = Ttot_line(a);
    %Orifice delta p
    Orifice_dP_OS(z) = Orifice_dP(a);
    %Ptot upstream of orifice
    Orifice_up_Ptot_OS(z) = Orifice_up_Ptot(a);
    %Pstat upstream of orifice
    Orifice_up_Pstat_OS(z) = Orifice_up_Pstat(a);
    z = z+1;
end

%%%%%%%%%%%%%%%%%%%%%%%%%%%%%%%%%%%%%%%%%%%%%%%%%%%%%%%%%%%%%%%%%%%%%%%%
%Find tunnel start time
%%%%%%%%%%%%%%%%%%%%%%%%%%%%%%%%%%%%%%%%%%%%%%%%%%%%%%%%%%%%%%%%%%%%%%%%
pp = 1;
for i = 1:Npsi
    if Ptot_free_up(i) > 0.007
        break
    end
    pp = pp+1;
end
clear i
tunnel_start_index = pp;
tunnel_start = pp/psi_fs; %Tunnel start time in seconds
reducestart = tunnel_start+tunnel_delay;
reduceend = reducestart+reductime;

%%%%%%%%%%%%%%%%%%%%%%%%%%%%%%%%%%%%%%%%%%%%%%%%%%%%%%%%%%%%%%%%%%%%%%%%
%Calculate Blowing Ratio
%%%%%%%%%%%%%%%%%%%%%%%%%%%%%%%%%%%%%%%%%%%%%%%%%%%%%%%%%%%%%%%%%%%%%%%%
%Geometry

```

```

%-----
%area of cooling holes (m^2)
A_holes = num_holes*pi*((hole_diam*(2.54/100))/2)^2;
%discharge coeff. of orifice plate
discharge_coeff = 0.62;
%area of orifice plate opening (m^2)
bore_area = pi*((0.2795*(2.54/100))/2)^2;

%Blowing Ratio
%-----
for i = 1:Npsi
    %Freestream
    %Static freestream temp upstream(K)
    Tstat_free(i)=(Ttot_free_OS(i)+Kelvin_con)/(1+0.2*M_up(i)^2);
    %Static freestream temp downstream(K)
    Tstat_free_down(i)=(Ttot_free_OS(i)+Kelvin_con)/(1+0.2*M_down(i)^2);
    %Upstream density(kg/m^3)
    rho_stat_free(i)=(Pstat_free_up(i)+Patm)*6894.75/(287*Tstat_free(i));
    %Downstream density(kg/m^3)
    rho_stat_free_down(i)=(Pstat_free_down_avg(i)+Patm)*6894.75/(287*...
        Tstat_free_down(i));
    %rho*u_free (kg/m^2-s)
    rhou_free(i)=rho_stat_free(i)*M_up(i)*sqrt(1.4*287*Tstat_free(i));
    %velocity @exit
    vel_down(i)=M_down(i)*sqrt(1.4*287*Tstat_free_down(i));

    mu(i)=0.00001716*((Ttot_free_OS(i)+Kelvin_con)/273.16)^1.5*(383.716/...
        ((Ttot_free_OS(i)+Kelvin_con)+110.556));%viscosity
    %Reynolds number @exit
    Re_down(i)=(rho_stat_free_down(i)*vel_down(i)*(C*2.54/100))/mu(i);

    %Coolant
    %Plenum total/stat pressure ratio
    Pr_plen(i)=(Ptot_plen(i)+Patm)/(Pstat_plen(i)+Patm);
    %Plenum Mach #
    M_plen(i)=sqrt(2/0.4*(Pr_plen(i)^(0.4/1.4)-1));
    pr_orf_up(i)=(Orifice_up_Pstat_OS(i)+Patm)/(Orifice_up_Ptot_OS(i)+...
        Patm);
    %Static temp upstream of orifice meter(K)
    Tstat_line(i)=(Ttot_line_OS(i)+Kelvin_con)*pr_orf_up(i)^(0.4/1.4);
    %Density of air entering flow meter(kg/m^3)
    rho_line(i)=(Orifice_up_Pstat_OS(i)+Patm)*6894.75/(287*Tstat_line(i));
    %Coolant mass flow(kg/s)
    mdot_coolant(i)=discharge_coeff*bore_area*sqrt(2*rho_line(i)*...
        Orifice_dP_OS(i)*6894.75);
    %Static temp in plenum(K)
    Tstat_plen(i)=(Ttot_plen_slide_OS(i)+Kelvin_con)/(1+0.2*M_plen(i)^2);
    %Density of air in plenum(kg/m^3)
    rho_plen(i)=(Pstat_plen(i)+Patm)*6894.75/(287*Tstat_plen(i));

    %Ratios
    DR(i) = rho_plen(i)/rho_stat_free(i);           %Density Ratio
    PR(i) = (Ptot_plen(i)+Patm)/(Ptot_free_up(i)+Patm); %Pressure Ratio
    BR(i) = (mdot_coolant(i)/A_holes)/rhou_free(i); %Blowing Ratio
end
clear i

%%%%%%%%%%%%%%%%%%%%%%%%%%%%%%%%%%%%%%%%%%%%%%%%%%%%%%%%%%%%%%%%%%%%%%%%
%Plot Exit MA/BR
%%%%%%%%%%%%%%%%%%%%%%%%%%%%%%%%%%%%%%%%%%%%%%%%%%%%%%%%%%%%%%%%%%%%%%%%
red_start_x = [reducestart,reducestart];
red_end_x = [reduceend,reduceend];
red_start_y = [0 40000];
red_end_y = [0 40000];

Mach_redtime = M_down(1,round(reducestart*psi_fs):round(reduceend*psi_fs));
BR_redtime = BR(1,round(reducestart*psi_fs):round(reduceend*psi_fs));
DR_redtime = DR(1,round(reducestart*psi_fs):round(reduceend*psi_fs));
Re_redtime = Re_down(1,round(reducestart*psi_fs):round(reduceend*psi_fs));
Ptot_free_redtime = Ptot_free_up(1,round(reducestart*psi_fs):...
    round(reduceend*psi_fs));

```

```

Ttot_free_redtime = Ttot_free_OS(1,round(reducestart*psi_fs):...
    round(reduceend*psi_fs));
Ttot_plen_slide_OS_redtime = Ttot_plen_slide_OS(1,...
    round(reducestart*psi_fs):round(reduceend*psi_fs));

Ptot_free_redtime_avg = mean(Ptot_free_redtime);
Ttot_free_redtime_avg = mean(Ttot_free_redtime);
mu_avg = mean(mu(1,round(reducestart*psi_fs):round(reduceend*psi_fs)));
Mex_avg = mean(Mach_redtime);
BR_avg = mean(BR_redtime);
DR_avg = mean(DR_redtime);
Re_avg = mean(Re_redtime);
Mstring = ['Mex = ' num2str(Mex_avg)];
BRstring = ['BR = ' num2str(BR_avg)];
DRstring = ['DR = ' num2str(DR_avg)];

figure
hold on
% plot(time_psi,BR,'b')
hl1=line(time_psi,M_down,'Color','b');
axis([tunnel_start 30 0 1.2])
xlabel('Time (s)'),ylabel('M_e_x_i_t')
line(red_start_x,red_start_y,'Color','r')
line(red_end_x,red_end_y,'Color','r')
ax1 = gca;
set(ax1,'XColor','b','Ycolor','b')
ax2=axes('Position',get(ax1,'Position'),'YAxisLocation',...
    'right','Color','none','XColor','k','YColor','k');
hl2=line(time_psi,BR,'Color','k','Parent',ax2);
axis([tunnel_start 30 0 3])
ylabel('BR')
text(20,0.5,{Mstring,BRstring,DRstring},'EdgeColor','black')
hold off
% plot(time_psi,M_down,'r')

%%%%%%%%%%%%%%%%%%%%%%%%%%%%%%%%%%%%%%%%%%%%%%%%%%%%%%%%%%%%%%%%%%%%%%%%
%Convert TFG voltages to Temperature
%%%%%%%%%%%%%%%%%%%%%%%%%%%%%%%%%%%%%%%%%%%%%%%%%%%%%%%%%%%%%%%%%%%%%%%%

if conv_TFG == 1
    disp('Converting TFG Voltages to Temperature...')

    Rline = 0.145; %Line resistance (ohms)
    Rs = 10000; %Series resistance of bridge (ohms)

    %Zero and obtain mean pre-run temp from t=0 to tunnel start
    %-----

    %Pre-run temp
    for i = 1:numberofTC
        TC_o(i) = mean(TC(1:tunnel_start*fs+1,i));
    end
    clear i
    TC_mean_o = mean(TC_o);

    %Zero TFG
    for i = 1:numberofgage
        %Average initial voltage from t=0 to tunnel start
        TFG_volt_o(i) = mean(TFG_volt(1:tunnel_start*fs+1,i));
        %Offset voltage to zero
        TFG_volt(:,i) = TFG_volt(:,i)-TFG_volt(1,i);
        %Correct calibration for day-to-day variation
        Kcor(i) = Kcalib(i)*(Rprun(i)-Rline)/R20(i);
        Rt(i) = Rs+Rprun(i);
        for j = 1:N
            %change in temp from initial
            del_T_Pt_TFG(j,i) = TFG_volt(j,i)*Rt(i)/(Kcor(i)*(Rs/Rt(i))*...
                Vbridgesupply-TFG_volt(j,i));
            %Temperature (degC)
            T_Pt_TFG(j,i) = TC_mean_o + del_T_Pt_TFG(j,i);
        end
    end
end

```

```

        if recovery == 1
            %Local Taw for uncooled (K)
            Trec(j,i) = (Ttot_free(j)+Kelvin_con)*((1+r*0.2*...
                M_loc(i)^2)/(1+0.2*M_loc(i)^2));
        elseif recovery == 2
            Trec(j,i) = (Ttot_free(j)+Kelvin_con)-Td(1,i);
        end
        phi(j,i) = (Ttot_free(j)-T_Pt_TFG(j,i))/(Ttot_free(j)-...
            Ttot_plen_slide(j));
    end

    end
    clear i j
end

%%%%%%%%%%%%%%%%%%%%%%%%%%%%%%%%%%%%%%%%%%%%%%%%%%%%%%%%%%%%%%%%%%%%%%%%
%Calculate Heat Flux using Laplace/FD Codes
%%%%%%%%%%%%%%%%%%%%%%%%%%%%%%%%%%%%%%%%%%%%%%%%%%%%%%%%%%%%%%%%%%%%%%%%
% TC_mean_o = 24.2;

if determine_q == 1

    if choose_code == 1
        disp('Determining q" using Laplace Code...')
        %Double-Layer Laplace FD Code
        for i = 1:numberofgage
            q(:,i) = SemiInfHeatFlux(T_Pt_TFG(:,i));
        end
        clear i

    elseif choose_code == 2
        disp('Determining q" using Finite Difference Code...')
        %Double-Layer FD Code
        Lm = [.2125,.2425,.2785,.3175,.36,.4025,.4475,.4875,.51875,...
            .1399,.23,.425,.504,.5137,.6452,.635,.52,.4975,.465,.425,.385];
        Lm = Lm*(2.54/100);
        backwalltemp=zeros(1,N)+TC_mean_o;
        for i = 1:numberofgage
            if (separate_plen==1 & (i== 9|i==10|i==11))
                q(:,i) = FiniteHeatFlux(T_Pt_TFG(:,i),Ttot_plen_slide,...
                    Lm(i),TC_mean_o);
            else
                q(:,i) = FiniteHeatFlux(T_Pt_TFG(:,i),backwalltemp,...
                    Lm(i),TC_mean_o);
            end
        end
        clear i
    end

    %%%%%%%%%%%%%%%%%%%%%%%%%%%%%%%%%%%%%%%%%%%%%%%%%%%%%%%%%%%%%%%%%%%%%%%%%
    %Calculate HTC/eta
    %%%%%%%%%%%%%%%%%%%%%%%%%%%%%%%%%%%%%%%%%%%%%%%%%%%%%%%%%%%%%%%%%%%%%%%%%
    disp('Calculating HTC and eta...')
    for i = 1:numberofgage
        k = 1;
        for j = round(reducestart*fs):round(reduceend*fs)
            y_axis(k,i) = q(j,i)/(Trec(j,i)-(Ttot_plen_slide(j)+...
                Kelvin_con));
            x_axis(k,i) = (Trec(j,i)-(T_Pt_TFG(j,i)+Kelvin_con))/...
                (Trec(j,i)-(Ttot_plen_slide(j)+Kelvin_con));
            k=k+1;
        end

        lineeq_o = polyfit(x_axis(:,i),y_axis(:,i),1);
        lineeq(1,i) = lineeq_o(1); %slope
        lineeq(2,i) = lineeq_o(2); %yint
        R_coef = corrcoef(x_axis(:,i),y_axis(:,i));
        R_squared(1,i) = R_coef(2,1)^2;
        evallinex(:,i)=(linspace((min(x_axis(:,i))-0.01),...
            (max(x_axis(:,i))+0.01),10))';
        evalliney(:,i) = polyval(lineeq_o,evallinex(:,i));
    end
end

```

```

HTC_avg(1,i) = lineeq(1,i); %Heat transfer coefficient
eta(1,i) = -lineeq(2,i)/lineeq(1,i); %Film-cooling effectiveness
phi_avg(i) = mean(phi(round(reducestart*fs):round(reduceend*fs),i));

end
clear i j

Nu_avg = HTC_avg*(C*(2.54/100))/0.03;

%Reduce HTC and Taw time history assuming eta is constant
%should only analyze results during time that eta is constant
for i = 1:numberofgage
    for j = 1:N
        %Taw(K)
        Taw(j,i) = eta(1,i)*(Ttot_plen_slide(j)+Kelvin_con-...
            Trec(j,i))+Trec(j,i);
        %HTC time history(W/m^2*K)
        HTC(j,i) = q(j,i)/(Taw(j,i)-(T_Pt_TFG(j,i)+Kelvin_con));
        theta(j,i) = (Ttot_plen_slide(j)-Ttot_free(j))/...
            (T_Pt_TFG(j,i)-Ttot_free(j));
    end
end
clear i j
xtextloc = 1.02*mean(x_axis);
ytextloc = 0.96*mean(y_axis);

for i = 1:numberofgage
    Taw_avg(i) = mean(Taw(round(reducestart*fs):round(reduceend*fs),i));
    T_Pt_TFG_avg(i) = mean(T_Pt_TFG(round(reducestart*fs):...
        round(reduceend*fs),i));
    Trec_avg(i) = mean(Trec(round(reducestart*fs):round(reduceend*fs),i));
    theta_avg(i) = mean(theta(round(reducestart*fs):...
        round(reduceend*fs),i));
    q_avg(i) = mean(q(round(reducestart*fs):round(reduceend*fs),i));
end
end

%%%%%%%%%%%%%%%%%%%%%%%%%%%%%%%%%%%%%%%%%%%%%%%%%%%%%%%%%%%%%%%%%%%%%%%%
%Plots
%%%%%%%%%%%%%%%%%%%%%%%%%%%%%%%%%%%%%%%%%%%%%%%%%%%%%%%%%%%%%%%%%%%%%%%%
%Mach Number
%-----
%Exit Mach number only
figure
hold on
xlabel('Time (s)'),ylabel('M_e_x_i_t'),title('Exit Mach Number')
line(red_start_x,red_start_y,'Color','r')
line(red_end_x,red_end_y,'Color','r')
axis([tunnel_start,30,0,1])
plot(time_psi,M_down)
hold off
%inlet/exit Mach number and freestream temp
figure
hold on
line(time_psi,M_down,'Color','g')
line(time_psi,M_up,'Color','b')
line(red_start_x,red_start_y,'Color','k')
line(red_end_x,red_end_y,'Color','k')
axis([tunnel_start 30 0 1.1])
xlabel('Time (s)'),ylabel('Mach Number')
ax1 = gca;
set(ax1,'XColor','k','YColor','k')
ax2=axes('Position',get(ax1,'Position'),'YAxisLocation',...
    'right','Color','none','XColor','k','YColor','k');
axis([tunnel_start 30 0 125])
line(time,Ttot_free,'Color','r','Parent',ax2)
ylabel('Temperature (degC)')
hold off
%Vane Mach Distribution
%-----
M_vane_loc = [0.010,0.064,0.116,0.189,0.279,0.373,0.448,0.492,0.579,...

```

```

    0.620,0.659,0.701,0.743,0.841,0.939,1.060,1.300,-0.044,-0.098,...
    -0.174,-0.302,-0.431];
%Uncooled Distributions for comparison
if fn_exit_mach == '0_60'
    M_vane_uncool = [0.082,0.123,0.195,0.299,0.494,0.657,0.715,0.734,...
        0.678,0.647,0.642,0.636,0.620,0.607,0.599,0.583,0.567,0.055,...
        0.074,0.089,0.133,0.154];
elseif fn_exit_mach == '0_80'
    M_vane_uncool = [0.082,0.124,0.213,0.341,0.584,0.824,0.961,0.1073,...
        1.000,0.946,0.940,0.934,0.927,0.906,0.893,0.872,0.835,0.071,...
        0.093,0.112,0.162,0.188];
elseif fn_exit_mach == '1_01'
    M_vane_uncool = [0.075,0.122,0.211,0.342,0.590,0.831,0.981,1.109,...
        1.154,1.056,1.039,1.041,1.059,1.084,1.116,0.993,0.943,0.072,...
        0.092,0.111,0.164,0.193];
end
Finding average M during reduction time
for j = 1:22
    M_vane_redtime(:,j) = M_vane(round(reducestart*psi_fs):...
        round(reduceend*psi_fs),j);
    M_vane_avg(1,j) = mean(M_vane_redtime(:,j));
end
clear j

figure
plot(M_vane_loc,M_vane_avg,'o')
hold on
plot(M_vane_loc,M_vane_uncool,'+r')
grid,xlabel('x/C'),ylabel('Mach Number')
title('Mach Number Distribution')
legend('Measured','Uncooled [2006]')
%BR
%-----
figure
hold on
xlabel('Time (s)'),ylabel('BR'),title('Blowing Ratio')
line(red_start_x,red_start_y,'Color','r')
line(red_end_x,red_end_y,'Color','r')
axis([tunnel_start,30,0,3])
plot(time_psi,BR)
hold off
%PR
%-----
figure
hold on
xlabel('Time (s)'),ylabel('PR'),title('Pressure Ratio')
line(red_start_x,red_start_y,'Color','r')
line(red_end_x,red_end_y,'Color','r')
axis([tunnel_start,30,0,2])
plot(time_psi,PR)
hold off
%DR
%-----
figure
hold on
xlabel('Time (s)'),ylabel('DR'),title('Density Ratio')
line(red_start_x,red_start_y,'Color','r')
line(red_end_x,red_end_y,'Color','r')
axis([tunnel_start,30,0,3])
plot(time_psi,DR)
hold off
% Gage Temperature traces
% -----
aa=1;
bb=8;
for j = 1:ceil(numberofgage/8)
    figure
    k=1;
    for i = aa:bb
        subplot(4,2,k),plot(time,T_Pt_TFG(:,i))
        hold on
    end
end

```

```

        line(red_start_x,red_start_y,'Color','r')
        line(red_end_x,red_end_y,'Color','r')
        hold off
        axis([tunnel_start,30,0,75])
        xlabel('Time (s)'),ylabel('Temp (degC)')
        title(['Gage ' num2str(i)])
        k=k+1;
    end
    if bb<(numberofgage-8)
        aa=aa+8;
        bb=bb+8;
    else
        aa=aa+8;
        bb=numberofgage;
    end
end
clear i j k aa bb
%Gage Heat Flux Traces
%-----
aa=1;
bb=8;
for j = 1:ceil(numberofgage/8)
    figure
    k=1;
    for i = aa:bb
        subplot(4,2,k),plot(time,q(:,i))
        hold on
        line(red_start_x,red_start_y,'Color','r')
        line(red_end_x,red_end_y,'Color','r')
        hold off
        axis([tunnel_start,30,0,30000])
        xlabel('Time (s)'),ylabel('q" (W/m^2)')
        title(['Gage ' num2str(i)])
        k=k+1;
    end
    if bb<(numberofgage-8)
        aa=aa+8;
        bb=bb+8;
    else
        aa=aa+8;
        bb=numberofgage;
    end
end
clear i j k aa bb
%Determining HTC/Effectiveness Plots
%-----
for i = 1:numberofgage
    hstring = ['h = ' num2str(round(HTC_avg(i))) ' W/m^2.K'];
    etastring = ['\eta = ' num2str(eta(i))];
    regstring = ['R^2 = ' num2str(R_squared(i))];
    figure
    hold on
    title(['Run ' run_number ', Gage ' num2str(i)])
    xlabel('(T_r-T_w)/(T_r-T_c)'),ylabel('q"/(T_r-T_c)')
    plot(x_axis(:,i),y_axis(:,i),'.','MarkerSize',4)
    plot(evallinex(:,i),evalliney(:,i),'-k')
    text(xtextloc(i),ytextloc(i),{hstring,etastring,regstring},...
        'EdgeColor','black')
    hold off
end
clear i
%Ttot_free,Taw,Trec,Tcoolant
%-----
for i = 1:numberofgage
    figure
    hold on
    axis([0 30 200 400])
    plot(time,(Ttot_free+Kelvin_con),time,Taw(:,i),time,Trec(:,i),time,...
        (Ttot_plen_slide+Kelvin_con))
    legend('T_t_o_t Freestream','T_a_w','T_r_e_c','T_c_o_o_l_a_n_t')
    line(red_start_x,red_start_y,'Color','r')

```

```

        line(red_end_x,red_end_y,'Color','r')
        xlabel('Time (s)')
        ylabel('Temperature (K)')
        hold off
    end
clear i
%Gage Heat Transfer Coefficients (assuming constant eta)
%-----
aa=1;
bb=8;
for j = 1:ceil(numberofgage/8)
    figure
    k=1;
    for i = aa:bb
        subplot(4,2,k),plot(time,HTC(:,i))
        hold on
        line(red_start_x,red_start_y,'Color','r')
        line(red_end_x,red_end_y,'Color','r')
        hold off
        axis([tunnel_start,30,0,2000])
        xlabel('Time (s)'),ylabel('h (W/m^2.K)')
        title(['Gage ' num2str(i)])
        k=k+1;
    end
    if bb<numberofgage
        aa=aa+8;
        bb=bb+8;
    else
        aa=aa+8;
        bb=numberofgage;
    end
end
clear i j k aa bb

%Nu Distribution
%-----
figure
plot(x_c,Nu_avg,'-o');
grid
xlabel('x/C'),ylabel('Nu')
title('Nu Distribution,' plot_name)
%HTC Distribution
%-----
figure
plot(x_c,HTC_avg,'-o')
grid,xlabel('x/C'),ylabel('HTC')
title(['HTC Distribution,' plot_name])
%Eta Distribution
figure
plot(x_c,eta,'-o')
grid,xlabel('x/C'),ylabel('\eta')
title(['\eta Distribution,' plot_name])
% Theta Distribution
% figure
% plot(x_c,theta_avg,'-o')
% grid,xlabel('x/C'),ylabel('\theta')
% title(['\theta Distribution,' plot_name])

%%%%%%%%%%%%%%%%%%%%%%%%%%%%%%%%%%%%%%%%%%%%%%%%%%%%%%%%%%%%%%%%%%%%%%%%
%Save Data to Excel Files
%%%%%%%%%%%%%%%%%%%%%%%%%%%%%%%%%%%%%%%%%%%%%%%%%%%%%%%%%%%%%%%%%%%%%%%%

if savedata ==1
    %Save blowing Data
    blowarray(:,1) = time_psi';
    blowarray(:,2) = BR';
    blowarray(:,3) = DR';
    blowarray(:,4) = PR';
    blowarray(:,5) = M_plen';
    blowarray(:,6) = Tstat_free';
    blowarray(:,7) = rho_stat_free';

```

```

blowarray(:,8) = mdot_coolant';
blowarray(:,9) = Ttot_plen_slide_OS';
blowarray(:,10) = Tstat_plen';
blowarray(:,11) = Ptot_plen';
blowarray(:,12) = Pstat_plen';
blowarray(:,13) = Orifice_up_Ptot_OS';
blowarray(:,14) = Orifice_up_Pstat_OS';
blowarray(:,15) = Orifice_dP_OS';
blowarray(:,16) = Ttot_plen_fit_OS';
blowarray(:,17) = Ttot_line_OS';
xlswrite(savename,blowarray,'Blowing History','A2')
%Save Freestream Data
freearray(:,1) = time_psi';
freearray(:,2) = M_down';
freearray(:,3) = Ptot_free_up';
freearray(:,4) = Pstat_free_up';
freearray(:,5) = Pstat_up_1';
freearray(:,6) = Pstat_up_2';
freearray(:,7) = Pstat_down_1';
freearray(:,8) = Pstat_down_2';
freearray(:,9) = Pstat_down_3';
freearray(:,10) = Pstat_down_4';
freearray(:,11) = Ttot_free_OS';
xlswrite(savename,freearray,'Freestream History','A2')
elseif savedata ==2
disp(['Saving Data...'])
%Save axis data
oddcount = 1;
evencount = 2;
for i = 1:numberofgage
axisdata(:,oddcount) = x_axis(:,i);
axisdata(:,evencount) = y_axis(:,i);
gagename3(oddcount) = i;
gagename3(evencount) = i;
oddcount = oddcount + 2;
evencount = evencount + 2;
end
xlswrite(savename,axisdata,'axisdata','B2')
clear oddcount evencount i
oddcount=1;
evencount=2;
num_rows = length(x_axis);
for i = 1:numberofgage
yy=1;
for j = 1:10:num_rows
axisdata_os(yy,oddcount) = x_axis(j,i);
axisdata_os(yy,evencount) = y_axis(j,i);
yy = yy+1;
end
gagename3(oddcount) = i;
gagename3(evencount) = i;
oddcount = oddcount + 2;
evencount = evencount + 2;
end
clear i j
xlswrite(savename,axisdata_os,'axisdata_os','B2')
%Save average values
xlswrite(savename,gagename2,'Average Values','B1')
avgarray(1,:) = HTC_avg(1,:);
avgarray(2,:) = Nu_avg(1,:);
avgarray(3,:) = eta(1,:);
avgarray(4,:) = R_squared(1,:);
avgarray(6,1) = Mex_avg;
avgarray(7,1) = BR_avg;
avgarray(8,1) = DR_avg;
avgarray(9,1) = Re_avg;
avgarray(11,1) = reducestart;
avgarray(12,1) = reduceend;
avgarray(14,1) = tunnel_start;
avgarray(16,:) = TC_mean_o;
avgarray(17,:) = TFG_volt_o(1,:);

```

```

avgarray(18,:) = Ptot_free_redtime_avg;
avgarray(19,:) = Ttot_free_redtime_avg;
avgarray(20,:) = mu_avg;
avgarray(21,:) = r;
avgarray(22,:) = lagTC;
avgarray(23,:) = choose_code;
avgarray(24,:) = Taw_avg(1,:);
avgarray(25,:) = Trec_avg(1,:);
avgarray(26,:) = T_Pt_TFG_avg(1,:);
avgarray(27,:) = theta_avg(1,:);
avgarray(28,:) = q_avg(1,:);
avgarray(29,:) = Td(1,:);
xlswrite(savename,gagename2,'Average Values','B1')
xlswrite(savename,avgarray,'Average Values','B2')
%Save Freestream Data
freearray(:,1) = time_psi';
freearray(:,2) = M_down';
freearray(:,3) = Ptot_free_up';
freearray(:,4) = Pstat_free_up';
freearray(:,5) = Pstat_up_1';
freearray(:,6) = Pstat_up_2';
freearray(:,7) = Pstat_down_1';
freearray(:,8) = Pstat_down_2';
freearray(:,9) = Pstat_down_3';
freearray(:,10) = Pstat_down_4';
freearray(:,11) = Ttot_free_OS';
xlswrite(savename,freearray,'Freestream History','A2')
%Save blowing Data
blowarray(:,1) = time_psi';
blowarray(:,2) = BR';
blowarray(:,3) = DR';
blowarray(:,4) = PR';
blowarray(:,5) = M_plen';
blowarray(:,6) = Tstat_free';
blowarray(:,7) = rho_stat_free';
blowarray(:,8) = mdot_coolant';
blowarray(:,9) = Ttot_plen_slide_OS';
blowarray(:,10) = Tstat_plen';
blowarray(:,11) = Ptot_plen';
blowarray(:,12) = Pstat_plen';
blowarray(:,13) = Orifice_up_Ptot_OS';
blowarray(:,14) = Orifice_up_Pstat_OS';
blowarray(:,15) = Orifice_dP_OS';
blowarray(:,16) = Ttot_plen_fit_OS';
blowarray(:,17) = Ttot_line_OS';
blowarray(:,18) = Ttot_free_OS';
xlswrite(savename,blowarray,'Blowing History','A2')
%Surface pressure
xlswrite(savename,Pstat_vane,'Vane Surf Press','B2')
%Surface Mach Number
xlswrite(savename,M_vane,'Vane surface Mach #','B2')
%Surface Mach number averaged
xlswrite(savename,M_vane_avg,'Avg Vane Surface Mach #','A2')
%Reduce time sheet
redarray(:,1) = Mach_redtime';
redarray(:,2) = BR_redtime';
redarray(:,3) = DR_redtime';
redarray(:,4) = Re_redtime';
redarray(:,5) = Ptot_free_redtime';
redarray(:,6) = Ttot_free_redtime';
redarray(:,7) = Ttot_plen_slide_OS_redtime';
xlswrite(savename,redarray,'Reduction Window','A2')
%Save Heat Flux Data
%Oversample to save
time_s = time(1:10:N,1);
for i = 1:numberofgage
    yyy=1;
    for j = 1:10:N
        T_Pt_TFG_OS2(yyy,i) = T_Pt_TFG(j,i);
        HTC_OS2(yyy,i) = HTC(j,i);
        q_OS2(yyy,i) = q(j,i);
    end
end

```

```

        Taw_OS2(yyy,i) = Taw(j,i);
        Trec_OS2(yyy,i) = Trec(j,i);
        Tcool_OS2(yyy,1) = Ttot_plen_slide(1,j);
        Ttot_free_OS2(yyy,1) = Ttot_free(1,j);
        yyy = 1+yyy;
    end
end
xlswrite(savename,gagename2,'T Pt TFG','B1')
xlswrite(savename,T_Pt_TFG_OS2,'T Pt TFG','B2')
xlswrite(savename,gagename2,'HTC','B1')
xlswrite(savename,HTC_OS2,'HTC','B2')
xlswrite(savename,gagename2,'Heat Flux','B1')
xlswrite(savename,q_OS2,'Heat Flux','B2')
xlswrite(savename,gagename2,'Taw','B1')
xlswrite(savename,Taw_OS2,'Taw','B2')
xlswrite(savename,gagename2,'Trec','B1')
xlswrite(savename,Trec_OS2,'Trec','B2')
%     xlswrite(savename,gagename2,'Ttot free','B1')
xlswrite(savename,Ttot_free_OS2,'Ttot free','B2')
%     xlswrite(savename,gagename2,'Tcool','B1')
xlswrite(savename,Tcool_OS2,'Tcool','B2')
end

```